MICROSTRUCTURE DEVELOPMENT IN BULK NIOBIUM FOLLOWING SEVERE PLASTIC DEFORMATION AND ANNEALING

A Dissertation

by

SHREYAS BALACHANDRAN

Submitted to the Office of Graduate and Professional Studies of
Texas A&M University
in partial fulfillment of the requirements for the degree of

DOCTOR OF PHILOSOPHY

Chair of Committee,	Karl T. Hartwig
Co-Chair of Committee,	Arun R. Srinivasa
Committee Members,	Raymundo Arroyave
	Peter McIntyre
Head of Department,	Andreas A. Polycarpou

May 2015

Major Subject: Mechanical Engineering

ABSTRACT

Niobium (Nb) finds application in the fabrication of Nb_3Sn superconducting wires for superconducting magnet applications, and SRF cavity applications. These applications need a favorable starting microstructure in precursor Nb to increase manufacturing reliability, reduce costs, and advance technology. The main problem with traditional Nb processing is that pure Nb is obtained by electron beam melting (EBM), which produces initial polycrystals tens to hundreds of centimeters in width/length, and can be comparable to the dimensions of the initial ingot. Breakdown of these initial cast microstructures, and to obtain consistent, fine grain microstructures in bulk product is a processing challenge. Generally, pure Nb, traditional thermo-mechanical processing methodologies such as: rolling, swaging, forging have been unable to effectively breakdown initial cast structures.

An objective of the thesis is to develop thermo-mechanical processing strategies involving severe plastic deformation (SPD) by Equal Channel Angular Extrusion (ECAE) for bulk Nb. ECAE enables grain refinement without appreciable crossectional area changes to the workpiece, which is a hallmark of ECAE. The microstructure refinement process by ECAE is not well understood for the breakdown of large grain Nb. We have shown that ECAE produces continuous orientation splitting, and hence grain refinement even when processed under a strain path that is perceived to be structure conserving (route 2C). Initial bi-crystal results indicate that significant convergence in microstructure is possible within two ECAE passes for extremely large grain Nb.

Processing strategies have been developed for effective control of grain size and texture in polycrystalline microstructures. The main results include effective grain

size control leading to uniform recrystallized grain sizes in the range of tens of microns, and texture control in Nb bars. Nb bars processed by this technique have better co-deformation characteristics as observed in Cu-Nb monocore wire experiments where a circularity greater than 0.85 is obtained for several textures , as compared to circularities of 0.5-0.7 using traditional processing. The methodology to adopt precursor Nb processed by thermomechanical processing by SPD to traditional tube development techniques such as area reduction extrusion are presented. The tubes formed by this approach show sufficient ductility (greater than 30%) along the circumferential and extrusion directions with tensile properties being very similar in perpendicular directions. The development of tube ECAE (tECAE) process produces textures very close to {111} parallel to tube normal directions that are considered to be favorable for hydroforming applications. This is the first report of such textures in a seamless tube. The processing strategies developed are able to homogenize and converge the microstructures in Nb leading to similar deformation behavior irrespective of the starting microstructure.

The grain refinement strategies for Nb presented in this thesis have the potential to be scaled up, and similar performance are expected irrespective of the Nb workpiece dimensions. The same processing strategies can be adapted to other bcc refractory metals including: tantalum (Ta), molybdenum (Mo), and tungsten (W) where the processing needs to be done at similar homologous temperatures/conditions where similar deformation mechanisms are active.

DEDICATION

I dedicate this thesis to my parents Balu, and Suma for supporting me all the way.

ACKNOWLEDGEMENTS

I would like to extend my special thanks to Dr. K. Ted Hartwig, and Dr. Arun Srinivasa, for their support, patience, and excellent mentorship throughout graduate school. Dr. Hartwig, I have enjoyed being around you, and have learnt a lot from you. I look forward for opportunities to continue working on interesting projects. Dr. Srinivasa, I would have never expected to wind up where I am today without your complete support. I am very thankful for your understanding and support during tough times.

Thank you to my committee members Dr. Raymundo Arroyave, and Dr. Peter McIntyre, for guiding me through graduate school. I have always enjoyed the discussions we have had. It has shaped my research thinking. Thank you for your time, and efforts in providing feedback. A special thanks to Dr. Patrick Shamberger, for making time, and willing to substitute, during my thesis defense presentation. I would like to thank Dr. Lance Cooley from Fermilab (FNAL) for his constant support, encouragement, and for asking me good questions that have motivated several areas of my research.

Dr. Zu Hawn Sung, and Dr. Peter Lee from the National High Field Magnet Lab (NHFML) deserve a special thanks, for providing assistance in helping me analyze the Nb bi-crystal samples. This work would have not been possible if not for the weeks that I spent at the Applied Superconductivity Center (ASC). In particular, discussions, and comments from Sung have been very helpful. I acknowledge the support of lab mates during my graduate school years. Dr. David Foley, Zach Levin (soon to be Dr. Levin), and Dr. Miao Song. I would like to thank you guys for your willingness to help, and offering the best suggestions whenever I needed them.

Thank you for the friendship. I would like to thank Dr. Siva Sankar, Dr. Steven Rios, and Dr. Dan Bufford who have contributed to my development.

A special thanks to Robert Barber, and Shear Form Inc for providing me all the raw material for my work. Robert I have learnt practical approaches beyond what textbooks can offer. Robert, I thank you for your friendship. Doug, I have always enjoyed your company (you know that!).

I would like to thank Andrea Cadima, Dr. Siva, Dr. Ashwin Rao, Dr. Guruprasad, and Dr. Sujay Deshmukh for being such good friends. I would have not been able to finish my PhD without your constant support. A special thanks to Dr. Pamela Lipe Revercomb, for guiding me during a very challenging time. Thank you, Laura Lee Revercomb for making this possible (It had to be arranged!). Thank you for the best wishes, and encouragement.

Finally, I would like to thank my parents, they have always made me feel special. They have taught me the importance of goodness, and I will always be indebted to them. I hope they realize how much I have watched, and learned from them.

TABLE OF CONTENTS

Page

ABSTRACT ii

DEDICATION iv

ACKNOWLEDGEMENTS v

TABLE OF CONTENTS vii

LIST OF FIGURES x

LIST OF TABLES xvi

1. INTRODUCTION AND LITERATURE REVIEW 1

1.1 Principal characteristics of deformation behavior in Nb 1
1.2 Qualitative understanding of Nb deformation 2
1.3 Production of high purity Nb 3
1.4 Conventional forming of Nb 4
1.4.1 Nb sheet production 5
1.4.2 Miscellaneous bulk Nb processing 9
1.4.3 Challenges to be overcome and gaps in knowledge 10
1.5 Severe plastic deformation by Equal Channel Angular Extrusion(ECAE)/ECAP 11
1.5.1 Description of ECAE 12
1.6 Microstructure development during ECAE of bcc metals 13
1.6.1 Experimental microstructure observations involving grain refinement of bcc metals as a consequence of ECAE 14

2. DEFORMATION OF A NIOBIUM BI-CRYSTAL 15

2.1 Introduction 15
2.2 Materials and Methods 15
2.2.1 Initial raw material 15
2.2.2 Billet cutting and extrusion details 16
2.2.3 Microstructure characterization 17
2.3 Experimental results 19
2.3.1 Macroscopic deformation characteristics 19
2.3.2 Initial orientation of bi-crystal 22

2.3.3 Microstructure characteristics after first pass ECAE 22
2.3.4 Microstructure characteristics after second pass ECAE 31
2.4 Discussion 35
2.4.1 Dislocation substructures 35
2.4.2 Orientation splitting 36
2.4.3 Orientation evolution 36
2.4.4 Summary and Conclusions 42

3. MICROSTRUCTURES IN NB BAR- EFFECT OF GRAIN SIZE AND TEXTURE ON DEFORMATION 43

3.1 Introduction 43
3.2 Materials and methods 48
3.2.1 Material and processing details for grain size study 48
3.2.2 Material and processing details for texture study 49
3.2.3 Manufacture of Cu clad Nb composite wires 50
3.2.4 Analysis method 50
3.3 Experimental results 51
3.3.1 Initial microstructure 51
3.3.2 Cu-Nb deformation characteristics after warm extrusions, and wire drawing 57
3.4 Discussion 62
3.5 Conclusions 65

4. MICROSTRUCTURE AND MECHANICAL PROPERTIES OF FINE GRAIN SEAMLESS NB TUBE BY SIMPLE SHEAR DEFORMATION 67

4.1 Background 67
4.2 Introduction 67
4.3 Materials and methods 69
4.3.1 Tube fabrication method 69
4.3.2 Microstructure characterization and mechanical testing 71
4.4 Results 71
4.4.1 Microstructures in recrystallized tubes 71
4.4.2 Mechanical testing 77
4.5 Discussion 77
4.6 Conclusions 81

5. SUMMARY AND CONCLUSIONS 82

5.1 Key Findings 82
5.1.1 Nb bi-crystal study 82
5.1.2 Microstructures in Nb bars produced by ECAE 83
5.1.3 Microstructure in Seamless Nb tubes 83

REFERENCES 85

APPENDIX A. GRAIN GROWTH IN RG NB 105

APPENDIX B. WELD HEALING OF A RRR NB TUBE BY MULTI PASS ECAE AND RECRYSTALLIZATION HEAT TREATMENTS 108

B.1 Background 108
B.2 Raw Material, processing Strategy, and characterization: Weld Healing 110
B.3 Results 111

LIST OF FIGURES

FIGURE Page

1.1 Example of large grain RRR Nb ingot from a 430 mm diameter ingot produced with the same EB melt furnace, with the melt rate, power and vacuum levels being constant. 4

1.2 Schematic of a 90^o ECAE die showing the deformation of a square element, as it passes through the die. The die axes are labeled in the figure where x=Extrusion Direction (ED); y= Normal Direction (ND); and z=Transverse Direction (TD). 12

1.3 Schematic of billet orientation between the first and second pass.The billet rotations about the axis provides changes in strain path between passes. 13

2.1 Schematic of the bi-crystal sample as it entered the ECAE die during: a) First pass (1A), and b) Second pass (2C). The billet was rotated by 180 ^{o} counterclockwise about the billet axis before reinserting back into the die as shown in (b). The global co-ordinate system which is attached to the die is as shown in the figure, where: x=Extrusion Direction(ED), y=Normal Direction (ND), and z= Transverse Direction (TD) 18

2.2 Deformation of the grid after ECAE deformation is shown: a) First pass (1A), b) Second pass (2C). The orientation of the grid is at 27^o to ED after 1A, and shape of the grid returns to roughly the original configuration of a square crossection of dimensions 2.5mm x 2.5mm. . 20

2.3 Representative optical micrographs of a large section from the ND-ED plane: (a-b) depict the deformation characteristics in Crystal 1, with the grain boundary at the center of (c), and (d) depicts the deformation characteristics in Crystal 2. 21

2.4 Representative optical micrographs of a large section from in the ND-ED plane: (a-b) depict the deformation characteristics in Crystal 1, with the grain boundary at the center of (c), and (d) depicts the deformation characteristics in Crystal 2. 23

2.5 Characteristics of the OIM of the initial bi-crystal. a) OIM of the initial crystal indicating the representative line segment for misorientation calculation, b) Misorientation profile of the two crystals indicating low misorientation in the grain interior and a spike at the GB, c) and d) are the {110} PF's for Crystal 1 and Crystal 2 respectively. 24

2.6 Representative microstructure of Crystal 1 away from the GB : a) and c) correspond to IPF in the TD direction, and b) and d) are corresponding IQ images 26

2.7 Misorientation profile representing dislocation local substructure formation in the matrix and band. a), and c) are IPFs of the matrix and band, b) and d) are the corresponding misorientation profiles taken along perpendicular lines to the observed structure 27

2.8 Representative microstructure of Crystal 2 away from the GB : a) IPF in the TD direction, and b) the corresponding IQ map 28

2.9 Misorientation profiles representing local dislocation substructure formation in the matrix and band. a), and c) are IPFs of the matrix and band, and b) and d) are the corresponding misorientation profiles taken along perpendicular lines to the observed structure 29

2.10 EBSD map of the GB region after 1 pass ECAE showing the differences in structure near the grain boundary in Crystal 1, and Crystal 2: a) IPF in the TD direction, and b) the corresponding IQ map, and c) the misorientation profile. The misorientation value at the GB is 52^o around the GB. 30

2.11 EBSD map showing representative microstructure in Crystal 1 after 2 pass ECAE: (a), (c) are IPF maps along TD, (c) and (d) are the corresponding IQ maps of the regions. 32

2.12 EBSD map showing representative microstructure in Crystal 2 after two ECAE passes, a IPF map along TD, b) is the corresponding IQ map of the regions. 33

2.13 EBSD map of the GB region after two ECAE passes showing differences in structure near the grain boundary in Crystal 1, and Crystal 2: a) IPF in the TD direction, and b) the corresponding IQ map, and c) the misorientation profile. The misorientation value at the GB is 44^o around the GB. 34

2.14 The fraction of misorientation boundaries in the interior of the two crystals are plotted scans of 300 μm x 300 μm; a), b) correspond to the first pass for Crystal 1 and Crystal 2 respectively, and c), and d) correspond to the second pass for Crystal 1, and Crystal 2 respectively. 37

2.15 Polycrystal simulation of 50 intial random bcc polycrystals by ECAE provides the following stable simple shear textures as shown by the {110} PF [11]. The symbols and text indicate specific stable orientations, which are provided in the following review paper [11](Table 2, pg: 438) 38

2.16 {110} Pole figures for one pass ECAE processed regions of the Nb bi-crystal: (a) and (b) represent regions away from the GB for Crystal 1, and Crystal 2 respectively; (c) and (d) represent regions around the GB in Crystal 1 and Crystal 2 respectively. The red, and blue points in the PF in (a), and (c) indicate the bands observed in the structure 40

2.17 {110} Pole figures for two pass ECAE processed regions of the Nb bi-crystal: a) and b) represent regions away from the GB for Crystal 1, and Crystal 2 respectively; (c) and (d) represent regions around the GB in Crystal 1 and Crystal 2 respectively. The blue, and green points in the PF in (a), and (c) indicate the bands observed in the structure. 41

3.1 Schematic of an internal tin wire architectures that are commonly used: a) Internal Tin single barrier wire commonly used for applications where magnetic stability is of primary importance, and b) Internal Tin distributed barrier conductor commonly used for applications needing high J_c. Courtesy:Peter Lee of NHFML/FSU 44

3.2 Fabrication process involved in the manufacture of an RRP conductor. The process involves multiple extrusion, and wire drawing steps. Nb_3Sn is formed after a high temperature,long soak heat treatment. The final wire dianmeter is of the order of 1000 μm's: Courtesy: Mike Field, OIST 46

3.3 Initial non-uniform deformation of Nb after extrusion (left), reshaped round Nb bar by machining and re-extruded (center), roundenss of the Nb bar retained after wire drawing (right)[103] 47

3.4 Representative microstructures of the starting Nb used in the fabrication of Cu-Nb monocore filaments. a) Cast sample with a grain size of 10-40mm; b) H.C. Stark Nb, average grain size of 1-4mm; c) ECAE processed and heat treated at 1150^{o}C, average grain size 70-170μm. and d) ECAE processed and heat treated at 950^{o}C, average grain size of 20-60μm. 52

3.5 Representative Nb microstructure after ECAE pre-processing by route 6B and recrystallization heat treatment at 950 ^{o}C/5400 sec. (a) Optical micrograph indicates a uniform starting microstructure with a grain size of 42 $\pm$ 10μm, (b) {110} PF indicates a medium strength texture, represented by {110}$\|$TD component 54

3.6 Optical micrographs indicating recrystallized microstructures in Nb after multi-ECAE processing by different ECAE routes: (a) Sample A-Route 4A, (b) Sample B-Route 4B, (c) Sample C- Route 4B$_c$, and (d) Sample D- Route 4E. The average recrystallized grain sizes are less than 30μm for all samples in consideration. 55

3.7 {110} PFs of multi-pass ECAE material processed under different ECAE routes in as worked and after recrystallization heat treatments (800^{o}C/ 5400 s); (a), (b), (c), and (d) are Pfs of as worked material, whereas (e), (f), (g), and (h) are recrystallized textures generated by routes 4A, 4B, 4B_c, and 4E respectively. The figure presents qualitative texture information. The max texture strengths are presented in Table 3.2. 56

3.8 Representative sections of the Cu-Nb interface of warm extruded monocore ro ID (grain sizes): (a) S1 (10000-40000) μm, (b) S2 (1000-4000) μm, (c) S3 (100$\pm$72) μm, (d)S4 (40$\pm$15 μm) 59

3.9 Macrographs of Cu-Nb monocore samples after warm extrusion, the sample ID (ECAE route) are :(a) A (4A), (b)B (4B). (c) 4B$_C$, (d) 4E. The Cu-Nb interface deformation is uniform, for all cases. 60

3.10 Seconday Electron image of as drawn Nb wire section at a final wire diameter of 1mm, with the Cu sheath etched off: a)S1- 10000-40000 μm, b) S2- 1000-4000μm, c) S3- 100$\pm$72μm, d) S4- 40$\pm$15μm 61

3.11 Optical Micrographs (OM) of as drawn Nb wire section at a final wire diameter of 1mm : a)A, b) B, c) C, and d) D. The initial grain sizes of the starting Nb was less than 50 μm, and the circularity is retained. 61

3.12 Variation of circularity as a function of wire diameter for various grain size ranges. Notice the poor circularity in Nb rods with starting grain sizes greater than 50μm. 63

3.13 Variation of circularity as a function of wire diameter for different initial texture strengths. All the Nb samples had grain sizes below 30μm. The circularity in Nb rods does not change significantly with warm extrusion followed by wire drawing 63

4.1 Illustration of the symmetric shear processing process of the tube, whereby a tube of initial internal radius of r_1 is expanded to r_2, and finally contracted back to the initial r_1. During the whole process the thickness of the tube remains a constant. 70

4.2 Schematic of the cutting plan for the tensile test samples: a) longitudinal direction (LD) sample as cut from the tube, b) circumferential direction (CD) sample cut from tube, and c) tensile specimen cut along CD after flattening. 72

4.3 Representative macrograph of area reduced tube after recrystallization at 900^{o}C. Banding of the microstructure in the central region was observed in these samples; a representative micrograph of one such band is shown. 73

4.4 Representative macrograph of the as shear processed tube with intermediate annealing after heat treatment of 900^{o}C. Banding of the microstructure was observed transmitted from inner to the outer surface were consistently observed along the circumference. 73

4.5 Representative macrograph of the as shear processed tube with no intermediate annealing after heat treatment of 900^{o}C. There were no consistent bands that were observed in this material. There was only one section along the circumference that showed macroscopic banding and is as presented. 75

4.6 {111},{110}, and {100} pole figures of thermomechanically processed samples after recrystallization annealing: a) as area reduced, b) one pass shear expansion with intermediate annealing, and c) one pass shear expansion with no intermediate annealing. 76

4.7 Tensile tests of recrystallized specimens in the longitudinal and circumferential directions: a) as area reduced, b) shear expansion with intermediate annealing, and c) shear expansion with no intermediate annealing. 79

A.1 Optical micrographs of ECAE processed Nb heat treated for 90 min in a vacuum of 2-8 x 10^{-6} torr at temperatures of: a) 700^{o}C, b) 800^{o}C, c) 900^{o}C, and d) 1000^{o}C 106

A.2 Optical micrographs of ECAE processed Nb heat treated for 90 min in a vacuum of 2-8 x 10^{-6} torr at temperatures of: a) 1100^{o}C, b) 1200^{o}C, c) 1300^{o}C, and d) 1400^{o}C 107

B.1 Crossection of a the Nb tube: a) Before ECAE processing, and b) After ECAE propcessing, the light gray overlap is the initial crossection. The crossection of the tube after ECAE processing is elliptical rather than circular. 111

B.2 Optical micrographs of EBW tube before and after ECAE processing and heat tretament. a-c, d-f correspond to the microstrctures of the different regions before and after the processing. 112

B.3 IPF maps in the sheet normal direction of the FZ, and the PM before after ECAE processing. a-b. IPF of the FZ ,and PM is EBW condition, and c-d are the corresponding PF's. e-f. IPF of the FZ ,and PM after ECAE processing and heat treatment at 700^oC, and g-h are the corresponding PF's 113

B.4 Hardness along the tube crossections along the PM, HAZ and FZ in the as-recieved, as worked, and ECAE processed and annealed conditions. 116

B.5 Tensile tests of samples cut along the axis of the tube corresponding to the FZ, and PM before and after thermomecghanical processing by ECAE. Note the converegence in the mechanical property of the FZ and PM after ECAE and heat treatment at 650^{o}C 117

LIST OF TABLES

TABLE Page

1.1 Common Slip planes observed in pure Nb 2

1.2 Ideal texture components of rolled and annealed bcc metals[140] . . . 6

2.1 Chemical Analysis of initial Nb billet as provided by the supplier (Niowave) 16

3.1 Characteristics of starting Nb bar with different starting initial grain sizes for the Cu-Nb composite wire drawing experiment 53

3.2 Summary of Nb microstructure characteristics for different texture options produced by multipass ECAE, and subsequent recrystallization heat treatment 58

4.1 Summary of the microstructure obtained during different thermomechanical processing conditions 74

4.2 Summary of Mechanical Properties 78

B.1 Summary of tensile testing data of EBW, and ECAE processed Nb tube115

1. INTRODUCTION AND LITERATURE REVIEW

Niobium is a body centerd cubic (bcc) metal. It belongs to the group of transition metals, has a high melting point (2469^{o}C) and has a relatively low elastic modulus (105GPa) in comparison with other high melting point metals such as Ta, W, and Mo. It is also a rare breed of element that shows Type II superconducting behavior (Tc=9.46 K [61]. On the negative side it oxidizes readily at temperatures over 200^{o}C, but the oxide has excellent corrosion resistance to most acids [51].

1.1 Principal characteristics of deformation behavior in Nb

The main variables that constitute the deformation behavior of a metal are: a) structure of the metal, b) orientation of the crystal, c) temperature and strain rate dependence, and d) impurity concentration. Nb is a bcc metal and deforms predominantly by slip. Slip occurs on the {110}, {112}, and {123} planes in the $\langle 111 \rangle$ direction [61] in pure Nb. Table 1.1 indicates the characteristics of slip in Nb. Note the temperatures at which the properties have been evaluated are not above 373 K, this is because Nb readily oxidizes, above 473 K, and hence this would nould be a Nb-O solid solution, and is no longer considered pure Nb. Observations of slip in Nb indicate that the main slip systems in Nb are the $\{110\}\langle 111 \rangle$, and $\{112\}\langle 111 \rangle$, there are observations of $\{123\}\langle 111 \rangle$ [26, 14] slip activated at room temperature as seen in Table 1.1 (row 4). The authors point out that these samples were contaminated by tunsten, and interstitials [14]. Twinning is observed at temperatures as high as 150 K in Nb [82, 14, 40, 107].

Table 1.1: Common Slip planes observed in pure Nb

Planes			Temperature (K)	Comments	Reference
{101}	{211}	{321}			
x	x		293		[30, 26]
x	x		298		[14]
x	x		225- 375	High Purity	[25]
x	x		77		[40]
x	x	x	293		[26, 14]
x	x	x	298		[56]
x	x		77		[107]
x	x		158	Lower Purity	[14]
	x		77-375		[25]
x			158	###	[66]
x			50	###	[82]

1.2 Qualitative understanding of Nb deformation

Slip is the major deformation mode in Nb, at temperatures above 77K [25]. Twinning has been observed in the low temperature regime of 4K-77K [96, 130, 107]. For bcc metals the major slip systems are the {112} plane at low temperatures, {110} plane at intermediate temperatures and {123} plane at high temperatures with the corresponding ⟨111⟩ direction in those planes. The ⟨111⟩ direction is the close packed direction and is the only obserevd slip direction in bcc metals irrespective of the slip plane.

The deformation of Nb like other bcc metals, is strain rate and temperature dependent [25, 28]. The reasons for this dependence are: interstitials, limited mobility of screw dislocations, fine precipitates, non-conservative motion of dislocation jogs, and cross-slip [61]. Mitchells [89] work on Nb single crystal show that the deformation behavior is highly dependent on impurity content. The shape of the stress strain curve changes with number of zone refining steps while the orientation of the single

crystal remains the same. As impurity content decreases, the yield behavior shifts until no single yield point observed. The effect of interstitials is to increase the flow stress without significant ductility change in dilute solid solutions [16, 14, 35, 133, 7]. Deformation is also affected by the temperature of deformation, keeping the other variables such as purity and orientation constant. As the temperature decreases below room temperature the variation in the critical resolved shear stress is large, suggesting different slip behavior, and an increased interplay of interstitials and individual dislocations[89] . Also, the deformation behavior of Nb is highly dependent on the slip systems that are activated. This has been shown by Taylor[131, **?**], and more recently by the work of Bieler and Baars et.al[13].

Critical issues that distinguish the behavior of bcc metals and fcc, and hcp metals have been the temperature , and strain rate dependence on deformation. Our main focus is Nb (group VB), however, these issues are general for group VB and VIB bcc elements[16]. Based on experimental data and observations, it is clear that most bcc metals undergo slip that deviates from Schmid law due to differences in activation of different kinds of dislocations. The screw dislocations have lower mobility than edge dislocations, and control the early slip behavior [119, 137]. However, ductile bcc metals like Nb form deformation structures known as dislocation cells very similar to medium and high stacking fault energy (SFE) fcc metals [128].

1.3 Production of high purity Nb

Refining the material from commercial purity levels to high purity levels is done using a powder metallurgical process or melt metallurgical processes. In the powder metallurgical process the powder is pressed and sintered at round 2000^{o}C under high vacuum conditions (10^{-7}- 10^{-8} torr). Sintering evaporates interstitial compounds and low melting impurities thus purifying the Nb. In a melt metallurgical process

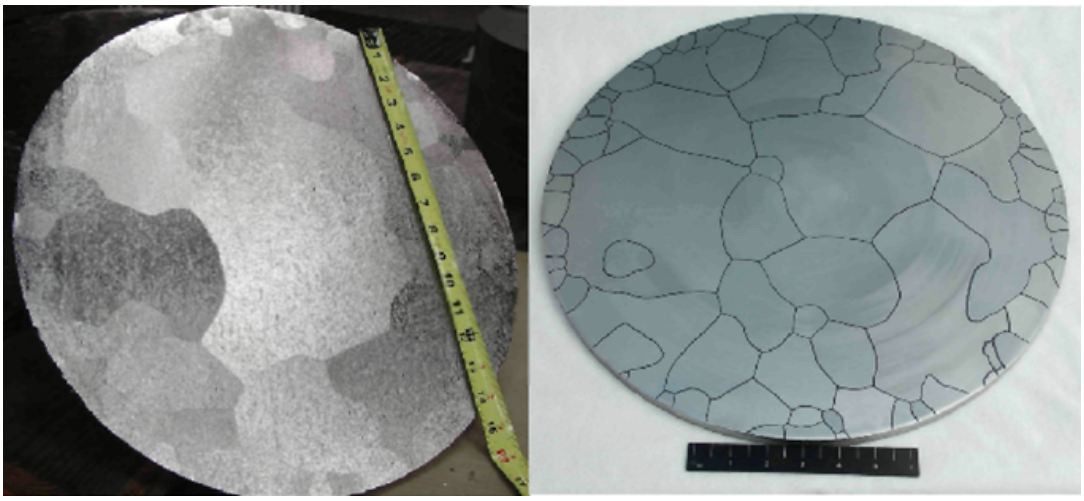

Figure 1.1: Example of large grain RRR Nb ingot from a 430 mm diameter ingot produced with the same EB melt furnace, with the melt rate, power and vacuum levels being constant.

the ingot is fed into an electron beam (EB) furnace and remelted atleast five to six times to remove the interstitial impurities. The Nb produced by this procedure can be of high purity as evidenced by a RRR value greater than 300 [46]. Although the same procedure is followed no two ingot slices have the same microstructure. Industry considers this to be the statistical nature of production [46]. There are also variations in the billet microstructure from different vendors implying that there is no preferential growth in Nb crystals from the melt [71].

1.4 Conventional forming of Nb

The initial EB melted large grain pure Nb microstructures needs to be broken down into finer grain sizes. Fine grain polycrystalline microstructures are preffered for metal forming applications. Some of the common shapes in which high purity Nb is available are Nb sheet/plate, round crossection Nb bar, and Nb tube. Typical reduction processing of EB meleted Nb for stock bar, slab, and sheet material includes extruison, swaging,forging, and rolling reductions.For the manufacture of tubing,

hollow billets are reduced to tube blanks (7:1) reduction, and then drawn over a mandrel[141].

When a b.c.c metal such as Nb is worked, certain orienations of crystals are commonly observed and they constitute the texture of the material. Texture denotes the relation between the crystal orientation and the geometry of the workpiece and processing direction. The most common textures that are observed in deformed, recrystallized bcc metals are as given in Table1.2[140]. {hkl} corresponds to a plane normal of the specimen geometry or process, and ⟨uvw⟩ corresponds to a specimen or process direction. Both these directions are normal to one another. For example, during rolling {hkl} is usually the sheet normal direction for rolled sheet. This is also called the normal direction (ND) and is represented as {hkl}‖ND; and ⟨uvw⟩ is the rolling direction (RD) and is represented as ⟨uvw⟩ ‖RD. The strength of a texture component is represented as multiples of random unit (m.r.d), which is the normalized strength of the texture component to the distribution obtained by a random distribution of orientations. Texture is plotted in the form a pole figure (PF) where a {100} PF refers to the position of all the {100} directions plotted as a projection on a 2D plane with the reference as the specimen/process co-ordinates. For a detailed discussion on texture, representation, calculation and types, an interested reader is reffered to the following articles/books [70][139][106]

1.4.1 Nb sheet production

RRR Nb sheets are a commodity product. They are not mass produced. The major goal of rolling is to accomplish: a) breakdown of microstructure, and b) preferential orientation change or texture development in sheet product. Rolling alone is not sufficient to breakdown the initial microstructure; Rolling reductions as high as 80% (which is equivalent to about a Von-Mises strain of 3) show significant in-

Table 1.2: Ideal texture components of rolled and annealed bcc metals[140]

Component	{hkl}⟨uvw⟩
Cube	{001}⟨100⟩
Rotated Cube	{001}⟨110⟩
####	{111}⟨110⟩
####	{111}⟨11$\bar{2}$⟩
####	{111}⟨110⟩
** *	{112}⟨110⟩
Goss	{110}⟨001⟩

fluence of prior microstructure at low temperature heat treatments of 900C /1hr for Nb [114][113]. The procedure used for conventional rolling by industry is proprietary [72][136], and usually involves a initial microstructure breakdown step involving a forging and heat treatment operation, and multiple rolling reductions and annealing steps to obtain the final rolled sheet. Experiments on rolling polycrystalline Nb have indicated the following:

- Common texture components present in rolled Nb are typically centered around the commonly observed orientations in bcc rolled metals. The main orientations that are observed in rolled and recrystallized Nb microstructures are: {001} ⟨100⟩,{001} ⟨110⟩ (rotated cube); {111}‖ ND (γ fiber components)[69],[136].

- Texture depends on the percent of rolling reduction ; rotated cube, and alpha fiber-{112}⟨110⟨ components dominate the texture upto 70% rolling reduction, and the gamma fiber strengthens after 75% rolling reduction [136][69].

- There is through thickness variability in the texture, and grain size from the center to the surface in rolled Nb sheets. [136],[69].

1.4.1.1 Occurence of common texture components in Nb

The common texture components observed in rolled Nb are similar to those observed in traditional bcc metals [105], and can be predicted by traditional crystal plasticity modeling, which indicate the presence of the main orientation components [29],[23]. The actual strengths of these components have not yet been explained well by any of these models. The emergence and stability of the γ fiber components has been predicted by the modeling of rolling texture with the inclusion of $123\langle 111\rangle$ slip in bcc metals, which are activated after heavy deformation [105]. One of the most important observation in rolling of polycrystalline rolled Nb sheet is the absence of $\{110\}\langle 001\rangle$ (Goss) component which occurs in the rolling of Fe-Si [88],[86],[120],[27] and is of technological importance in possible SRF cavity fabrication due to a low work function [69] is absent. Single crystal studies on Nb rolling [114],[127] have shown that the Goss grain is unstable in rolling, which strengthens the acceptability of modeling efforts which predict the instability of the Goss component under plane strain loading conditions [105]. The stability of the Goss component in Fe-Si alloys have been attributed to formation of intense local shearing in shear bands involving complex processes paths and recrystallization [24].

1.4.1.2 Through thickness variations in sheet microstructures in Nb

Through thickness variations in microstructures are commonly observed in Nb sheets. There could be several reasons for the inhomogeneous textures between the surface and center of the Nb sheet : a) friction effects between the rolls and the surface, and b) deformation zone geometry. Intense shearing occurs at contact between the work piece and rolls, leading to microstructures that correspond to shear type textures at the surface of the sheets; this is typically observed in Nb rolling experiments where there was no lubrication of the rolls. A more common

occurrence could possibly explain the changes in the through thickness deformation behavior is the change in deformation zone geometry; which is defined by a term called the shape factor (SF)[135]. The SF is the ratio between the mean sheet thickness and roll contact length ratio. Observations indicate SF greater than one leads to larger inhomogenities in the through thickness texture in Nb (up to 70% rolling) than in Al [85]. Traditionally, this process can be controlled during rolling by either taking huge reductions per pass in the presence of low friction, or by having rolls of larger diameter. Larger rolls enable lower SF. Since the SF keeps varying with the thickness of the sheet; the ratio increases as the sheet thickness decreases for a constant rolling diameter. Another, view of this problem is to assume rolling gap as a convergent channel, which leads to location based strain variation in the metal leading to differences in strain history at different locations[74]. Either view points are able to explain the presence of texture components in the material, however the exact distribution or location specific descriptions have often been impossible to predict in any of the approaches leading to conjecture that initial orientations may have an influence on the final microstructures.

1.4.1.3 Possible influences of initial microstructures

In a production setting, lubrication of rolls, and the deformation zone geometry can be traditionally controlled, however studies on batches of Nb sheets indicate that there are differences in the through thickness textures in commercially available Nb sheets [68]. One of the leading authority in the physical metallurgy of Nb, Dr. Bieler often says No Nb sheet that I have seen are the same. From large grain rolling studies of Nb, it is clear that the rolling microstructure depend significantly on the initial orientation (texture) of the sample. It is clear that $110\langle 100\rangle$ orientation is broken down effectively during rolling, and recrystallization of this grain after

rolling reduction greater than 70%, and a 900^{o}C heat treatment produces finer grain sizes [114],[113],[127]. However, an initial $\{100\}\langle 100\rangle$ oriented crystal on rolling is very stable to the deformation and recrystallization does not significantly alter the orientation after low temperature heat treatments [127]. One could hypothesize that the Nb microstrcurture in rolled sheet could thus depend on the strain history of Nb billet prior to rolling. It has been known that strain path changes can lead to better grain refinement in metals [73], [94],[142] [97]. A common technique that industry employs to produce Nb sheet is by cross rolling Nb [67]. Even with this approach the problem persists.

1.4.2 Miscellaneous bulk Nb processing

High purity Nb is also manufactured in smaller quantities in the form of swaged and forged bars for Nb-Sn wire applications and Nb seamless tubes for potential SRF cavity applications. There is paucity in literature regarding microstructures in bulk Nb other than rolled Nb. Nb is chemically very similar to Ta which is also a VA metal. The characteristics of mechanical behavior of Nb and Ta appear are very similar, with both showing similar characteristic responses in hardening/softening behavior in the presence of interstitial solutes[133], plastic anisotropy characteristics [119], hardening behavior[93],[90]. It is hence assumed that experimental observations made in bulk Ta processing could also be applicable to Nb processing. Textures once generated in intermediate processing operations could not be eliminated, example:Side forged Ta plates creates a $001\langle 100\rangle$ texture which persists after rolling, the presence of this texture could not be eliminated even by plain rolling and recrystallization steps [18]. Heavily deformed and recrsyatllized vacuum arc melted Ta (shear strain greater than 4) in the forged, swaged, extruded, and rolled forms show non-uniform microstructures with several regions unrecrystallized irrespective

of the deformation process [18][17][112][65][87]. This indicates that the strain is not well distributed by conventional processing for effective breakdown of the initial microstructure, although the overall strain is very large and conventionally acceptable for breakdown of microstructures by conventional methods[61].

With the need to develop SRF Nb cavities for ILC, and other accelerator projects, further development work in the area of fabrication of seamless Nb tubing for hydroforming applications need to occur. Seamless Nb tubing is typically formed by the following methodos: a) back extrusion, b) back extrusion and flow forming [21], c) deep drawing of Nb sheet and spinning [123][98, 100], [99],and d) explosive bonding of Nb on Cu tubes [121]. There have not been many microstructure studies in these areas. Observations have indicated that back extrusion of Nb tubing has not given consistent results. The main problem seems to be that there are regions in the back extruded tube that have grain sizes of the order of 500 μm, and texture gradients which limit the ductility of the material during hydroforming applications [123], [44]. The best results for hydroforming of cavities come from work on fine grain Nb sheet of nominal grain sizes of less than 50 μm followed by deep drawing and spinning [124],[122]. There are manufacturing schedules that have used intermediate heat treatment steps and strain steps to achieve the goal of cavity fabrication by hydroforming [129]. In summary there appears to be no commercial approach today to achieve suitable microstructures in seamless RRR Nb for hydroforming applications.

1.4.3 Challenges to be overcome and gaps in knowledge

The previous sections indicate the need to develop processing strategies for pure Nb. This is because

- The initial EBM process creates large grain Nb material with grains of the

order of 100's of mm in length and width. The challenge in refractory metals for both Nb , and Ta is to consistently breakdown the cast structure to form uniform fine grain in bulk material.

- There is a gap in our understanding of how fine grain microstrucrues form in bulk Nb material. There have been very few studies involving processing of pure bulk Nb.

- Seamless Nb tubing for hydroforming is a viable alternative for cavity fabrication, however consistentcy in hydroforming has been a challenge, with deep drawing/spinning startegy providing the best results to date. There is a lack of development work in thw fabrication of seamless Nb tubing by extrusion processes. Correlations between mechanical properties and microstructure for seamless Nb tubes are absent from the current literature

1.5 Severe plastic deformation by Equal Channel Angular Extrusion(ECAE)/ECAP

From the above sections it can be seen that incomplete breakdown of initial microstructures and inhomogenities in the starting material leads to undesirable deformation characteristics. For the purpose of grain refinement of as cast structures severe plastic deformation process such as high pressure torsion (HPT)[145], cyclic extrusion and compression (CEC)[108], and ECAE could be applied to improve microstructural breakdown. ECAE has been found to successfully produce ultra fine grain (UFG) microstructures in the range of 150-300 nm in a variety of metals and alloys [134].

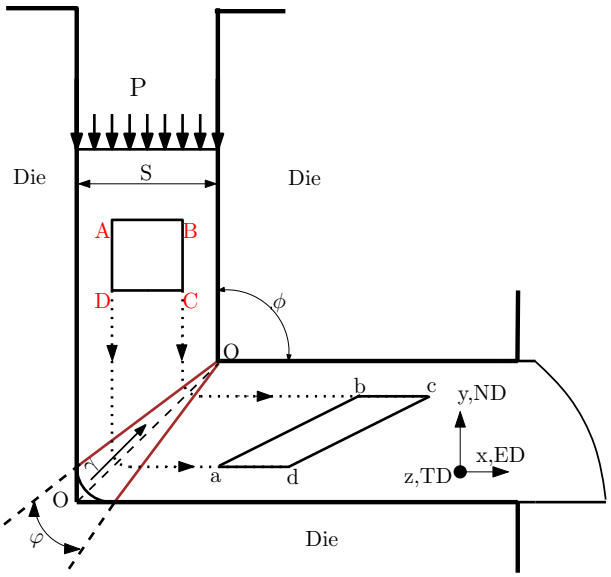

Figure 1.2: Schematic of a 90^o ECAE die showing the deformation of a square element, as it passes through the die. The die axes are labeled in the figure where x=Extrusion Direction (ED); y= Normal Direction (ND); and z=Transverse Direction (TD).

1.5.1 Description of ECAE

ECAE is based on the principle that simple shear deformation is an effective method to breakdwown the microstructure of bulk material. [95], [118]. ECAE involves deformation of a billet at the intersection of a two channels of equal crossection; leading to shear deformation at the intersection . The commonly used intersecting die angles (ϕ) are: 90^o, 120^o,, and 135^o. The schematic in Figure1.2 shows an initial square element ABCD sheared along the line OO, to form a parallelogram abcd.

The key features of this deformation method are:

- For an intersecting die with a sharp corner the shear strain (ϵ) is expressed in terms of ϕ as: $\epsilon = (2N/(3)^{1/2})$*cot($\phi$), where N is the number of passes [116]. The shear strain per pass in a $\phi = 90^o$ die, is 1.15.

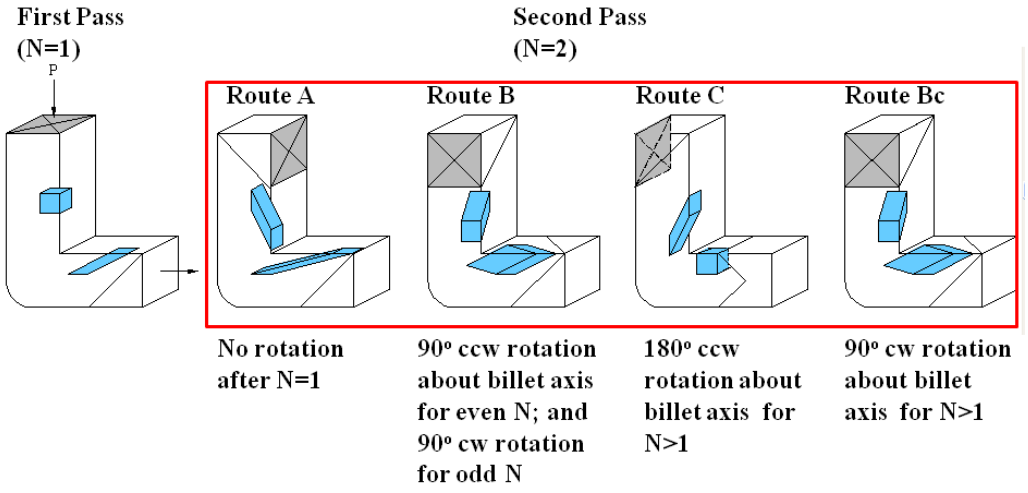

Figure 1.3: Schematic of billet orientation between the first and second pass.The billet rotations about the axis provides changes in strain path between passes.

- For a material with sufficient ductility strain space is unlimited. Note that the workpiece crossection remains unchanged, as a result of extrusion.

- Rotations between passes along the billet axes are possible leading to changes in strain path and hence different microstructure/ texture outcomes. Figure 1.3 depicts a schematic of the commonly used routes to process material.

1.6 Microstructure development during ECAE of bcc metals

ECAE has been used to produce UFG microstructures in cubic and hcp metals and alloys. There is vast literature on the production of UFG for fcc, we are citing some work done here at TAMU on : Al [20, 31, 109], Cu[55], hcp: Mg[1, 10, 34], Ti[104, 144, 143], and more recently for bcc metals [15, 3, 2, 5, 83, 84, 101, 111] . Our main interest is in the application of ECAE towards development of microstrcuture in Nb which is a refractory bcc metal.

1.6.1 Experimental microstructure observations involving grain refinement of bcc metals as a consequence of ECAE

- UFG grain size: Grain refinement during ECAE reaches a steady state value after a critical amount of strain is reached [57][138][84]. This critical amount of strain for Nb and Ta is approximately 10 [101]. The critical UFG grain size seems to be dependent on the metal, and for Nb and Ta it is approximately 200-300nm [83, 84].

- Misorientation angle: Observations suggest that high angle misorientation increases with deformation, it has been observed that there is a steady increase in misorientation angle with increasing strain (as high as 20) although the UFG size saturates [101].

- Dependence of grain refinement on route: TEM characterization based on ECAE processing of IF steel suggest rapid grain refinement was found in Route C after 2 passes, and Bc after 4 passes [81] for a 90^o die. However, an EBSD study on IF steel suggests the grain refinement occurs most efficiently in the following order after 4 passes, Bc⟩B⟩A⟩C[41]. Whereas, a similar EBSD study on IF steel suggests the contrary indicating that 4A produces better refinement than 4Bc [12].

This prior work indicates certain consistent results from ECAE processing: grain refinement, and the formation of a stable UFG microstructure. Recrystallized ECAE processed microstructures in bcc metals (Ta, Fe) show finer grain size distributions than rolled/forged process [83, 84][60]. However, aspects of microstructure refinement which are strain path dependent, and influence grain refinement, like formation of HAGB's are not well understood in bcc metals processing by ECAE.

2. DEFORMATION OF A NIOBIUM BI-CRYSTAL

2.1 Introduction

It is evident from the previous chapter that ECAE has been applied to produce UFG microstructures by different processing routes. To this date the ECAE induced microstructure refinement processes are not yet well understood in a polycrystalline material. One of the reasons for this could be the limited number of studies done with controlled test cases such as work on: single and bi-crystals. Currently, studies on single crystals are mainly done on fcc metals: Al[37, 36, 52], Cu [38, 39, 53, 91, 92], Ni [45, 48]. Little work has been done on ECAE processing of single crystal bcc metals except for the works of Sandim [110], and Zhu [146, 148, 147].

To clarify microstructure breakdown, and orientation evolution and in a simple polycrystal, a bi-crystal is chosen because: a) there is a possibility of well controlled initial orientation, and b) the grain to grain interaction is limited to one grain. The ECAE route used in this experiment is 2C, which has been claimed to lead to texture reversal based on crystal plasticity simulations [49, 50, 64]. In the present study, the Nb bicrystal is processed at room temperature upto two passes, and the microstructure evolution is investigated by electron back scatter diffraction.

2.2 Materials and Methods

2.2.1 Initial raw material

The Nb used for this study was a electron beam (EB) melted large grain Nb ingot, of starting dimensions of 250 mm x 50 mm x 50 mm.The Nb billet had a residual resitivity ratio (RRR) of 176±10. The chemical analysis of this Nb test material is as shown in Table2.1. The major subsititutional impurity present is tantalum (Ta).

The interstitial content was fairly low with carbon (C) and nitrogen (N) content less than 50 ppm, and the oxygen (O) content was less than 100 ppm.

Table 2.1: Chemical Analysis of initial Nb billet as provided by the supplier (Niowave)

Element	ppm	Element	ppm
Ta	551	Al	< 10
Fe	< 10	H	< 10
C	< 30	Ti	< 13
O	97	Ni	< 20
N	34	Cr	< 10
Zr	7	B	< 1
Mo	< 50	Co	< 1
W	< 18	Hf	< 25
Si	< 20	Be	< 1

2.2.2 Billet cutting and extrusion details

The 250 mm x 50 mm x 50mm large grain Nb bar was lightly etched in a 1:2:2 HF: HNO_3: H_2O, mixture to reveal the macroscopic grain structure. A billet was extracted from the large bar by electro discharge machining (EDM) so that this bar was composed of a bi-crystal with a grain boundary (GB) running along the center line of the billet. An initial square grid of dimensions 2.5 mm x 2.5mm was scribed on the billet side (flow plane) using a 1mm end-mill.

The billet of nominal dimensions 25 mm x 25 mm x 200 mm was processed by two passes of ECAE, at room temperature (303 K). The die used for this study had the following characteristics: a) die angle of 90 ^{o}, b) sharp corner, c) sliding walls to reduce friction between workpiece and die, and d) 25mm x 25mm square crossection, inlet and outlet channels. The extrusion speed was 1mm/sec for both extrusions.

The schematic in Figure2.1(a) indicates the orientation of the bi-crystal as it entered the die. The dashed line represents the grain boundary. For the entire study the global co-ordinate system fixed to the die is used as shown by directions: ED, ND, and TD in Figure2.1.

After the first extrusion pass, a sample of nominal dimensions 25mm x 25mm x 50mm was extracted for microstructure characterization. The billet of nominal dimensions 25 mm x 25 mm x 150 mm was then rotated by 180 ^{o} about the billet axis, which corresponds to ED in the global (die) co-ordinate system was re-inserted into the die as shown in Figure2.1(b). This route is commonly referred to as 2C in literature. After two passes were completed, a sample of material of nominal dimensions 25 mm x 25mm x 10 mm was extracted for further microstructure characterization. Care was taken to keep track of the billet orientation.

2.2.3 Microstructure characterization

Representative samples were taken from the ED-ND plane, from different locations of the billet to characterize the deformation near the grain boundary (GB), and away from the GB for both of the sample crystals. Micro-texture was characterized using orientation imaging microscopy (OIM). The sample preparation technique for OIM analysis included traditional grinding and polishing. The final step of the polishing included vibratory polishing for several hours (greater than 10 hours for some samples) to obtain flat and damage free samples, this procedure has been found very effective to characterize brittle Nb intermetallics. The sample that was then lightly etched using a 1:3:10, HF: HNO_3:H_2O solution for 10-15 seconds to remove any surface deformation. OIM was performed in a Zeiss 1540EsB, scanning electron microscope (SEM), with high resolution OIM imaging (high speed Hikari Camera). The step sizes for rough scans to determine large scale features were done using

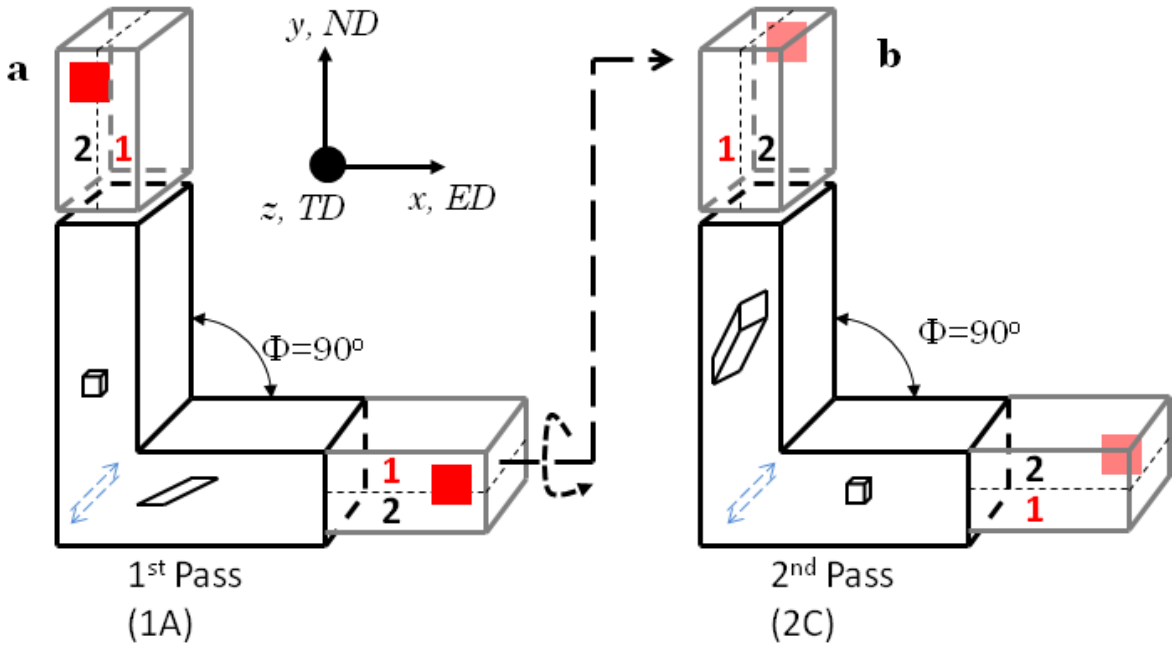

Figure 2.1: Schematic of the bi-crystal sample as it entered the ECAE die during: a) First pass (1A), and b) Second pass (2C). The billet was rotated by 180 ^{o} counter-clockwise about the billet axis before reinserting back into the die as shown in (b). The global co-ordinate system which is attached to the die is as shown in the figure, where: x=Extrusion Direction(ED), y=Normal Direction (ND), and z= Transverse Direction (TD)

a spot diameter of 2-3μm. Higher resolution scans were done with a spot size of 300nm.The results were interpreted using the TSL- OIM software to plot the pole figure (PF), with corrections to the orientation representations being carried out by an in-house MATLAB code. Microstructure characterization are done by analysis of the inverse pole figure (IPF) maps, image quality (IQ) maps, and PF's. All the IPF maps shown in this study are in the ED-ND plane, the poles represented in the IPF maps are color coded in the transverse direction (TD). In this study, the microstructure were analyzed based on OIM of regions that were representative and located in two distinct locations: a) away from the GB, and b) in the vicinity of the GB.

2.3 Experimental results

2.3.1 Macroscopic deformation characteristics

2.3.1.1 Grid deformation

The deformation of the billet after the first pass of the bi-crystal appears to macroscopically uniform as shown in Figure 2.2(a). The orientation of the grid is uniformly sheared at an angle of 27^o across the GB of the bi-crystal. After a rotation of 180^o about the centerline of the billet for the second pass of ECAE, it is observed that the grid to a large extent returns to its original shape as shown in Figure 2.2(b). Note the non-uniform deformation zones extending about 25mm on either end of the bar.

2.3.1.2 Optical microscopy

Polishing and light etching of the billet revealed the macro-structure of the deformed bi-crystal. Optical micrographs (OM) in the ND-ED plane after the first pass are as shown in Figure 2.3 (a-d). The characteristics of deformation seem to be

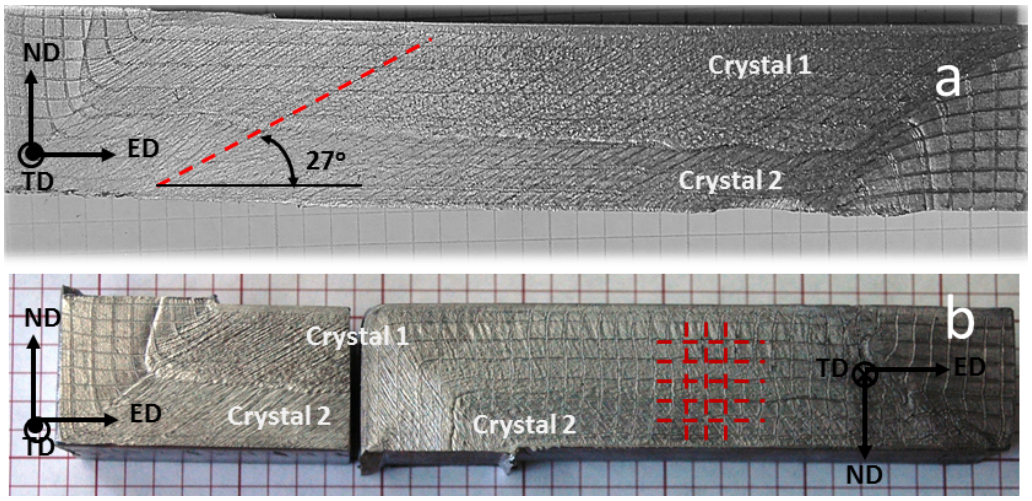

Figure 2.2: Deformation of the grid after ECAE deformation is shown: a) First pass (1A), b) Second pass (2C). The orientation of the grid is at 27^o to ED after 1A, and shape of the grid returns to roughly the original configuration of a square crossection of dimensions 2.5mm x 2.5mm.

very different in Crystal 1 and Crystal 2. Crystal 1 has bands which are oriented at 27^o to ED as shown in Figure 2.3(a-c). The width of these bands are 100 $\pm$30μm. The spacing between the bands is not consisten. These bands are seen throughout Crystal 1, and extend toward the boundary. There are some finer structures that occur in Crystal 1 in between these bands, which could be resolved well with OM. In Crystal 2 there is a characteristic 45^o trace to ED as shown in Figure 2.3(c-d).

After second pass, the macro-structure is more complex as indicated by Figure 2.4(a-d). Crystal 1 contains two sets of bands as shown in Figure2.4(a-b). The abnds that run across Crystal 1 are oriented along 63^o to the ED direction. There are a second set of bands that are oriented at an angle of 138^o to ED. The bands from Crystal 1 appear to curve towards the GB in Crystal 1. There are MBs that also occur in Crystal 2 after the second pass of deformation as shown in Figure 2.4 (c-d).

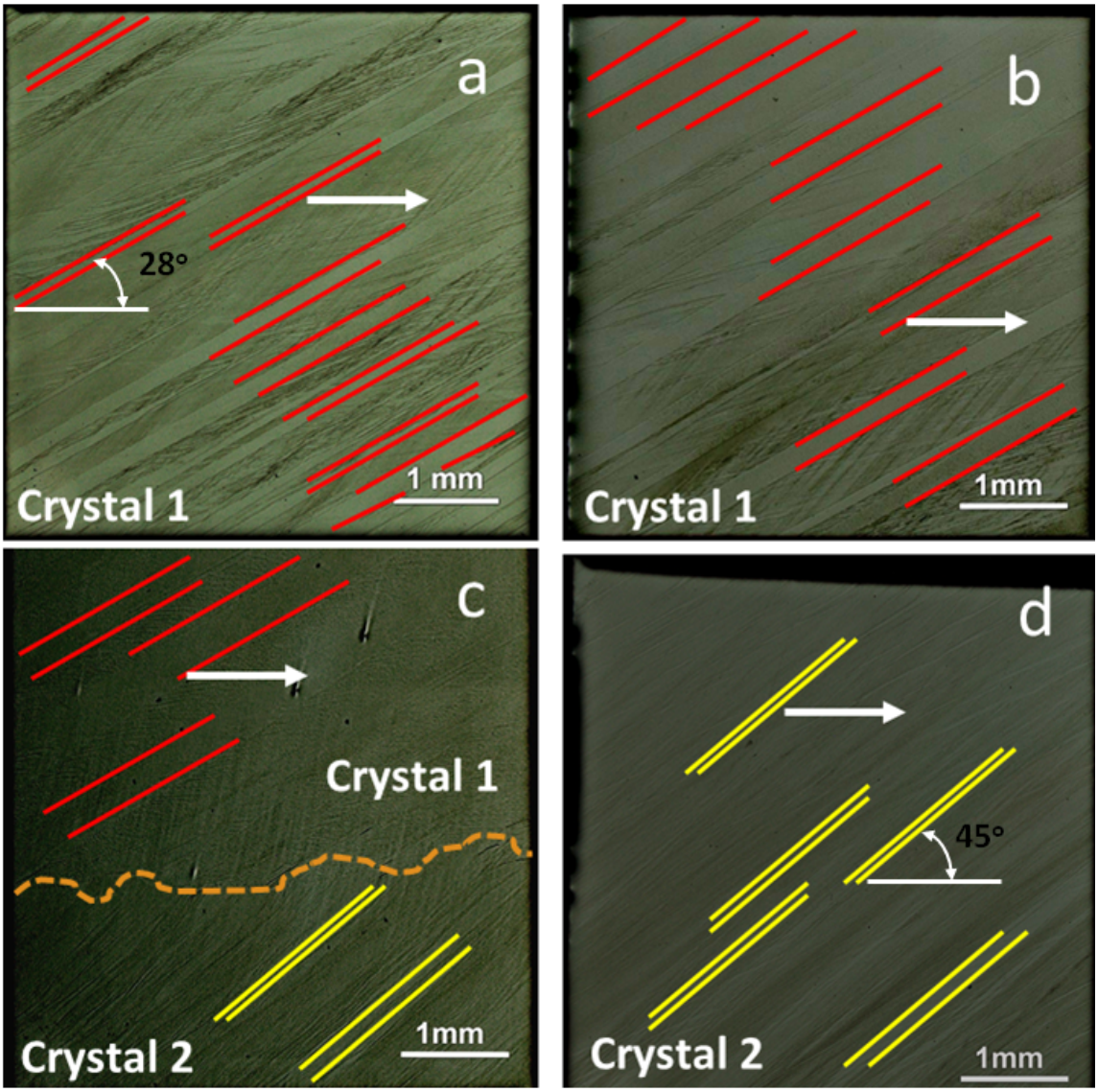

Figure 2.3: Representative optical micrographs of a large section from the ND-ED plane: (a-b) depict the deformation characteristics in Crystal 1, with the grain boundary at the center of (c), and (d) depicts the deformation characteristics in Crystal 2.

The MBs in Crystal 2 are oriented around 45^o to ED, and similar to Crystal 1, there are several secondary bands that occur oriented around 157^o to ED. Similar to the observation from Crystal 1, the band structure appears to curve towards the GB in Crystal 2.

2.3.2 Initial orientation of bi-crystal

OIM of the initial bi-crystal indicate that the orientation with respect to the Euler angles were, (313.2^o,71.3^o,25.7^o) for Crystal 1, and (338.2^o,40.3^o, 69.0^o) for Crystal 2. The Miller indices of crystal axis correspondence to the ECAE die axis is as follows: Crystal I- $[\overline{5}\ 6\ \overline{5}]\|$ ED, and $[7\ \overline{1}\ \overline{7}]\|$ ND, Crystal II- $[\overline{5}\ \overline{6}\ 6]\|$ ED, and $[5\ \overline{2}\ 6]\|$ ND. Based on the OIM measurements the spread in the initial orientations were calculated to be within 2^o for both the crystals. An average of ten measurements across the GB as shown in Figure 2.5 (a), indicates that the GB is a high angle GB with an initial misorinetation of 48.1^o. The initial spread in orientation of the crystals was less than 0.5^o.

2.3.3 Microstructure characteristics after first pass ECAE

2.3.3.1 Crystal 1

After the first ECAE pass Crystal 1 forms bands in the microstructure. Figure2.6(a-d) show the representative microstructure away from the GB. The matrix and band region are clearly misoriented from the each other, as observed by the orientation differences. The bands were aligned close to 28^o to the ED direction. There was a slight difference in the orientation of the bands (i.e, the color between the bands changes representing slight differences in the orientation) as seen in Figure 2.6 (a), (c). However, these orientation changes were small, and the bands in Figure 2.6 (a), (c) are not considered to be different bands. The contrast difference in the IQ maps in Figure 2.6 (b),(d) are able to provide a clearer picture of possible dislocation

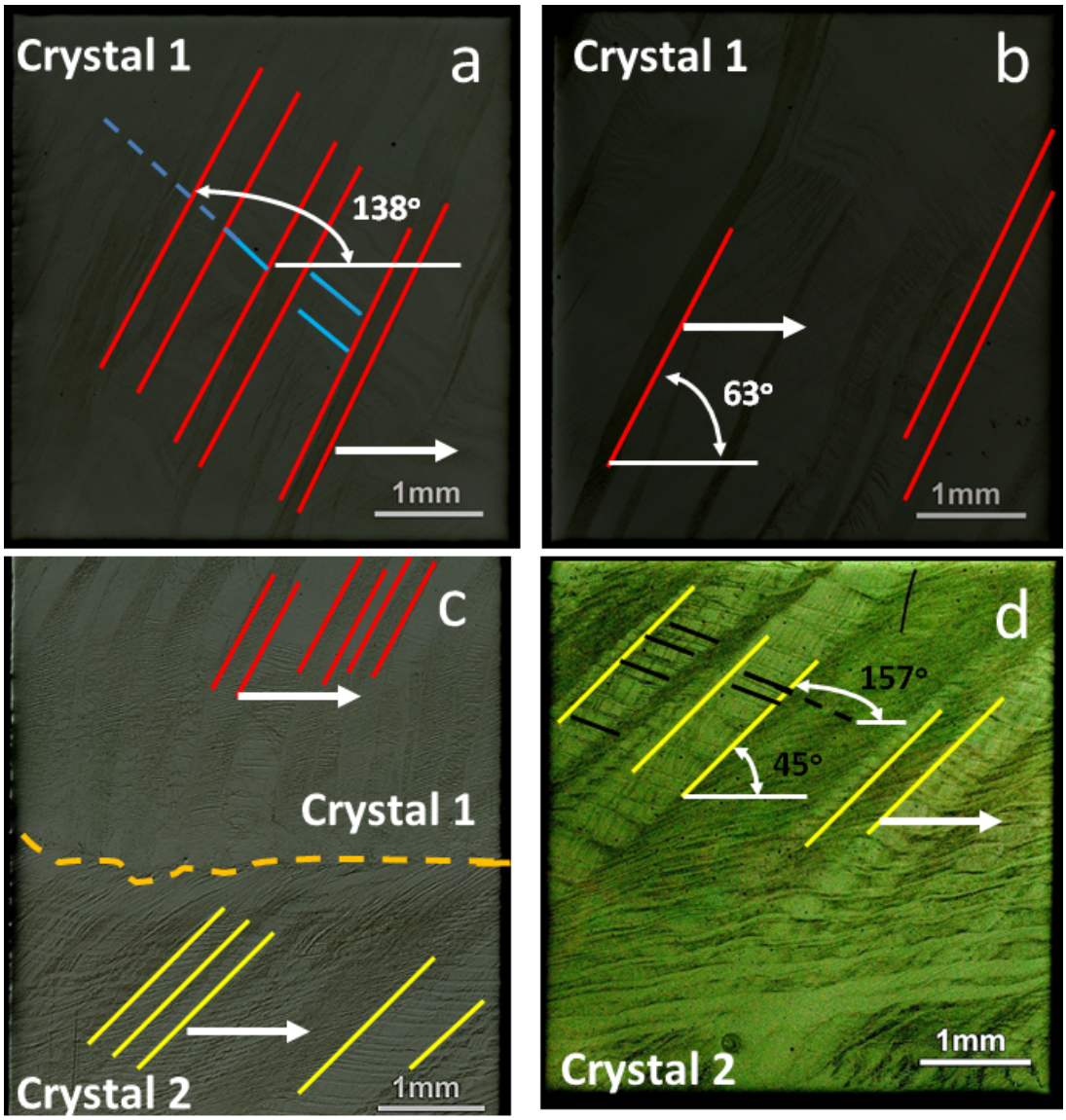

Figure 2.4: Representative optical micrographs of a large section from in the ND-ED plane: (a-b) depict the deformation characteristics in Crystal 1, with the grain boundary at the center of (c), and (d) depicts the deformation characteristics in Crystal 2.

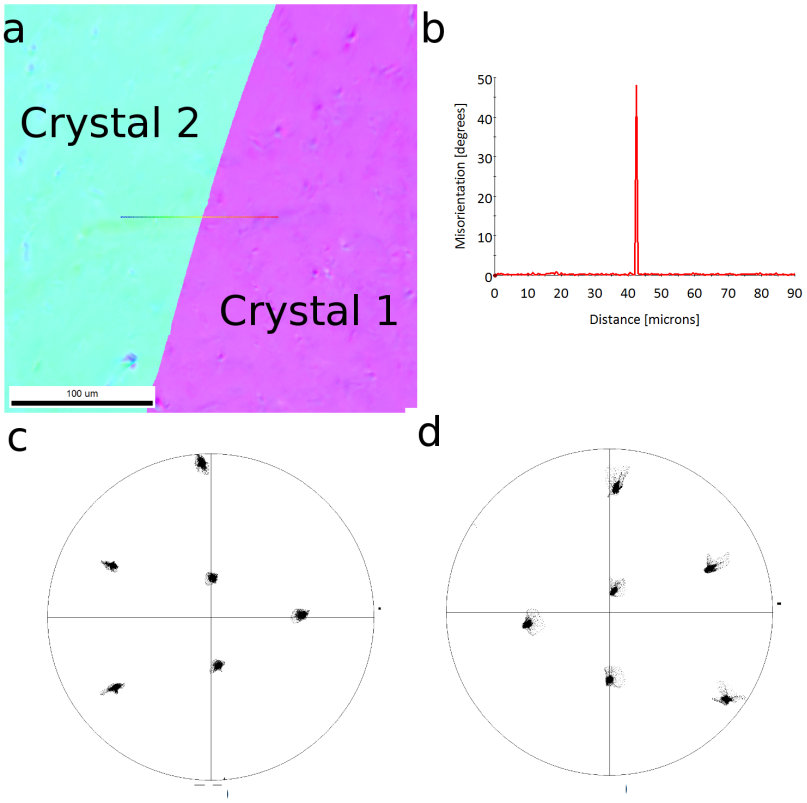

Figure 2.5: Characteristics of the OIM of the initial bi-crystal. a) OIM of the initial crystal indicating the representative line segment for misorientation calculation, b) Misorientation profile of the two crystals indicating low misorientation in the grain interior and a spike at the GB, c) and d) are the {110} PF's for Crystal 1 and Crystal 2 respectively.

storage, with the lighter regions having a lower overall dislocation density, and hence a better signal than darker regions. The finer structures in the band and the matrix indicate dislocation motion in both the matrix and the band regions. Smaller area scans of the matrix and the band regions as shown in Figure 2.7 (a)-(d). The lamellar dislocation substructure is evident in the matrix and the band region, and is aligned at approximately 53^o to the ED axis, and about at 45^o in the case of the bands. The local fluctuations in misorienation are observed along a perpendicular line to the structure as shown in Figure 2.7 b, and d. There is a characteristic length scale for the matrix structure which is about 1-2 μm, as observed by consistent rise and fall of the misorientation angle. However, in the band the misorientation differences between neighboring points are lower. Since the angular accuracy of the EBSD is $\sim 2^o$ there could be misorienations that are not resolvable in the dislocation structures. However, it appears from the IQ map, and misorientation line profile that the dislocation substructures in the band are not yet fully developed after the first ECAE pass.

2.3.3.2 Crystal 2

After first ECAE pass Crystal 2 forms dislocation structures that are oriented at 45^o to ED. The main differences between the microstructure in Crystal 1, and Crystal 2 are the absence of misorientation bands in the Crystal 2 microstructure. There are however orientation changes that were observed as depicted by the pink/yellow transitions in the IPF in Figure 2.8 (a). The IQ map in Figure 2.8 (b) indicates that these regions may have slightly higher dislocation content and hence there maybe orientation differences between with the lattice. Smaller area scans on Crystal 2 are as shown in Figure 2.9, the crystal indicate substructure development as represented by periodic high misorientation changes in the direction perpendicular to the

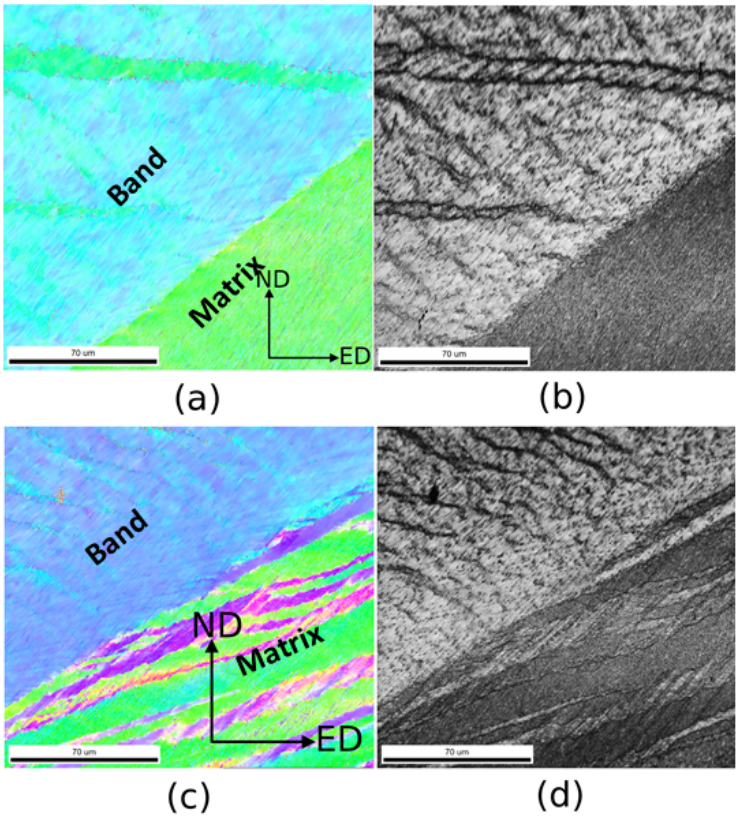

Figure 2.6: Representative microstructure of Crystal 1 away from the GB : a) and c) correspond to IPF in the TD direction, and b) and d) are corresponding IQ images

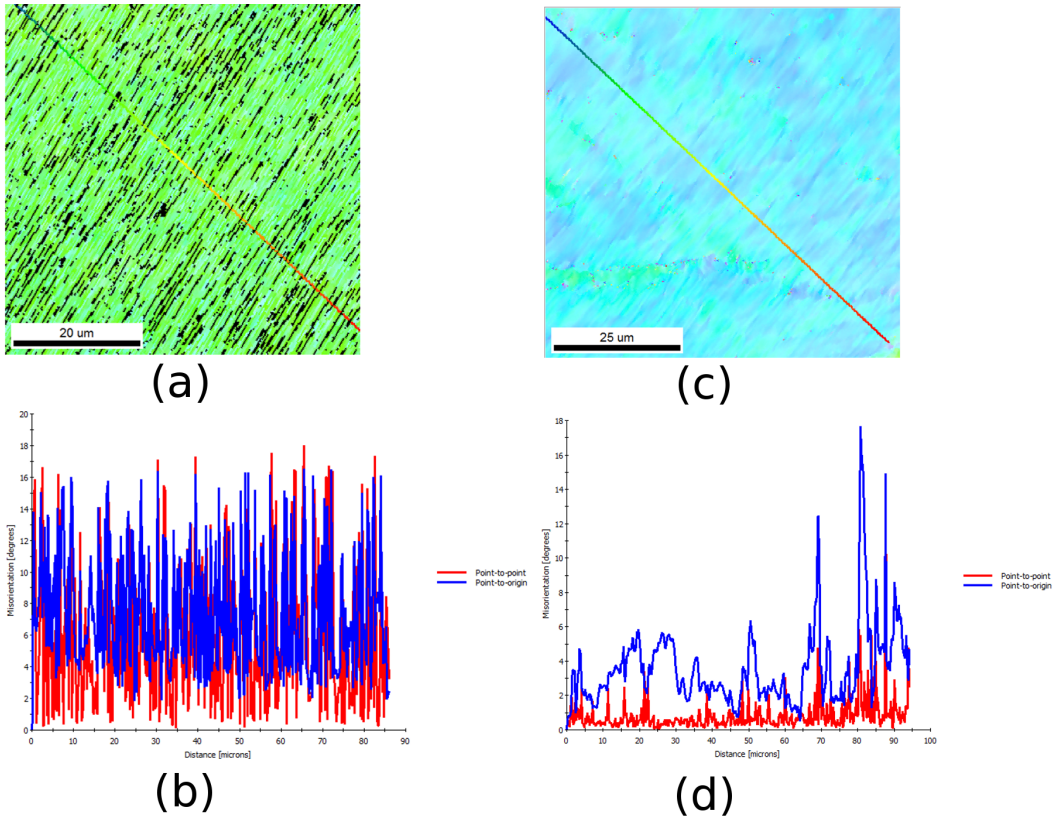

Figure 2.7: Misorientation profile representing dislocation local substructure formation in the matrix and band. a), and c) are IPFs of the matrix and band, b) and d) are the corresponding misorientation profiles taken along perpendicular lines to the observed structure

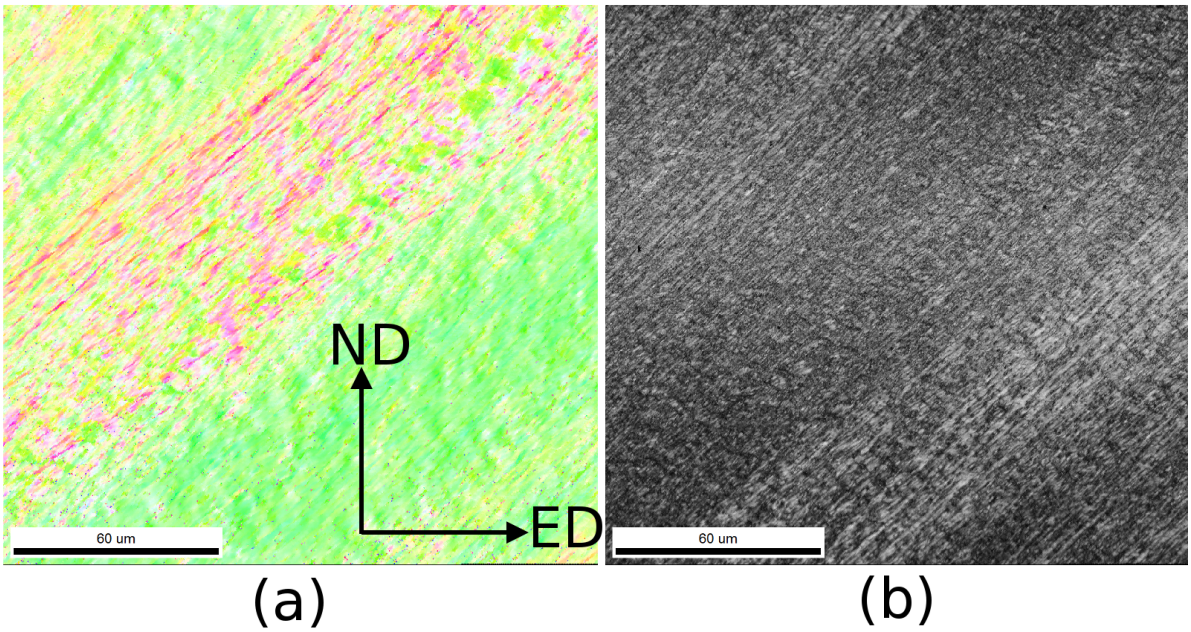

Figure 2.8: Representative microstructure of Crystal 2 away from the GB : a) IPF in the TD direction, and b) the corresponding IQ map

dislocation activity as shown in Figure 2.9 (b,d).

2.3.3.3 GB region

The GB region after the first pass indicates that the microstructure in the two crystals is different from the region away from the grain boundary. Figure 2.10 (a), presents the IPF of the region around the GB. There are two kinds of bands present in the region around the grain boundary in Crystal 1 (represented as 1 in Figure 2.10 (a)), oriented at about 35^o, 135^o to ED. Crystal 2 represented by 2 in Figure 2.10 (a) has dislocation structures that are oriented at 45^o, and 135^o to ED, whereas away from the GB the 135^o structures are absent. The misorientation angle of the GB has also increased after the first pass of deformation. The misorientation of the grain boundary is 54 ± 3^o, which is much higher than the initial misorieintation angle (48.2 ± 1). The IQ map does not show significant contrast around the GB region.

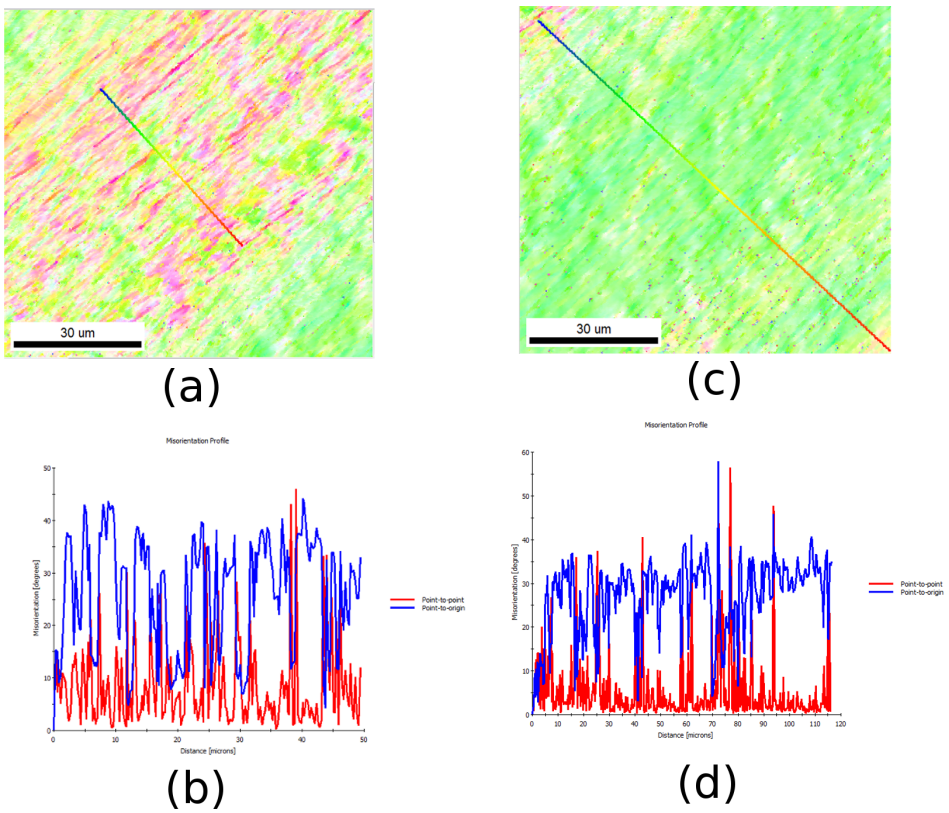

Figure 2.9: Misorientation profiles representing local dislocation substructure formation in the matrix and band. a), and c) are IPFs of the matrix and band, and b) and d) are the corresponding misorientation profiles taken along perpendicular lines to the observed structure

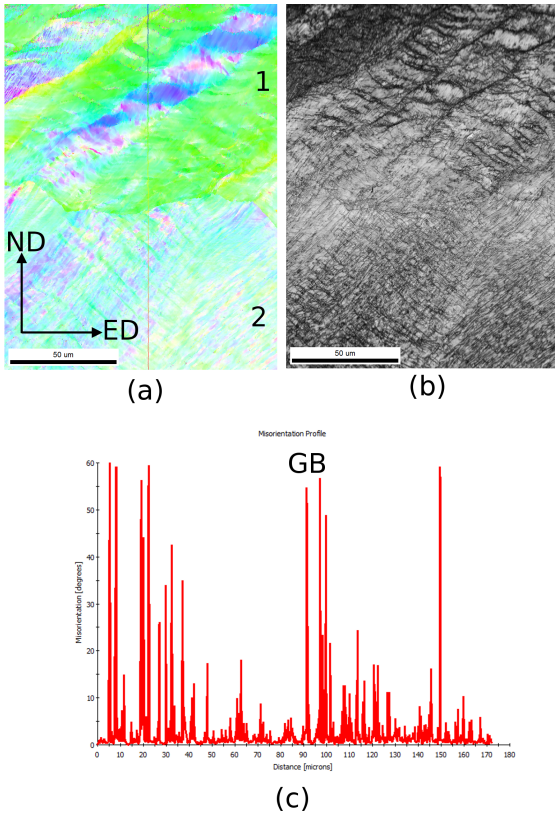

Figure 2.10: EBSD map of the GB region after 1 pass ECAE showing the differences in structure near the grain boundary in Crystal 1, and Crystal 2: a) IPF in the TD direction, and b) the corresponding IQ map, and c) the misorientation profile. The misorientation value at the GB is 52^o around the GB.

2.3.4 Microstructure characteristics after second pass ECAE

One of the observations after second pass processing indicated a complex deformation pattern. Finer scans as done in Figure 2.7, and Figure 2.9 were not done, and this is a work in progress.

2.3.4.1 Crystal 1

Crystal 1 after two ECAE passes still consists of a matrix and band structure as shown in Figure 2.11 (a). The bands extend through the matrix. The thickness of the bands vary between 90-10 μm .The banded structure is much more complex than in the case of the bands produced after the first pass. There is in increased dislocation activity/storage which leads to very poor contrast in the IQ map. The matrix is presented in Figure 2.11 (c). There are diffuse curved microbands that extend towards in the matrix region. Resolving these microbands need finer scans of spot sizes around 150-200 nm.

2.3.4.2 Crystal 2

EBSD scans of Crystal 2 after two passes of ECAE, showed that the microstructure consisted of curved bands throughout the microstructure. A representative EBSD scan is as shown in Figure 2.12,these bands are not easily distinguishable from one another as the orientation in TD are very similar. However, these will be discussed further in the section on orientation evolution (in the Discussion section. Dislocation structures are still visible in the IPF, however we need finer scans to resolve these structures. A significant aspect to notice in the microstructural characteristics of the bi-crystals after the second pass is that both Crystal 1 and 2 orient themselves along a particular pole along TD as indicated by the similar green coloring in Figures 2.11, and 2.12.

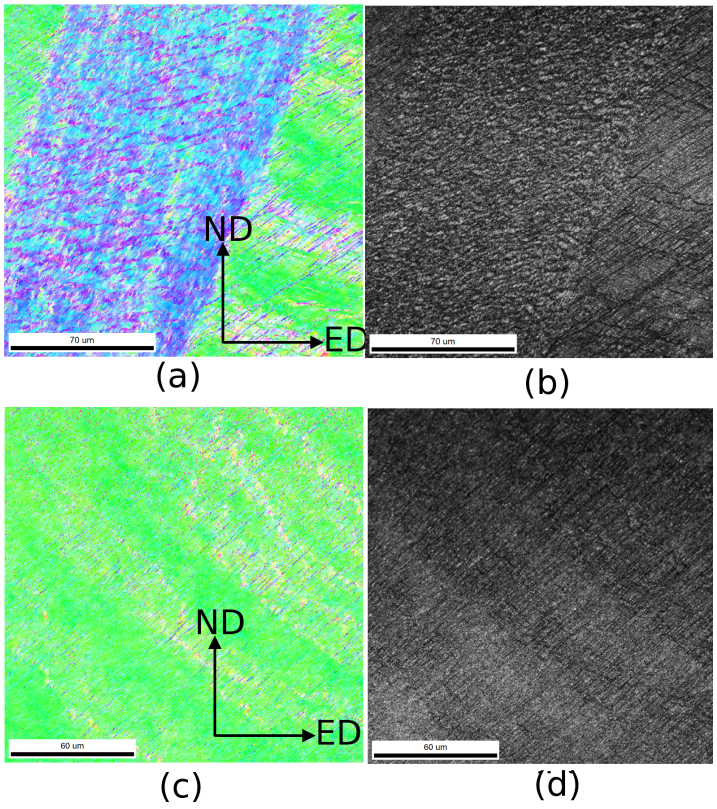

Figure 2.11: EBSD map showing representative microstructure in Crystal 1 after 2 pass ECAE: (a), (c) are IPF maps along TD, (c) and (d) are the corresponding IQ maps of the regions.

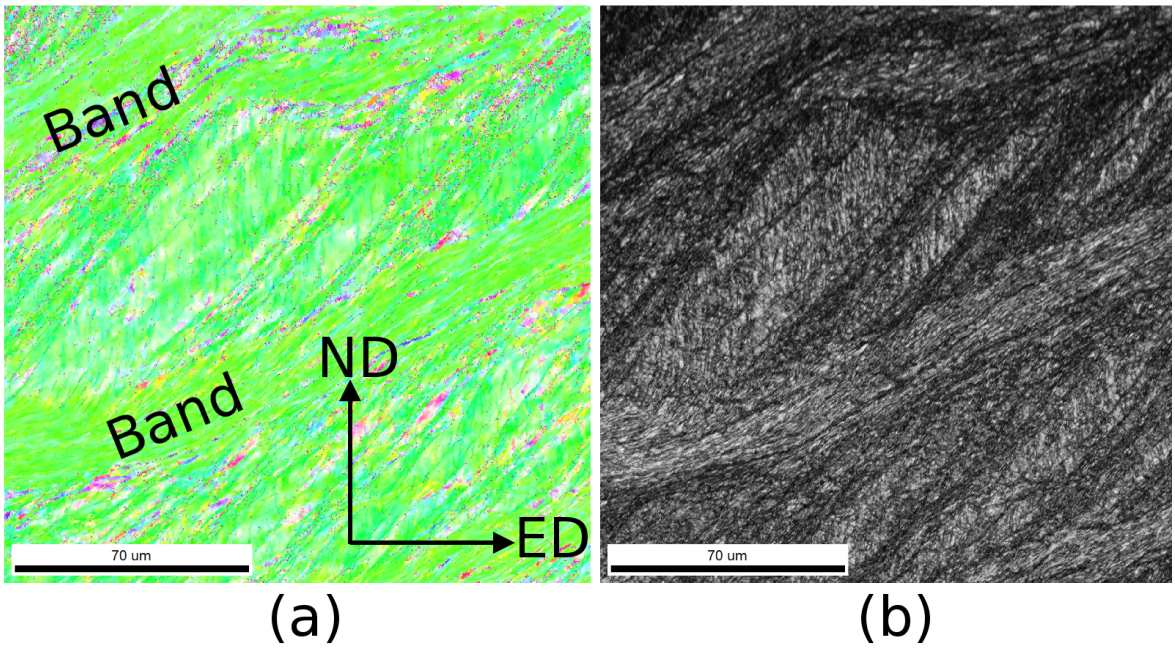

Figure 2.12: EBSD map showing representative microstructure in Crystal 2 after two ECAE passes, a IPF map along TD, b) is the corresponding IQ map of the regions.

2.3.4.3 GB region

EBSD scans of the GB region are as shown in Figure 2.13, reveal the microstructure around the GB region is oriented such taht the poles are very similar in orientation along the TD direction. An important observation is that the misorientation angle decreases between the two grains after 2 passes. The average misorientation angle decreases from 54 ± 3^o, to 44 ± 2^o, which is closer to the initial misorientation angle between the two grains 48.2 ± 1^o. The dislocation substructures that are present in the GB region are complex and need finer scans to resolve the structure.

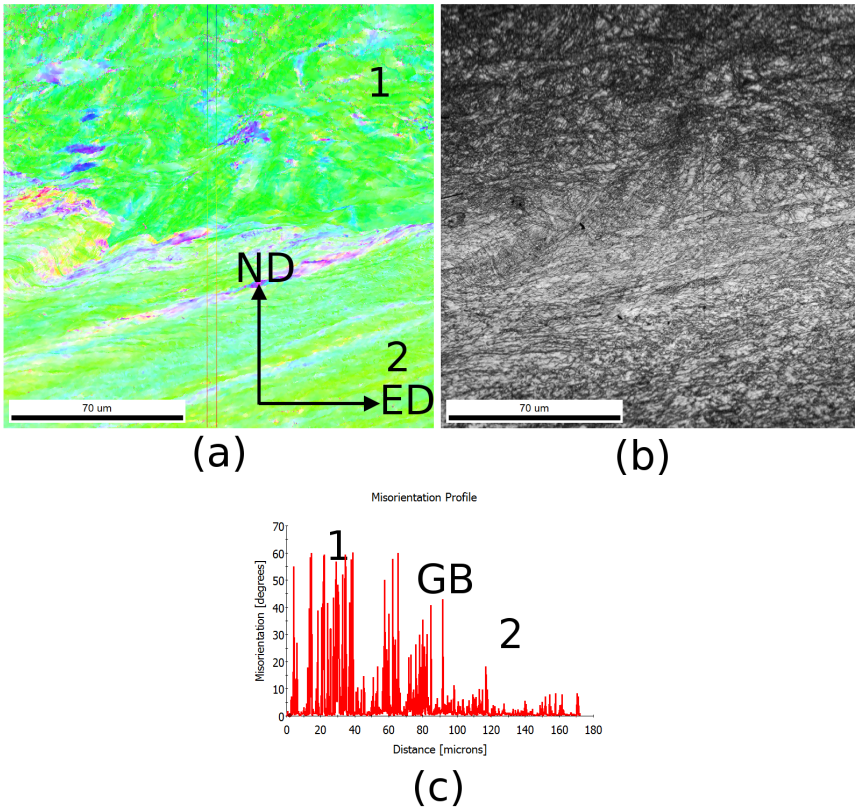

Figure 2.13: EBSD map of the GB region after two ECAE passes showing differences in structure near the grain boundary in Crystal 1, and Crystal 2: a) IPF in the TD direction, and b) the corresponding IQ map, and c) the misorientation profile. The misorientation value at the GB is 44^o around the GB.

2.4 Discussion

2.4.1 Dislocation substructures

Grain substructure formation and breakup processes during plastic deformation are very similar in metals with medium to high SFE. The deformation is slip dominant, and the structures are similar although the deformation mode, activation, and deformation temperatures are different. According to these observations, two types of dislocation boundaries are expected: a) boundaries formed due to statistical trapping of dislocations and are called incidental dislocation boundaries (IDBs), and b) boundaries formed between regions that have different local slip systems activated, these are called geometrically necessary boundaries (GNBs). The GNBs tend to align along the crystal axis/macroscopically with the deformation axis. In this study dislocation structures are observed in both the bi-crystals that orient themselves at 45^o to the ED direction as seen in Figures 2.7(a),(c), 2.9 (a). At least during the first pass of ECAE, the orientations on these GNBs show alternating orientation changes suggesting that similar combination of slip systems are activated on either side of the boundary, and the orientation change may only be due to a strain amplitude that differs. The effect of the GB is considered to be very local during the deformation, According to Hauser and Chalmers[58] , in the vicinity of the GB slip activity changes: there are more number of slip systems that need to be activated to accomadate the deformation of the individual crystals. This phenomenon is commonly described as multislip. Multislip is observed in our case in Crystal 2 after first pass around the GB as shown in Figure 2.10, which is evident from the crossed pattern. The pattern represents activity of more than one slip system.

2.4.2 Orientation splitting

Dislocation boundaries are created when lattice rotations occur, which can cause trapping of further dislocations and increases in the number of boundaries created. The misorientations for different dislocation boundaries (IDB's and GNB's) increase with strain. Therefore the fraction of GNB's and HAGB's could be a good indicator of the degree of orientation splitting.

From, Figure2.14 it can be seen that there is an orientation dependence of the percent HAGBs depending on the crystal orientation. With increasing strain the percent of HAGBs increase irrespective of the initial orientation [54]. Although Crystal 1 during the first pass develops bands in the microstructure, the percent of HAGBs are only about 4-8%. This supports the observation that the banded region probably has fewer HAGBs as shown by the contrast difference in the IQ maps in Figure 2.6. Crystal 2 is the most fragmented with a HAGB percent of 44-54%. It can be concluded that Crystal 2 gets divided more severely than Crystal 1 from these results.

2.4.3 Orientation evolution

The deformation mode is ECAE is generally considered to be simple shear to the first approximation. In fact, the grid lines on the initial billet and the macroscopic deformation correspond to the theory that ECAE can be considered to be simple shear to the first approximation. To understand the orientation evolution {110} pole figures have been plotted for: interior of Crystal 1, and Crystal 2, and in the vicinity of the GB for Crystal 1, and Crystal 2 after the first and second pass ECAE.

Texture development during the ECAE process has been investigated in comparison with the simple shear deformation for bcc metals [11],[81]. This analysis was done on a random polycrystal subjected to ECAE using the Taylor model.The

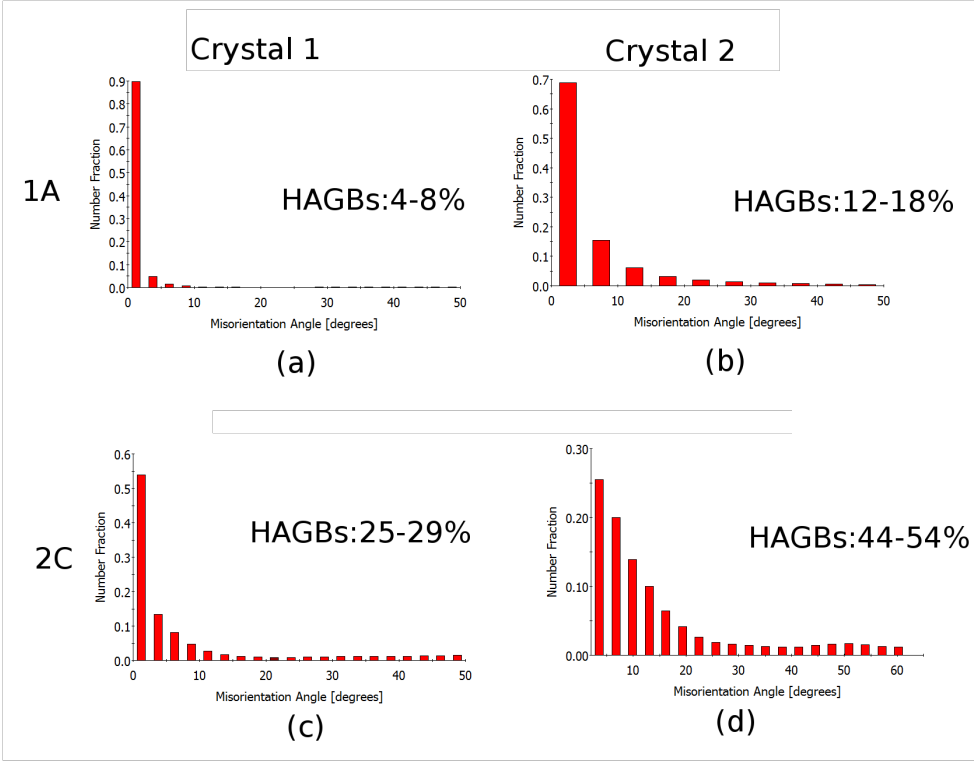

Figure 2.14: The fraction of misorientation boundaries in the interior of the two crystals are plotted scans of 300 μm x 300 μm; a), b) correspond to the first pass for Crystal 1 and Crystal 2 respectively, and c), and d) correspond to the second pass for Crystal 1, and Crystal 2 respectively.

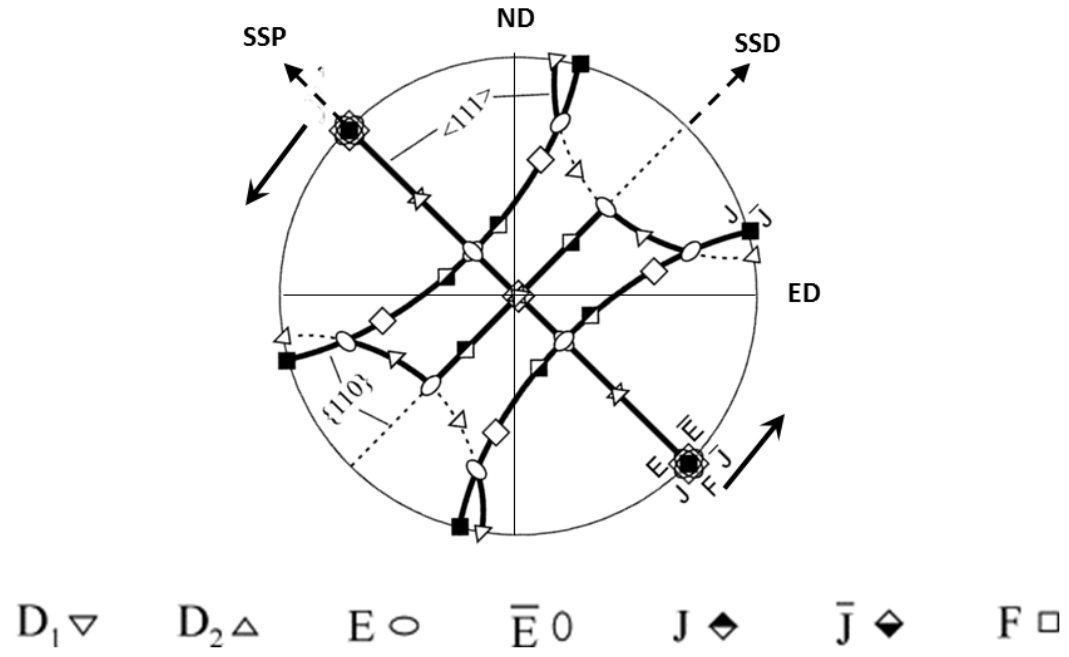

Figure 2.15: Polycrystal simulation of 50 intial random bcc polycrystals by ECAE provides the following stable simple shear textures as shown by the {110} PF [11]. The symbols and text indicate specific stable orientations, which are provided in the following review paper [11](Table 2, pg: 438)

ideal orientations correspond to either {110}‖ to the simple shear plane (SSP) or the ⟨111⟩ ‖ to the simple shear direction (SSD). Figure 2.15 represents the ideal ECAE textures for a bcc material on a {110} PF. All comparisons will be made using the ideal texture components. The symbols presented in Figure 2.15 are ideal/stable orientations that was got with the polycrystal simulation, and an interested reader is directed to the review paper by Beyerlein [11](Table 2, pg: 438).

2.4.3.1 First pass ECAE

Figure 2.16 gives the orientations of different parts of the crystal. Away from the GB Crystal 1 deforms by having a matrix-band structure. From Figure 2.16(a) one can infer that the matrix structure is spread between the ideal components D2-F.

D2 corresponds to $(11\bar{2})\|$SSP) and $[111]\|$ to SSD. The band is also oriented along a direction in which $\langle 111\rangle \parallel$ SSP. The spread in orientations in the matrix/band regions is low for Crystal 1; this is corroborated by the low percent of HAGBs in Crystal 1 after first pass. The deformation of Crystal 2 is more complicated. The PF in Figure 2.16 (b) indicates that the deformed Crystal 2 has orientations that are spread around the orientations that are aligned along the SSP/SSD or an ideal orientation. It is however difficult to separate the individual orientations. Comparisons between Figures 2.16(a) and (c) indicate that similar orientations exist near the GB after deformation, and there is an existence of a new orientation (as given by the black dots in Figure 2.16, this has been observed previously in Cu grains deforming under tension upto a strain of 25%, shows evolution of new orientations close to the GB [58], and this effect is localized. In our study Crystal 2 shows a similar mean orientation around the GB to that away from the GB as shown in Figures 2.16(b) and (d). This suggests that the region around the GB does not rotate as much as the lattice away from the GB, i.e. the region around the GB is somewhat harder to deform in Crystal 2. This is verified by the double slip crossed pattern around the GB in Crystal 2 (refer Figure 2.10(a)).

2.4.3.2 Second pass ECAE

The texture in Crystal 1 after 2C is quite complicated as indicated by Figure 2.17, and there is no definite mean orientation that can be easily determined. However, all the matrix and bands lie on the $\langle 111\rangle \|$SSD or $\{110\}\|$SSP or one of the ideal orientations. Figures 2.17 (b)-(d) is a remarkable finding indicating that the orientations begin to converge as a consequence of ECAE 2C processing. There are stable orientations that are experimentally observed in fcc, and bcc crystals under ECAE [37, 36, 38, 39, 45, 148, 147] and our results strengthen this notion.

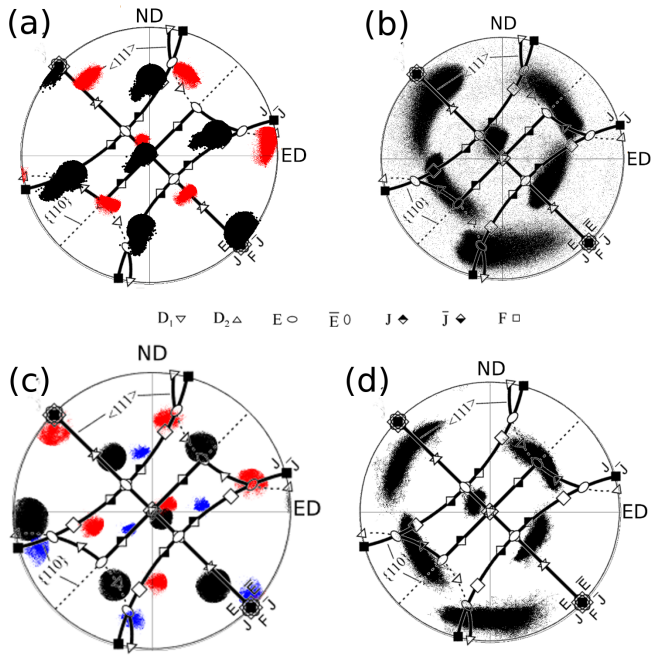

Figure 2.16: {110} Pole figures for one pass ECAE processed regions of the Nb bicrystal: (a) and (b) represent regions away from the GB for Crystal 1, and Crystal 2 respectively; (c) and (d) represent regions around the GB in Crystal 1 and Crystal 2 respectively. The red, and blue points in the PF in (a), and (c) indicate the bands observed in the structure

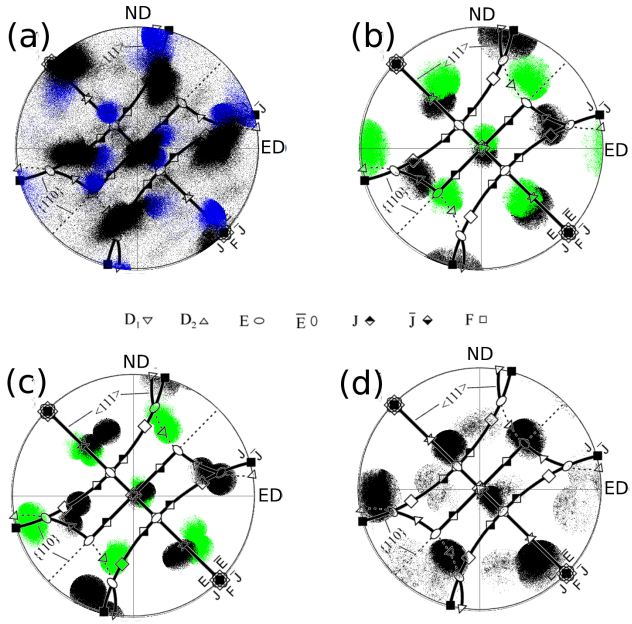

Figure 2.17: {110} Pole figures for two pass ECAE processed regions of the Nb bicrystal: a) and b) represent regions away from the GB for Crystal 1, and Crystal 2 respectively; (c) and (d) represent regions around the GB in Crystal 1 and Crystal 2 respectively. The blue, and green points in the PF in (a), and (c) indicate the bands observed in the structure.

2.4.4 Summary and Conclusions

In summary, the deformation in a bi-crystal sample was very inhomogeneous, with banding observed in Crystal 1, whereas uniform deformation in Crystal 2 especially after the first pass. The initial orientation was not reversed in any of the crystals after 2C. ECAE route 2C is microstructurally irreversible, as formation of dislocation structures are continous, and dislocation location motion is irreversible (leads to dissipation of heat).

The orientations in the initial single crystals are very strong and ECAE deformation produces newer orientations, and large orienation spreads which consitute the breakdown of microstructure. The newer orientations created do not follow the ideal orientations predicted by common polycrystal models. However, they are aligned along, $\langle 111 \rangle \parallel$SSD or $\{110\} \parallel$SSP.

Although initially the crystals had a large misorientation angle, the texture converge as early as the second ECAE pass.

In conclusion,the ECAE process can be employed to breakdown large grain polycrystals and has potential to homogenize different starting polycrystal structures due to process of converegence of micriostructures. This methodology could be effectively applied to any high SFE metal system.

3. MICROSTRUCTURES IN NB BAR- EFFECT OF GRAIN SIZE AND TEXTURE ON DEFORMATION

As shown in the previous chapter ECAE could be used as an effective tool to breakdown large grain polycrystal structures in Nb. Presented in this chapter is a validation and practical application of the microstructural breakdown strategy which can be directly applied to Nb-Sn superconductor wires.

3.1 Introduction

The main motivation for the development of microstructures in bulk Nb bar material is to improve the Nb_3Sn performance for various applications through the US conductor development program[22]. The performance of Nb3Sn strand is directly dependent on the Cu:Nb:Sn ratios. From the works of Peter Lee and others [79][102, 59, 78, 43, 76, 77], it is seen that high Sn:Nb ratios are beneficial for the formation of a homogeneous distribution of the Nb-Sn A15 compound. Obtaining the right ratios of Cu:Nb:Sn involves a complex interplay between the Nb strand size,amount of Cu , architecture of the wire, and the manufacturing process. The Nb_3Sn wires come in different architectures, and the architecture that we are concerned with is the internal tin architecture. There are two kinds of conductors that are used in the internal tin type wires, Figure 3.1 shows the different architectures used: a) single barrier (SB)and b) distributed barrier (DB). The kind of wire architecture is dictated by the application. The SB strands have high performance in applications that involve low hysteresis losses with moderate current densities (Jc) such as the ITER toroidal field (TF) coils, whereas the DB strands are used in applications (Nuclear Magnetic Resonance) where Jc is the most important property [33]. In the architectures above, the magnetic field loss (and hence the stability at low

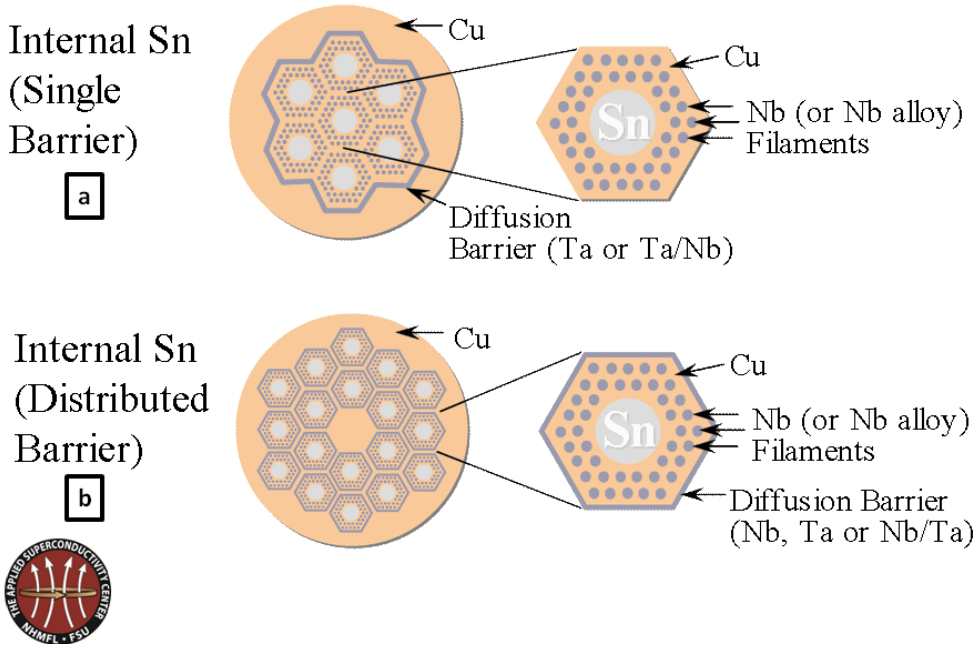

Figure 3.1: Schematic of an internal tin wire architectures that are commonly used: a) Internal Tin single barrier wire commonly used for applications where magnetic stability is of primary importance, and b) Internal Tin distributed barrier conductor commonly used for applications needing high J_c. Courtesy:Peter Lee of NHFML/FSU

magnetic fields [42],[9]), and high Jc are competing variables. High non- Cu Jc is attained by increasing the area of Nb-Sn reaction and Sn accessibility to allow complete and full reaction to form Nb_3Sn which is observed in distributed barrier conductors [79] , however the limitation of a distributed barrier conductor is the increased effective filament diameter(D_{eff}) which contributes significantly to stability at low magnetic fields. However, the problem of stability is largely mitigated in the SB strand because the D_{eff} can be controlled easier because of better drawability[103].

High Energy Physics (HEP) applications require conductors with high Jc and better stability in regions that are exposed to lower magnetic fields, this requirement leads to a manufacturing challenge of trying to decrease the Nb rod size, and

increase the Nb content to make filaments that could potentially have high Jc as well as maintain stability. A successful fabrication technique developed by OIST to achieve this goal, in a distributed barrier internal tin conductor is the rod restack process (RRP)[102]. Steps involved in manufacturing an RRP conductor is as shown in Figure 3.2. Nb bars of 6 in diameter are jacketed in Cu-sheath, and the composite Cu-Nb bars are stacked depending on the number of filament per stack, wrapped with a Ta/Ta-Nb sheet and extruded. The Cu core is then removed and tin is inserted into the core of the billet. This composite Cu-Nb-Sn billet is restacked in Cu and redrawn to reach the final wire dimensions which corresponds to about 1mm, the final heat treatment is a 650^{o}C/2hr heat treatment. The full heat treatment schedule depends on the Nb content and varying temperatures and times are employed [103]. This approach offers significant advantages: a) better control over Cu to Nb ratios and hence Cu interfilament distance and b) easy scalability The method includes extrusion and drawing of Nb rods in a Cu- matrix.

The issue related to the manufacture of wire is of Nb co- deformation in a Cu matrix, leading to non-uniformity of filaments during the initial extrusion steps. A particular situation of non-uniform deformation is provided in Figure3.3 , in order to remedy the problem OIST introduced a machining step to remove the jacketed Cu and the Nb fringes to obtain a circular Nb rod which was then drawn which maintained necessary circularity. This procedure is impractical considering the number of elements in one stack and the cost of the wire (dollar/kA).

An alternate proposed solution to the problem is to start with precursor Nb microstructures that are favorable to drawing and maintain good co-deformability in a Cu-matrix without any remedial machining. Presented in this chapter is the development of Nb microstructures for superior co-deformability through thermo-mechanical processing of precursor Nb including experimental evidence of Cu-Nb

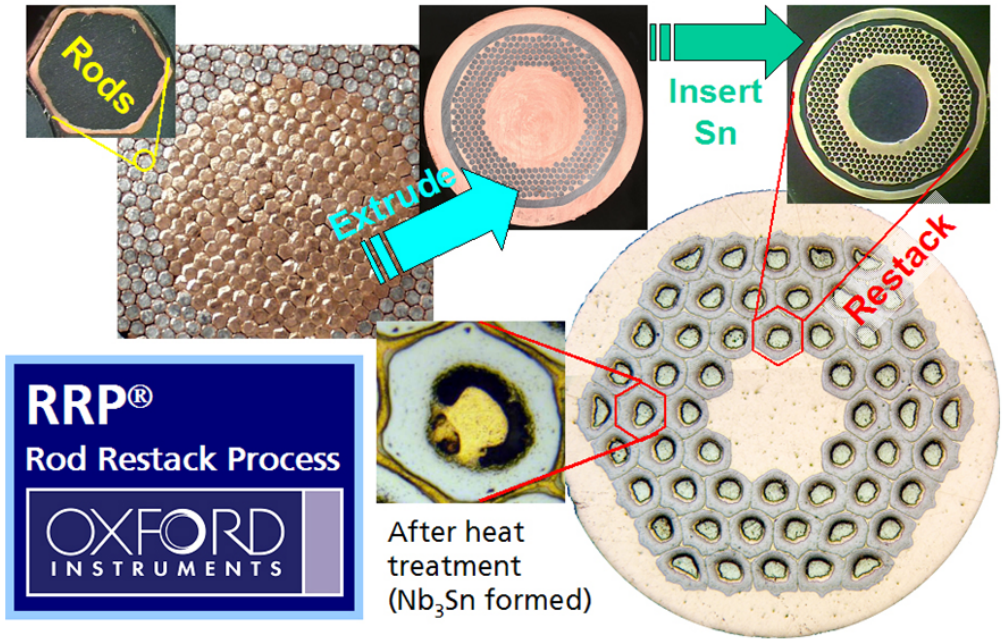

Figure 3.2: Fabrication process involved in the manufacture of an RRP conductor. The process involves multiple extrusion, and wire drawing steps. Nb_3Sn is formed after a high temperature,long soak heat treatment. The final wire dianmeter is of the order of 1000 μm's: Courtesy: Mike Field, OIST

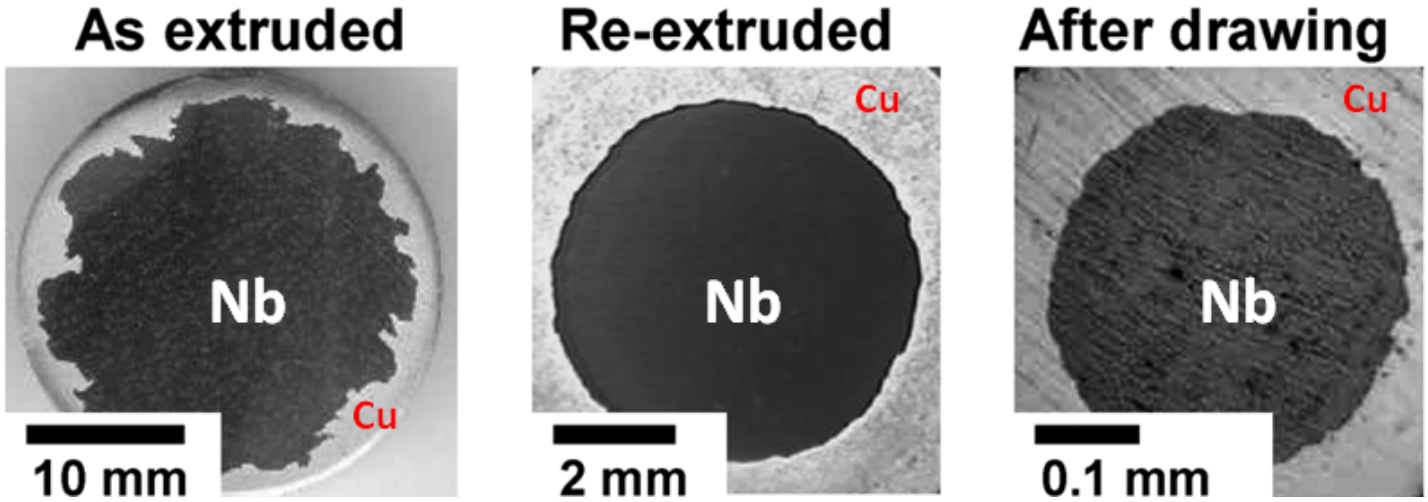

Figure 3.3: Initial non-uniform deformation of Nb after extrusion (left), reshaped round Nb bar by machining and re-extruded (center), roundenss of the Nb bar retained after wire drawing (right)[103]

prototype deformation experiments.

3.2 Materials and methods

All the Nb used in this study was Grade I Nb, with typical composition of 99.9% Nb, 1500 ppm Tantalum (Ta) and trace amounts of carbon, hydrogen, nitrogen and oxygen. All the Nb samples baring two samples for the grain size study underwent initial thermomechanical processing steps. The processing involved multiple ECAE passes, with recrystallization heat treatments. Details of obtaining the samples for the grain size; and texture effects on Cu-Nb monocore deformation are presented in this section.

3.2.1 Material and processing details for grain size study

Four bars with different starting grain sizes were used in this study. All the bars were cut to nominal dimensions of 50mm x 50mm x 250mm using a wire EDM. To obtain different grain sizes in the Nb bars the following procedure was employed. A large grain sample (S1) was generated from the As EBM bar stock which had a starting grain size in the order of tens of centimeters. A grain size with a order of magnitude less than S1, within the range of one to ten centimeters was obtained directly from HC Starck (courtesy: Peter Jephson). This sample was designated as S2. Although, technically this material was Grade I NB, it was informed that this material was contaminated with Ti. No chemical testing was done to verify this claim. Sample S3, and S4 were samples generated by employing thermomechanical processing by multiple ECAE, and recrystallization heat treatments.

The processing details for S3, and S4 involved processing as EBM Nb bars of nominal dimensions 50mm x 50mm x 250mm by a hybrid ECAE processing schedule, that involved an initial homogenization step, and a final processing step. The initial homeogenization step consisted of an initial two pass ECAE, subsequent recrystal-

lization at 1100^{o}C. The final processing step was four pass ECAE. Sample S3 was recrystallized at 1150^{o}C, and S4 at 950^{o}C to obtain grain sizes in the range of hundreds of micron in S3, and tens of microns in S4. All the heat treatments, were done under vacuum conditions of 2-8 x 10^{-6} torr, the duration of heat treatments for all cases was 5400 sec. The heat treatment schedule involved introducing the samples into the hot zone of the furnace when the set temperature was reached (within five percent, and after 5400 seconds, the furnace was turned off, and the samples were allowed to furnace cool to room temperature under vacuum conditions. The selection of the heat treatment temperature is based on previous recrystallization, and grain growth studies of ECAE processed Grade I Nb. One such study is presented in Appendix 1 in the form of micrographs obtained after the above recrystallization heat treatment schedule for Grade I Nb processed via multiple pass ECAE.

3.2.2 Material and processing details for texture study

The starting material for the texture study was Grade I Nb, with a similar composition as bars S3, and S4, as described above. All the billets for the texture study involved a pre-processing step using an hybrid ECAE route 6B, and underwent recrystallization heat treatment at 950^oC, for 5400 seconds. The heat treatment schedule used during this study is the same as the previous section. Four samples designated as A, B, C, and D with initial starting dimensions of 50mm x 50mm x 178mm were further processed by different ECAE routes to obtain textural differences. Sample A was processed by route 4A, Sample B by 4B, Sample C by 4B$_c$, and sample D by 4E. To obtain similar grain sizes in the range of tens of microns, all the samples were recrystallized at 800^oC (refer Appendix (), for choice of recrystallization temperature).Characterization samples were cut from the as-worked and recrystallized fully worked regions for microstructure evaluation

as shown in Figure **??**. From here on we refer to the uniform heavily worked region as the bar/wire front end (FE), and the non-uniform region as the back end (BE). There are differences in the work zone geometry depending on the route and number of passes, at either ends of the billet in ECAE and depends on the route. In the worst possible scenario the non-uniform zone could extend upto 50mm after four passes depending on the route[8]. Here the back end (BE) is the zone that is not fully worked to the same number of passes as the middle. The warm extrusion and wire drawing were done in the same direction as ECAE with the FE pointing into the die.

3.2.3 Manufacture of Cu clad Nb composite wires

An electro discharge machining (EDM) setup was used to machine the above described ECAE processed Grade I Nb billets to a diameter of 45 mm and a length of 80 mm, for fabrication into Cu-Nb composite bars. The composite wires were fabricated at OIST and included an initial warm extrusion of a 51 mm OD Cu-Nb composite rod to 16 mm diameter bar. This composite bar was then cold drawn to a final wire diameter of 1 mm. The wire drawing reduction ratio for each drawing step was 10% to 15%. Samples were cut after warm extrusion and at intermediate drawing steps for further shape analysis.

3.2.4 Analysis method

Standard metallographic procedures were used to polish the Nb and Cu-Nb composite samples. The samples were etched with a 1:3:3 HF:HNO_3:lactic acid solution for microstructure characterization. Texture was measured along the extrusion direction for the starting material, and for the rod and wire samples were measured along the extrusion and wire drawing directions using a Bruker D8 Discover Diffractometer with radiation at 40 kV and 40 mA. Pole figures and inverse pole figures

were calculated using PopLA. To evaluate the circularity of the Nb cores in the extruded and drawn wires, circularity was determined using the ImageJ software from optical micrographs of the sectioned wires. Circularity is mathematically defined as specified in Equation 3.1. For a perfect circle the value of circularity equals one. The circularity quantifies the deviation of shape from a circle; a circle with a jagged boundary will have a circularity less than one. The higher the jaggedness, the lower the circularity value as the perimeter increases, whereas the area remains mostly unchanged.

$$Circularity = \frac{4\pi.Area}{Perimeter^2} \tag{3.1}$$

3.3 Experimental results

In this section, experimental results on microstruture of the starting Nb bars will be presented. Results on Nb crossectional changes during warm extrusion, and wire drawing of Cu-Nb monocore composites from diffrent Nb microstructure options generated will be presented.

3.3.1 Initial microstructure

Initial starting microstructures in Nb samples S1, S2, S3, and S4 showed expected variation in grain sizes due to differences in heat treatment. Representative micrographs of the samples for the grain study (S1-S4) are presented in Figure 3.4(a-d). Table 3.1 provides a summary of the initial microstructure and corresponding hardness values. Sample S1, has the largest grain size in the order of 10000-40000 μm, Sample S2, provided by HC Starck, had a grain size of 2000$\pm$1500μm. Sample S3, and S4 which are thermomechanically processed by ECAE and recrystallized had grain sizes corresponding to 100$\pm$72μm, and 40$\pm$15μm respectively. The hardness

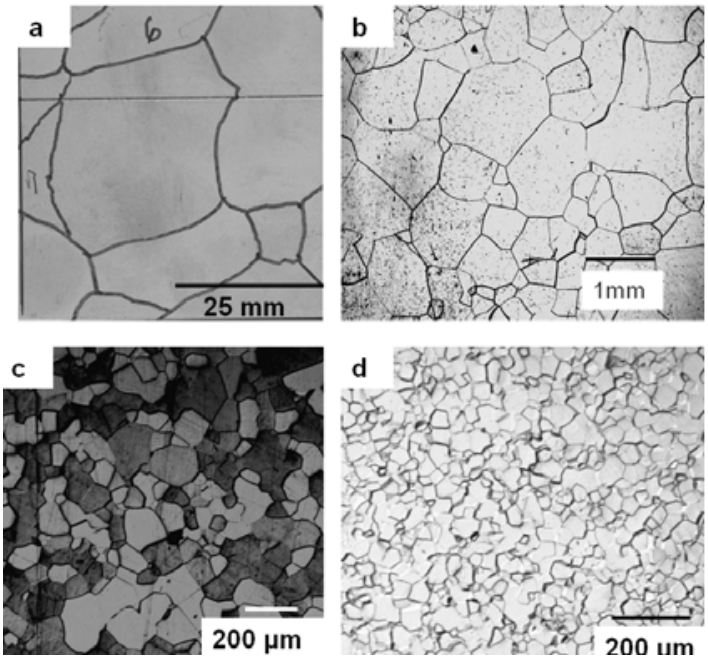

Figure 3.4: Representative microstructures of the starting Nb used in the fabrication of Cu-Nb monocore filaments. a) Cast sample with a grain size of 10-40mm; b) H.C. Stark Nb, average grain size of 1-4mm; c) ECAE processed and heat treated at 1150^{o}C, average grain size 70-170μm. and d) ECAE processed and heat treated at 950^{o}C, average grain size of 20-60μm.

values of all the samples as presented in Table 3.1 indicate that the microstructures are fully recrystallized with hardness values in the range of 50-66 HV(300g). Sample S2, has a slightly higher hardness than the other samples, possibly indicating the effect of the above mentioned contamination.

The initial microstructure of Nb bars used in the texture study was uniform as seen in Figure 3.5(a). The calculated average grain size was 42 $\pm$10μm. The texture of the sample as indicated by the PF in Figure 3.5(b), shows a strong $\{110\}\|$TD texture, with a maximum texture intensity of 5.28 m.r.d. This starting bar material was processed via different ECAE routes and recrystallized to obtain texture variations. Figure 3.6 (a-d), depicts the grain structure of processed material by

Table 3.1: Characteristics of starting Nb bar with different starting initial grain sizes for the Cu-Nb composite wire drawing experiment

Monocore ID Number	**Processing**	**Grain size (μm)**	**HV 300**
S1	As cast	10000-40000	54±2
S2	As received from HC Starck	1000-4000	63±3
S3	Multi-pass ECAE and recrystallized at 1150^{o}C	100±72	56±1
S4	Multi-pass ECAE and recrystallized at 950 C	40±15	57±2

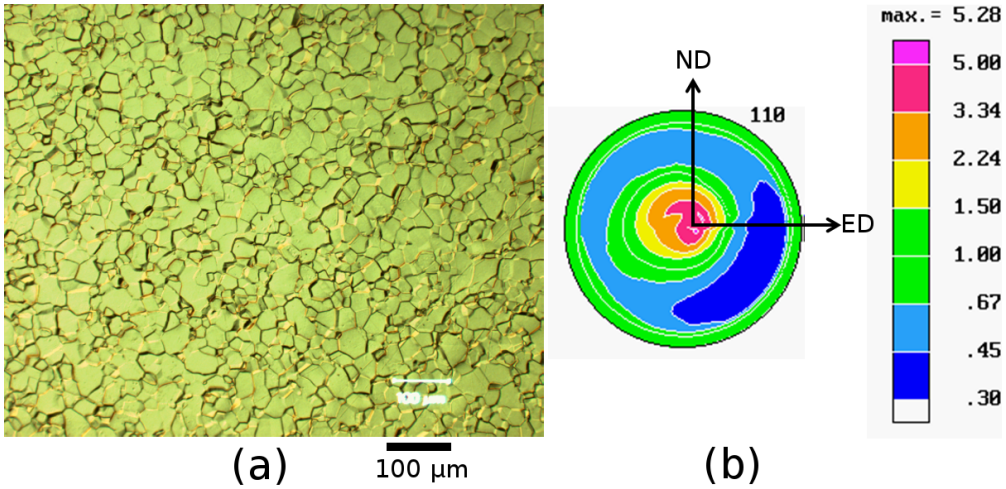

Figure 3.5: Representative Nb microstructure after ECAE pre-processing by route 6B and recrystallization heat treatment at 950 ^{o}C/5400 sec. (a) Optical micrograph indicates a uniform starting microstructure with a grain size of 42 $\pm$ 10μm, (b) {110} PF indicates a medium strength texture, represented by {110}$\|$TD component

different routes, the grain sizes are in the range of 10-30μm. Figure 3.7 depicts the texture variation in the samples after the different processing schedules. It is clear that there are variations in the texture after processing as indicated by the PFs in Figure 3.7(a,b,c, and d). Sample A, B, and C, processed by routes 4A, 4B, and 4B$_c$ have strong {110}$\|$TD peaks. The {110} poles are offset from the center in case of Sample D, processed by route 4E. After recrystallization the texture changes in all cases as observed in Figure 3.7(e,f,g, and h). The recrystallization texture evolves in such a way such that {110} poles tend to align with the ND direction for samples B, C, D, and is slightly offset from this position for sample A. Irrespective of the processing path all the PFs indicate diffuse texture components.

The microstructure for samples A-D are quantified in terms of grain size and texture strength and are presented in Table 3.2. There grain sizes are uniform in all samples after multi-pass ECAE and recrystallization, as indicated by the standard

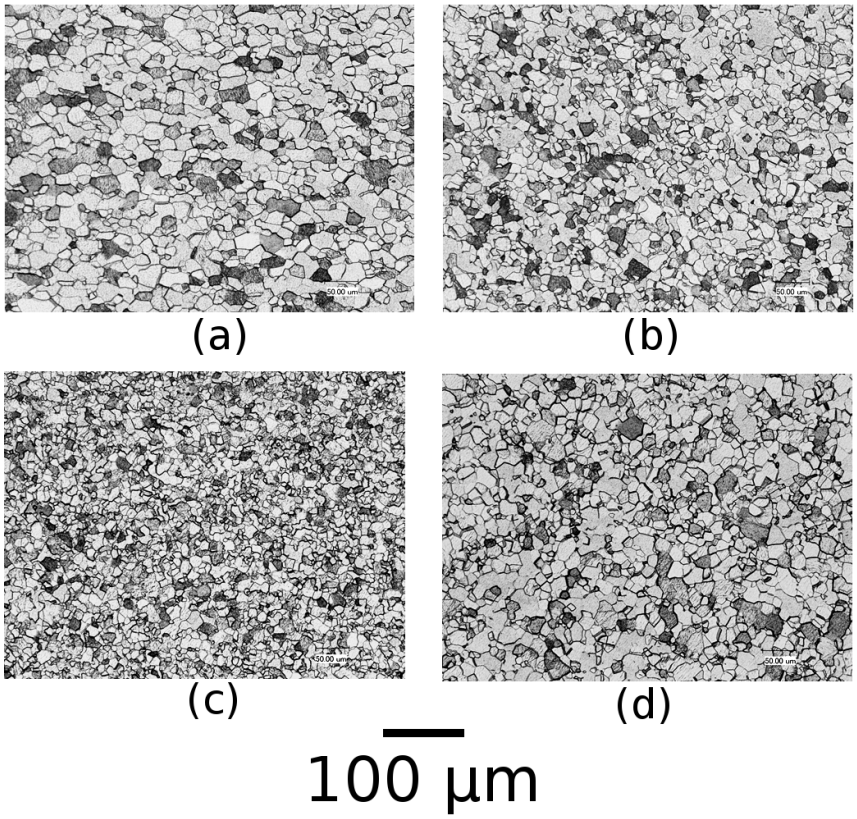

Figure 3.6: Optical micrographs indicating recrystallized microstructures in Nb after multi-ECAE processing by different ECAE routes: (a) Sample A-Route 4A, (b) Sample B-Route 4B, (c) Sample C- Route $4B_c$, and (d) Sample D- Route 4E. The average recrystallized grain sizes are less than 30μm for all samples in consideration.

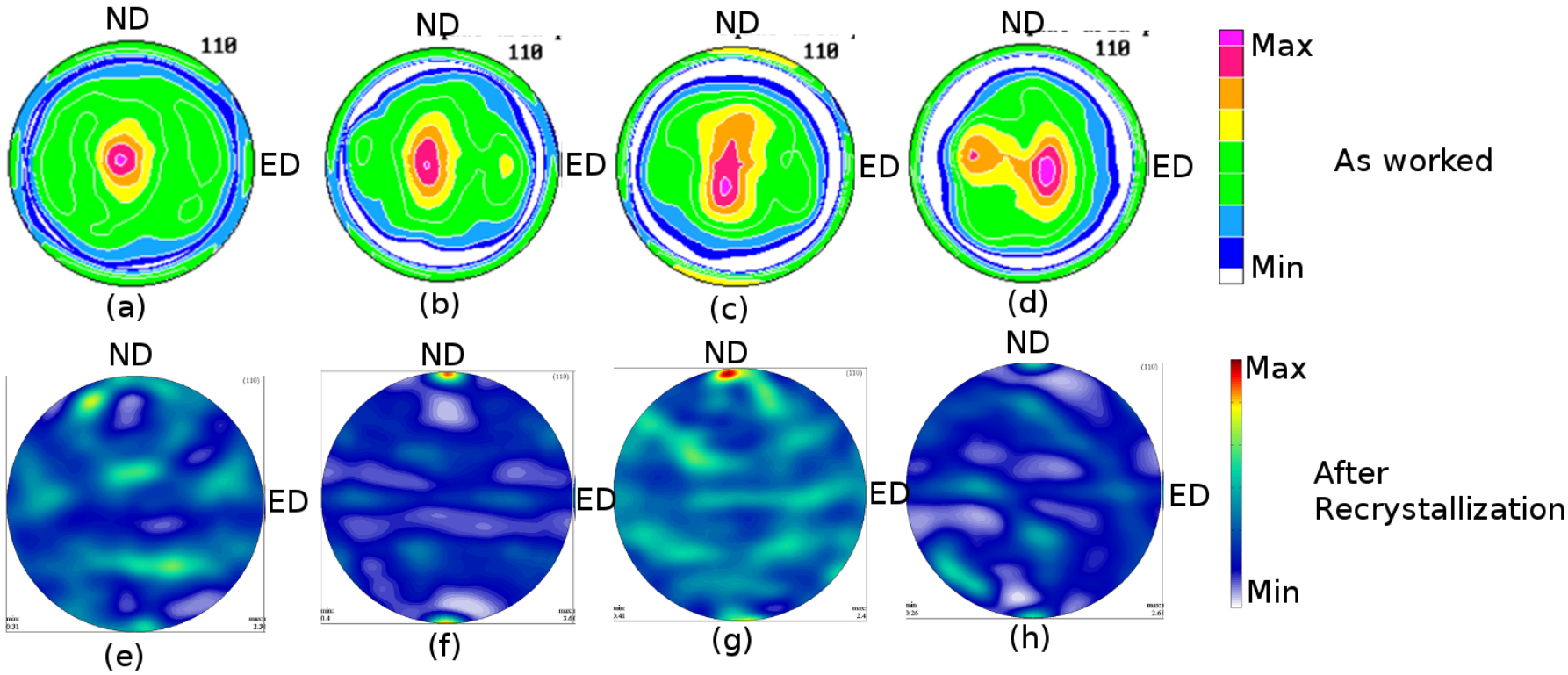

Figure 3.7: {110} PFs of multi-pass ECAE material processed under different ECAE routes in as worked and after recrystallization heat treatments (800°C/ 5400 s); (a), (b), (c), and (d) are Pfs of as worked material, whereas (e), (f), (g), and (h) are recrystallized textures generated by routes 4A, 4B, $4B_c$, and 4E respectively. The figure presents qualitative texture information. The max texture strengths are presented in Table 3.2.

deviation about the mean values. The average grain sizes are in the range of 20-30μm for samples A, B, and D. Sample C has a slightly finer average grain size of 12 $\pm$3μm. Texture strength variations with ECAE route depend on the processing route. For routes 4A, and 4B texture strength increases after ECAE processing from an initial value of 5.3 m.r.d to 10.4 m.r.d, and 11.6 m.r.d, respectively in the worked state respectively. The texture strength does not vary significantly after processing by Routes B_c, and E, as indicated by the texture strength values of Sample C, and D after working. On recrystallization the texture strength drops for all processing routes. The texture strengths after recrystallization are weak and below 4 m.r.d as shown in Table 3.2. The texture strength drops significantly from the worked state for Samples A, and B whereas less dramatically for Samples C, and D.

3.3.2 Cu-Nb deformation characteristics after warm extrusions, and wire drawing

Samples S1, S2, S3, and S4 which had different starting grain sizes showed significant differences in cross-section after being warm extruded by an area reduction ratio of approximately 9. The initial and final crossections of the die were circular. Figure 3.8(a-d), show the differences in cross-sections in various samples. Sample S3, and S4 appear to be more circular than S1, and S2 whose shape resemble polygons instead of a circle. Samples A, B, C, and D which had different starting textures deform more uniformly as observed in Figure 3.9(a-d). The initial circular Nb billets remain circular even after warm extrusion

The as warm extruded Cu-Nb rods were drawn down to a final wire diameter of 1mm. The total strain that the Cu-Nb composite experiences from the hot extruded to wire drawn state is about 5.5. The cross sectional shapes of the Nb rods after wire drawing are presented in Figure 3.10, and Figure 3.11. For the samples in which the grain size was varied, there is a clear difference between the Nb cross sections.

Table 3.2: Summary of Nb microstructure characteristics for different texture options produced by multipass ECAE, and subsequent recrystallization heat treatment

Sample ID	Processing Route	Initial Grain size (μm)	Maximum texture strength (m.r.d)	
			As worked	After Recrystallization
Pre-processing	6B	42 ± 10	—	5.3
A	4A	26 ± 8	10.4	2.3
B	4B	22 ± 4	11.6	3.6
C	4Bc	12 ± 3	5.4	2.4
D	4E	28 ± 6	5.9	2.6

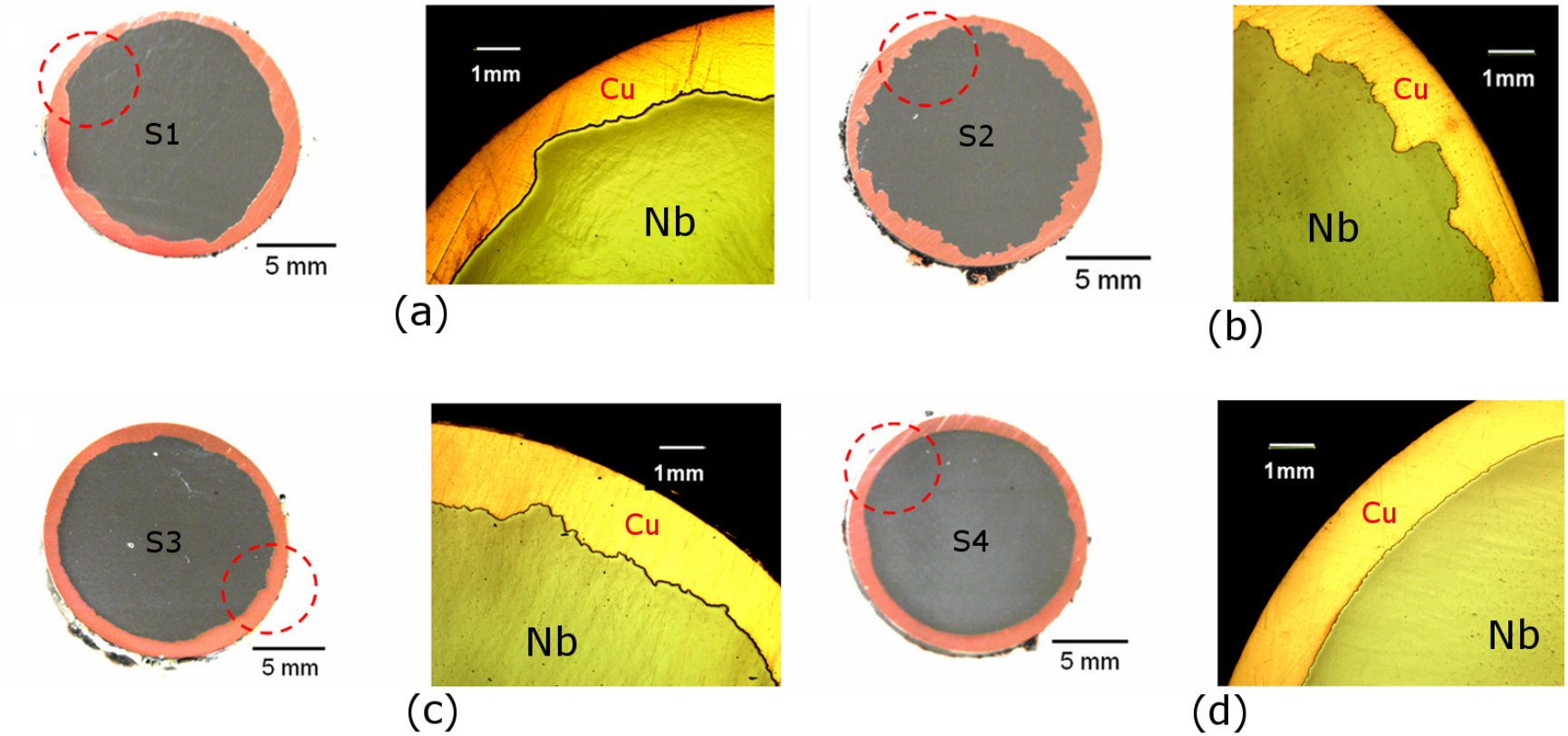

Figure 3.8: Representative sections of the Cu-Nb interface of warm extruded monocore ro ID (grain sizes): (a) S1 (10000-40000) μm, (b) S2 (1000-4000) μm, (c) S3 (100$\pm$72) μm, (d)S4 (40$\pm$15 μm)

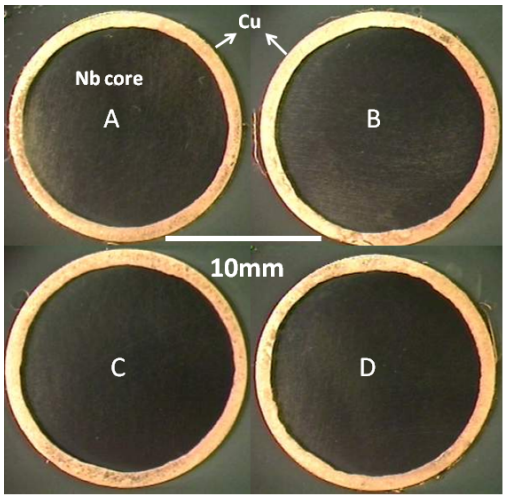

Figure 3.9: Macrographs of Cu-Nb monocore samples after warm extrusion, the sample ID (ECAE route) are :(a) A (4A), (b)B (4B). (c) $4B_C$, (d) 4E. The Cu-Nb interface deformation is uniform, for all cases.

From Figure 3.10 (a-b) we observe that Sample S1, S2 which deformed poorly after warm extrusion show a worsened behavior after wire drawing. S3, and S4 are have a better cross section retention after wire drawing as observed from Figure 3.10(c-d). In the case of samples A,B, C, and D all the samples retain their circular shape after the wire drawing operation from the warm extruded state as suggested by the macro graphs in Figure 3.11(a-d).

It is clear from these results that the deformation behavior is strongly co-related to the initial grain size of the Nb bar used in these studies. In order to study the deformation characteristics, circularity of the wires at various stages of the deformation were calculated using Eq3.1 for all the samples. The circularity was plotted against the wire diameter. Figure 3.12 shows the variation of circularity for various initial Nb grain sizes. The circularity of the large grain samples S1 (10000-40000 μm), and S2 (1000-4000 μm) after warm extrusion (represented by the wire diameter of 16mm) are 0.74, and 0.5 respectively. For the finer grain sizes less than

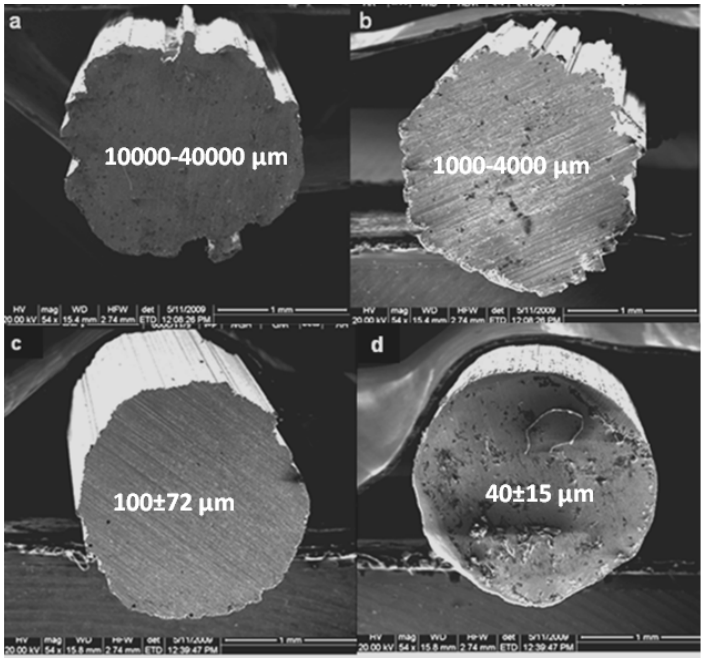

Figure 3.10: Seconday Electron image of as drawn Nb wire section at a final wire diameter of 1mm, with the Cu sheath etched off: a)S1- 10000-40000 μm, b) S2- 1000-4000μm, c) S3- 100$\pm$72μm, d) S4- 40$\pm$15μm

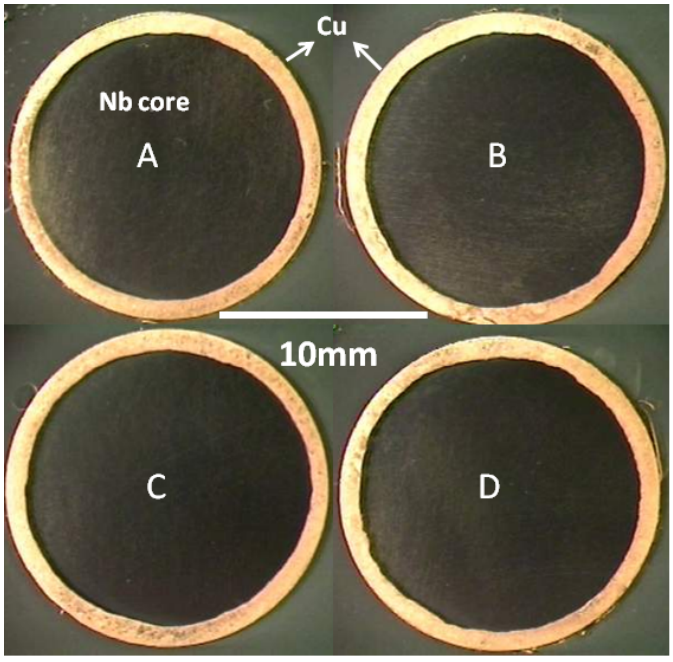

Figure 3.11: Optical Micrographs (OM) of as drawn Nb wire section at a final wire diameter of 1mm : a)A, b) B, c) C, and d) D. The initial grain sizes of the starting Nb was less than 50 μm, and the circularity is retained.

50μm, which correspond to samples S4, A, B, C, and D the circularity values are above 0.9 after warm extrusion. General trend indicates that the circularity of the wire deteriorates in all cases as drawing commences after the warm extrusion step. There is a slight improvement in the circularity of the wires as observed by the increase in the circularity after 4mm in the case of sample S1, and at 2mm in the case of samples S2 (1000-4000 μm), S3 (100$\pm$72 μm) , and C(12$\pm$3 μm). A similar plot of circularity with varying texture as denoted by the texture strengths is shown in Figure 3.13, there is no significant change in the circularity of the wires from the as warm extruded rod (16mm diameter) to the as drawn wire at a final diameter of 1mm. All the samples have starting circularity value greater than 0.9 after warm extrusion, and have circularity values greater than 0.85 after wire drawing. All these samples had grain sizes less than 50 μm. A key result from this study is that for ECAE processed and recrystallized samples the circularity of the wires with grain sizes less than 50 μm maintain their circularity even when drawn down to large starin values in a Cu- matrix.

3.4 Discussion

To analyze the roughness phenomenon, the process of roughening can be broken down into several parts: a) creation of instability, b) instability reaching a critical value, and c) propagation of the instability and worsening of interfacial roughness. Thilly et. al suggested that during the drawing of Cu-Ta interfaces, the creation of roughness depends on the instability due to differences in the shear modulus between interfacial surfaces in contact [47],[132]. The shear moduli of Cu and Nb are 46 GPa and 37.5 GPa, respectively,.In fact alloys containing Cu-Nb, Cu-Ag have been used for high strength conductor applications due to formation of very fine complex microstructures [126],[125]. The microstructures present in these systems

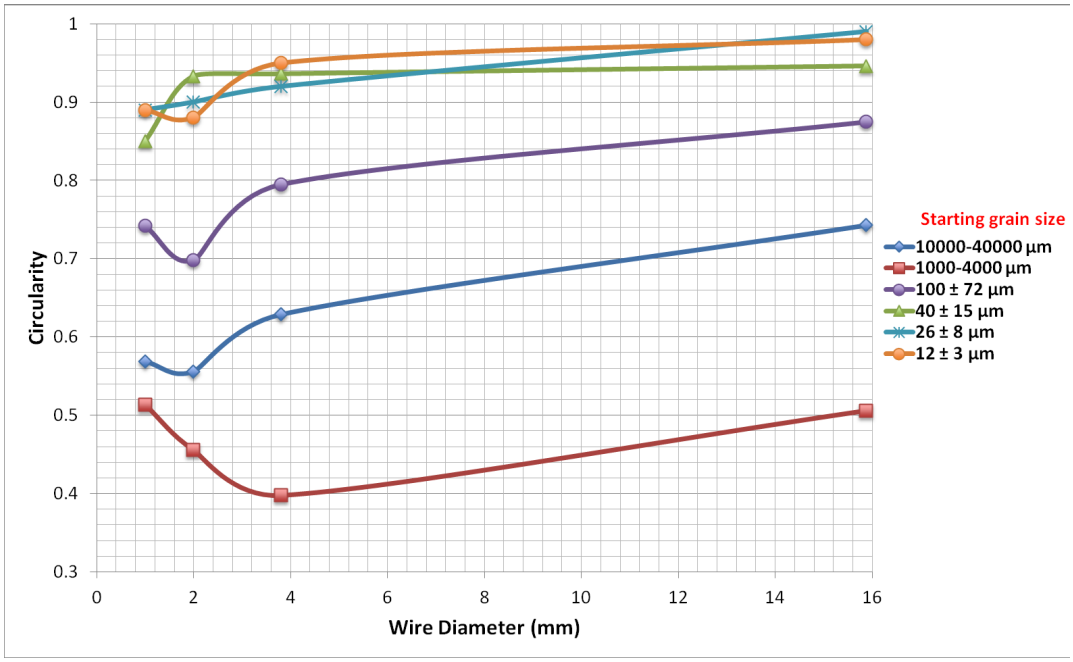

Figure 3.12: Variation of circularity as a function of wire diameter for various grain size ranges. Notice the poor circularity in Nb rods with starting grain sizes greater than 50μm.

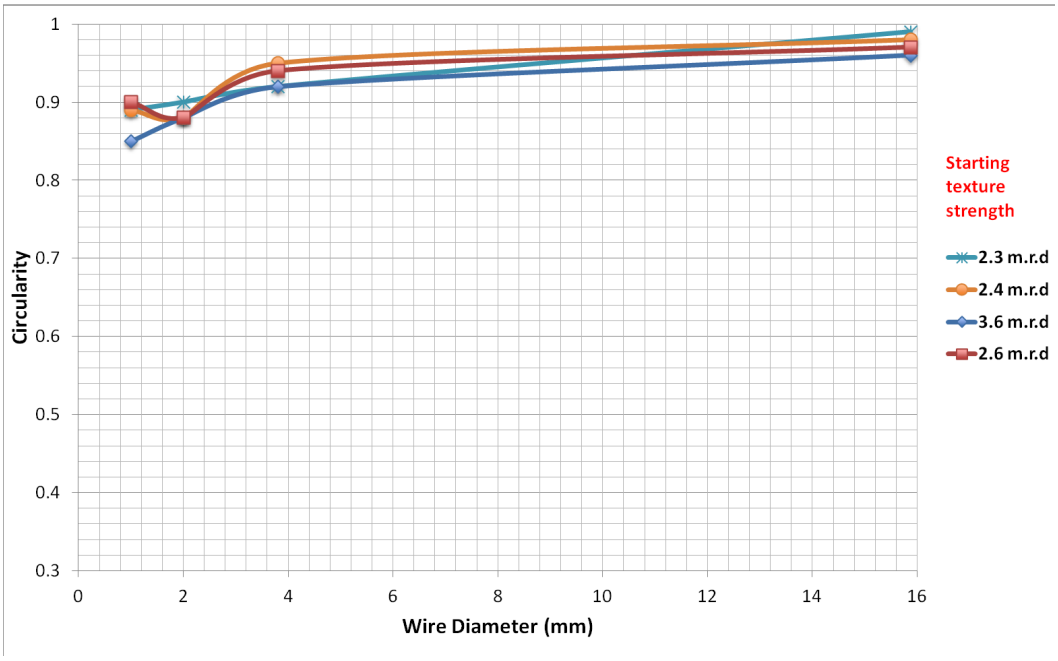

Figure 3.13: Variation of circularity as a function of wire diameter for different initial texture strengths. All the Nb samples had grain sizes below 30μm. The circularity in Nb rods does not change significantly with warm extrusion followed by wire drawing

show incompatible deformation at the interface of Cu-Nb or Cu-Ag [52]. At the atomic level, these elements do not form solid solutions due to differences in lattice parameters in case of Cu-Ag, and differences in crystal structure in case of Cu (fcc)-Nb (bcc), and hence there is an incompatibility in deformation at the interface. These aspects are beyond the scope of our discussion. Our interest is limited to the macro roughness or incompatibility seen in Cu-Nb monocores, and worsening of the roughness during deformation. In our opinion the propagation of roughness is based on initial and continually evolving microstructural features: i.e grain size, and texture.

In general any mechanical processing operation reorients the grains to favorable orientations which show up as the texture of the material after processing[61]. In the presence of applied stresses, the major deformation of the grains is in the form of stretch and rotation. The deformation of the grain shows up as the roughness on a free surface, which is the interface in our case. This would mean that the bigger the grain and the more unfavorable the initial orientation, the larger will be the deformation and bigger the displacement left behind on the surface. The results suggest that there is a strong correlation between the initial grain size and the interface roughness generated after the warm extrusion. Figures 3.8, and 3.10 suggest that larger the grain size higher the roughness/ lower the circularity. Figures 3.8(a, b) suggest that the initial instability that is created in the form of roughness features is of the order of initial grain size, which is in the order of mms observable through optical micrographs. These cannot be observed in macrographs for finer grain sizes, however secondary electron images of the 1mm wires in Figure ZZZ show the possible remnants and propagation of roughness features where initial grain sizes are greater than 50 μm. Figure 3.10(d) shows a smooth surface at the same magnification. There is not much change in the circularity of the wires with starting

intial grain sizes of less than 50 μm. If we consider stability in terms of maintaining circularity, a grain size of less than 50μm leads to stability.

An unfavorable orientation under deformation should also lead to development of incompatibilities. Among the several texture options that we created, there was no dependence of the texture for grain sizes below 50μm. The key reason for this result is due to the fact that: the starting textures in all the recrystallized polycrystalline samples were low. This is a common observation in ECAE processed polycrystalline and recrystallized cubic metals [32], [80]. The maximum texture strengths in the fine grain polycrystalline materials were around 3 m.r.d (see Table 3.2. This is low compared to other processing techniques; example: recrystallized rolling textures in Nb are typically in the order of tens of m.r.d for Nb [13]. Also, extrusion and drawing textures in Nb are predominantly the {110}‖ major axes textures [62],[63], and all the textures that we observed after ECAE had {110} ‖ TD/ ND (see Figure 3.7). This means that not only were the textures low, they were stable orientations that Nb attains after drawing. This translates to lesser reorientation and possibly lesser changes in macroscopic shape. The possibility of texture variations may become important when the texture strengths are higher.

3.5 Conclusions

- Initial grain size has a significant impact on the drawability of Nb in a Cu matrix. Initial grain sizes of over 50μm are expected to show poor deformation behavior. Low textures which are typical of multi pass ECAE do not have an impact on drawability.

- ECAE has been demonstrated to be a viable processing tool to create microstructures for Nb bars for Nb-Sn applications. ECAE is able to provide excellent microstructure control, which could be tuned in the range of tens to

hundreds of microns.

- With careful control over the ECAE yield, the complete billet could be used. The end effects produced during multi-pass ECAE do not have an impact on the final wire dimensions.

- This thermomechanical processing strategy could be scaled up to process Nb billets of larger crossections, and has potential for possible future conductor applications.

4. MICROSTRUCTURE AND MECHANICAL PROPERTIES OF FINE GRAIN SEAMLESS NB TUBE BY SIMPLE SHEAR DEFORMATION

4.1 Background

In the previous chapter it was shown that ECAE could be applied to refine bulk Nb microstructures in the form of Nb bars for Nb-Sn superconductor wire applications. In a proof of concept experiment the idea of development of seamless tube from a Electron Beam Welded (EBW) was developed. The main results of this project led to the development of tube ECAE(tECAE) process. The experimental methods that led to the development of the process, and key results are presented in Appendix B. This chapter has been published elsewhere.*Permissons required for usage have been obtained.

4.2 Introduction

Seamless polycrystalline Niobium (Nb) tubing is attractive in the manufacture of superconducting radio frequency (SRF) cavities by hydroforming. The reasons for this include: a) the possibility of lower net manufacturing costs of a multi-cell cavity, and b) elimination of equatorial welds, and the associated heat affected zones. These are possible defect regions and can be the origin of hot spots that are observed during associated cavity tests [19]. The main objective of this work is to develop processing strategies for seamless Nb tube that give a uniform through thickness microstructure and desired mechanical properties suitable for hydroforming. The current technical

*Reprinted with permission from "Microstructure and mechanical properties of fine grain seamless Nb tube by a novel shear deformation process" by S Balachandran, N Seymour, R Mezyenski, R Barber, and KT Hartwig, 2014. Advances in Cryogenic Engineering: Transactions of the International Cryogenic Materials Conference ICMC, 197-203, Copyright 2014 by AIP Publishing LLC[6].

specifications for a Nb seamless tube requires a recrystallized grain size of less than 50μm, and elongation at break of greater than 30%. There is no specification for microstructural uniformity.

The most common fabrication methods of polycrystalline seamless Nb tube that have been previously used are [121]: a) back extrusion, b) back extrusion and flow forming , and c) deep drawing and subsequent spinning. Single, and multicell cavities have been successfully fabricated by the above techniques. Accelerating voltage gradients in excess of 30MV/m have been achieved in these cavities. One of the problems that has persisted is process repeatability. In our view the main fabrication problem associated with the manufacture of polycrystalline Nb cavities by sheet or tube has been the persistence of initial microstructural non-uniformity of starting raw material.

Traditional practices for grain refinement of bulk Nb involve swaging, forging, or rolling lead to retention of initial cast structures, and non-uniform strain distribution in the material leading to non-uniform recrystallized microstructures. A successful thermomechanical approach to decrease the severity of this problem is to grain refine bulk Nb by severe plastic deformation (SPD) steps and subsequent annealing [3, 2] to obtain a uniform starting microstructure. The authors here present a thermomechanical processing approach by SPD involving simple shear and area reduction extrusion. The work reported here follows the development of microstructures in seamless Nb tube, fabricated by a forward extrusion technique [4]. The scope of this work is limited to recrsyatllized microstructure development and mechanical property relationships in a Nb tube formed by this novel approach.

4.3 Materials and methods

The Nb used in this study was as received in the electron- beam melted condition and had an initial RRR of 185. The as received grain size was on the order of tens of centimeters. The initial workpiece bars had nominal dimensions of 50mm x 50mm x 250mm was subjected to SPD and annealing cycles to obtain a finer and more uniform starting microstructure for the tube making process. The details of the above procedure has been presented earlier. [4]

4.3.1 Tube fabrication method

A thick walled tube of the subject material was machined from ECAE processed bar stock. It had a length of 200 mm, an outer diameter (OD) of 25 mm, and a thickness of 8 mm. It was forward extruded to obtain the desired shape with an OD of 38 mm and a thickness of 3mm. The total area reduction obtained by the forward extrusion was 3:1, which corresponds to a strain of about 1.1. This tube then underwent a shear deformation process as shown in the schematic in Figure 4.1. This innovative shear deformation process consists of two deformation steps, a shear expansion and a shear contraction step. The main highlight being the tube dimensions are unchanged after a complete cycle (expansion and contraction). The shear strain(γ) that the material receives depends on the die angle(2ϕ) . The equivalent Von- Mises ϵ_{vm} can be determined by the following relations [116]:

$$\gamma = 2cot(\phi) \tag{4.1}$$

$$\epsilon_{vm} = \frac{\gamma}{\sqrt{3}} \tag{4.2}$$

For $2\phi = 135^o$ a total $\epsilon_{vm} = 1.9$ is achieved. This corresponds to four passes of shear deformation through a 135^o die angle as illustrated in Fig 1. Results on

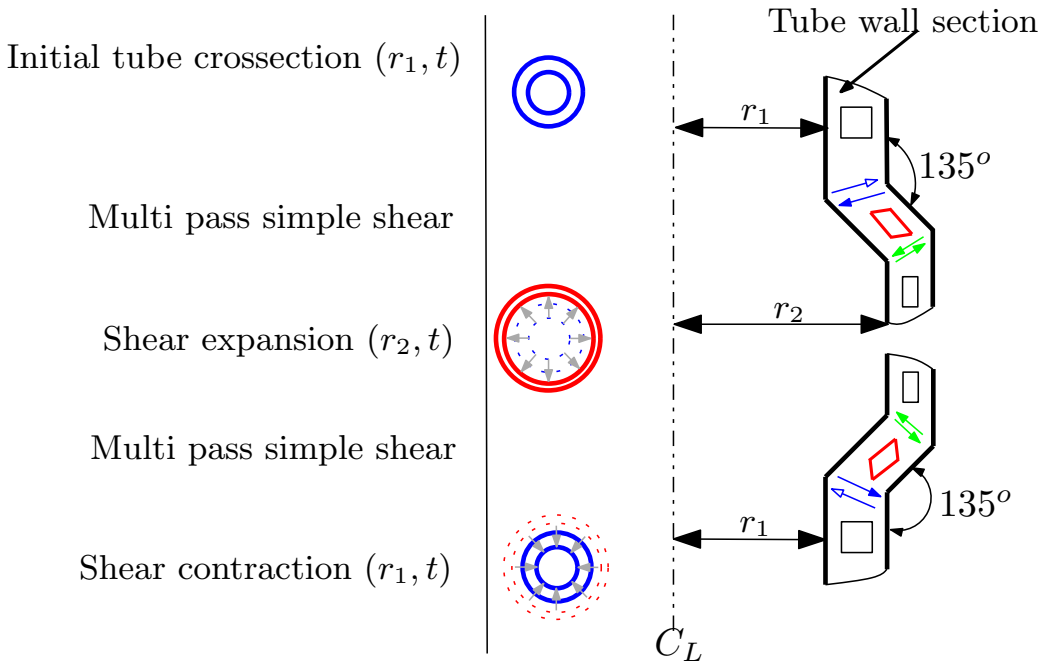

Figure 4.1: Illustration of the symmetric shear processing process of the tube, whereby a tube of initial internal radius of r_1 is expanded to r_2, and finally contracted back to the initial r_1. During the whole process the thickness of the tube remains a constant.

tubes reported in this work have undergone only one tube expansion process, which corresponds to a (evm) of 0.95. Two different thermo-mechanical conditions were considered: with and without intermediate annealing between the area reduction and shear expansion steps. All recrystallization heat treatments were done under moderate vacuum conditions($< 1x10^{-5}$ torr) for two hours.

4.3.2 Microstructure characterization and mechanical testing

Optical metallography was performed on all the tube samples, to obtain representative microstructural details along different crossections of the tube. Standard sample preparation techniques were employed to grind and polish the Xray diffraction was performed on the polished sample sections using a Bruker D8 Discover Diffractometer with a Cu Ka radiation at 40KV and 40mA. The slit width used was 1mm in all cases. The pole figures (PFs) were plotted and further analyzed using a open source toolbox for MATLAB called MTeX [115].

Vickers microhardness (HV) tests were done using a Leco LM300 AT microhardness machine; all the samples were mounted in bakelite and polished flat; the load and dwell time used was 300g and 13s respectiveley. Tensile tests were performed on recrystallized tube material, in the longitudinal (LD) and circumferential (CD) directions. The circumferential tensile specimens were cut out from the tube by flattening out a section of the tube in the as worked condition, which was followed by subsequent recrystallization heat treatment. Figure 4.2. shows the orientation of the samples with respect to the co-ordinate axis of the tube.

4.4 Results

4.4.1 Microstructures in recrystallized tubes

Representative micrographs of the recrystallized tubes are shown in Figure 4.3-4.5. The crossections of the area reduced (AR) tube as shown in Figure 4.3, and

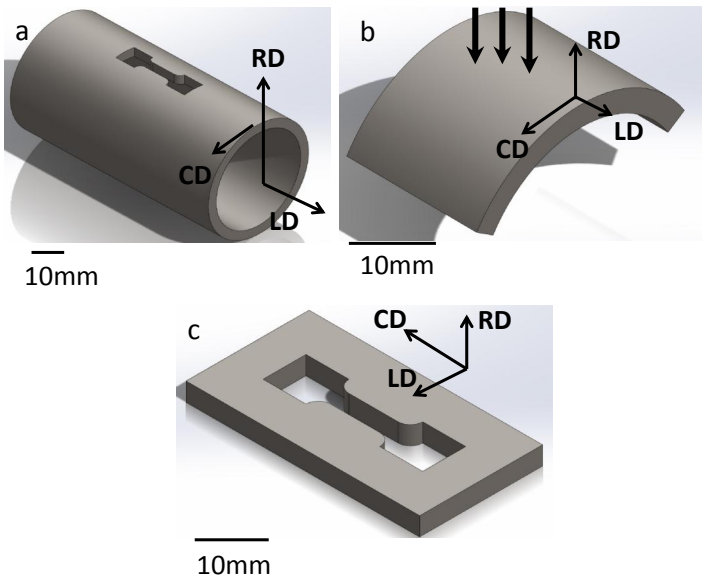

Figure 4.2: Schematic of the cutting plan for the tensile test samples: a) longitudinal direction (LD) sample as cut from the tube, b) circumferential direction (CD) sample cut from tube, and c) tensile specimen cut along CD after flattening.

shear expansion(SE) with intermediate anneal in Figure 4.4 show grain size banding. The average grain size in the finer regions of the banded microstructure is about 10μm. The microstructure bands seem to originate from the free surface of the tube. There is no clear indication that these bands are uniformly distributed around the circumference of the tube. The angle of the bands, relative to the tube outside surface is shallower for the AR tube, compared to the SE tube. The SE tube with no intermediate annealing reduced banding with an average grain size of 20$\pm$17 μm as seen in Figure 4.5. Table 4.1, provides a summary of the grain sizes for the various cases. The large standard deviation values are indicative of grain size banding in the material.

The textures observed in the recrystallized tubes correspond to common b.c.c

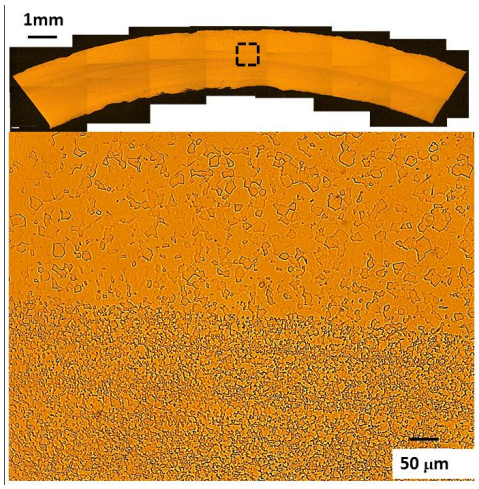

Figure 4.3: Representative macrograph of area reduced tube after recrystallization at 900°C. Banding of the microstructure in the central region was observed in these samples; a representative micrograph of one such band is shown.

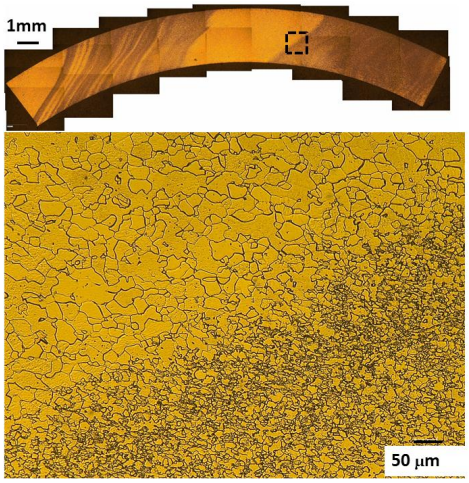

Figure 4.4: Representative macrograph of the as shear processed tube with intermediate annealing after heat treatment of 900°C. Banding of the microstructure was observed transmitted from inner to the outer surface were consistently observed along the circumference.

Table 4.1: Summary of the microstructure obtained during different thermomechanical processing conditions

Condition	Grain size (μm)	Predominant Texture	
	CD	{hkl} ‖ RD ¡uvw¿ ‖ CD	Intensity (m.r. d)
Area Reduction	63±34	(0.0 1.0 0.0) ⟨0.7 0 0.7⟩	9.4
SE- Intermediate Anneal	40±18	(0.0 0.0 1.0) ⟨-0.8 -0.6 0.0⟩	9.0
SE- No intermediate Anneal	20±17	(0.1 0.1 0.9) ⟨-0.6 0.7 0.0⟩	6.0

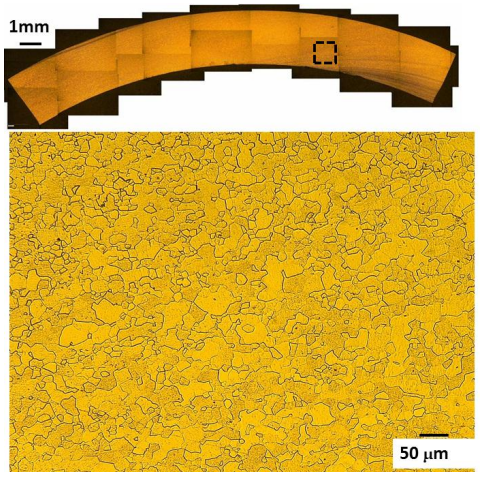

Figure 4.5: Representative macrograph of the as shear processed tube with no intermediate annealing after heat treatment of 900^{o}C. There were no consistent bands that were observed in this material. There was only one section along the circumference that showed macroscopic banding and is as presented.

fiber textures, and are represented by the pole figure maps in Fig. 6(a-c). The main texture components observed in the recrystallized materials depend on the thermomechanical heat treatment. The AR sample has a strong $\langle 010 \rangle$ ||RD and $\rangle 101 \langle$ ||CD with an intensity of 9.4 m.r.d (Figure4.6(a)). The texture components are different in the shear processed samples and vary slightly depending on the thermomechanical processing steps. The shear processed sample with intermediate annealing, has a predominant (001)||RD texture component which is rotated about the [001] axis by a 30^{o}C , with a maximum intensity of 9.0 m.r.d as shown in Figure4.6(b). The sample with no intermediate annealing shows similar texture components to the previous sample, however the axis is not aligned perfectly with the cube component, as observed from the pole figures Figure4.6(c). The maximum intensity of texture component is lower than previous cases and corresponds to 6.0 m.r.d. It can represented by the following directions: (0.12, 0.14,0.98)|| RD and [0.65,-0.76,0.03]|| CD

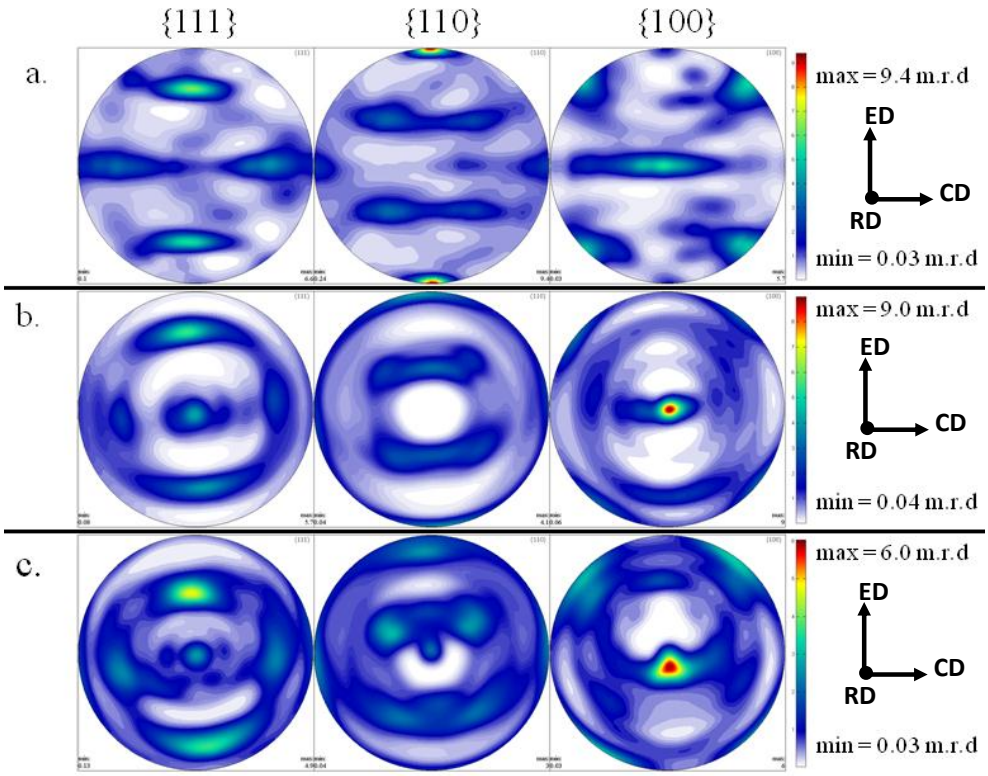

Figure 4.6: {111},{110}, and {100} pole figures of thermomechanically processed samples after recrystallization annealing: a) as area reduced, b) one pass shear expansion with intermediate annealing, and c) one pass shear expansion with no intermediate annealing.

4.4.2 Mechanical testing

The Vickers Hardness (HV)of all the recrystallized samples was between 60-80, in all cases indicating complete recrystallization. Tensile tests conducted along the CD and ED directions of the different tube samples are as shown in Figure 4.7(a-c). A summary of the tensile results is presented in Table 2. The AR tube had similar tensile properties in the CD and LD directions, as seen in Figure 4.7(a), with a strain hardening exponent (n) of 0.16, an ultimate tensile strength (UTS) of about 205 MPa, and a ductility of 35 to 40 percent along orthogonal directions. The mechanical properties of the shear processed sample depended on the intermediate anneal. The SE sample with an intermediate anneal had varying n values depending on the direction of testing, with a low value of 0.12 in CD compared to 0.25 in LD. The variation in UTS and strain at failure was not significant. For the SE sample with no intermediate annealing, the UTS values varied depending on the testing direction, with the strength in the LD direction being greater than the CD direction. However, there was no difference in strain hardening or failure strain depending on the direction of testing.

4.5 Discussion

The microstructure characteristics of the tube material indicates grain size banding that occurs in tube crossections. It is most severe in the case of the shear expanded tube with intermediate annealing than in the tube with no intermediate annealing as seen in Figures 4.3-4.5. The occurrence of banding is related to instabilities in the flow of the material during forming, and can occur due to: a) precursor non-uniform microstructure and local chemistry variations, b) non-uniform deformation zone geometry during deformation, and c) frictional effects between the die and workpiece. The material used in this study was pre-processed to a total strain of

Table 4.2: Summary of Mechanical Properties

Condition	**Hardness (HV)**	**Tensile Properties**					
		n		**UTS (MPa)**		**Strain at failure (%)**	
		LD	**CD**	**LD**	**CD**	**LD**	**CD**
Area Reduction	72 ± 7	0.16	0.16	210	205	37	42
SE- Intermediate Anneal	75 ± 10	0.25	0.12	172	187	47	39
SE- No intermediate Anneal	67 ± 3	0.2	0.2	202	172	45	46

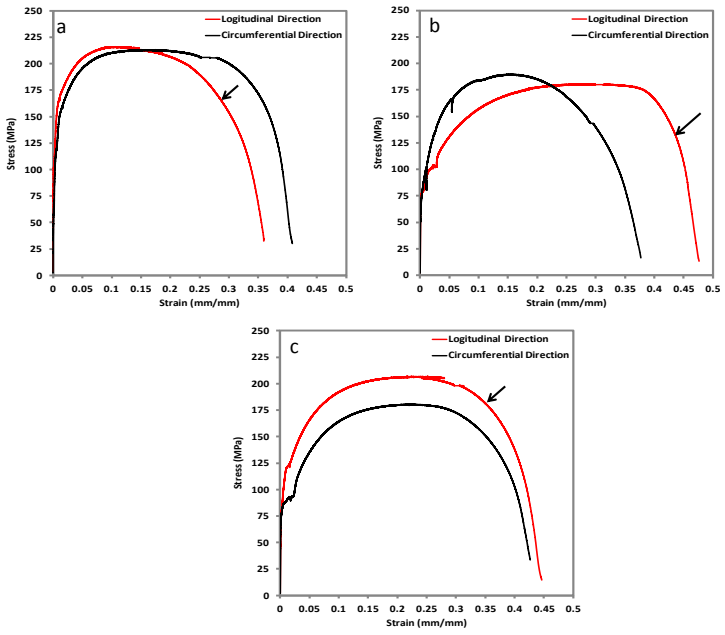

Figure 4.7: Tensile tests of recrystallized specimens in the longitudinal and circumferential directions: a) as area reduced, b) shear expansion with intermediate annealing, and c) shear expansion with no intermediate annealing.

approximately 9, with intermediate recrystallization. This leads to severe breakdown of grain size and hence reduced deformation banding. Hence it is unlikely that the origin of the deformation banding in this case is due to the precursor starting microstructure.

The non uniform deformation zone during shear processing with sharp die angles is restricted to about 0.1 times the characteristic thickness, hence we do not expect the deformation bands to originate from the deformation zone geometry changes along the thickness of the tube [117].

The bands running from the outer to inner surface of the tube as seen in Figure 4.4., indicate that friction may be responsible for causing non-uniform deformation and instability, leading to grain and possible texture banding. These sorts of de-

formation bands are often seen in material processing operations when high contact friction conditions are experienced (eg extrusion, rolling etc) [75, 108]. The surface to volume ratio is high for processing a tubular material; hence friction instabilities could propagate through the thickness of the sample if the flow stress of the material is low, as in the case of annealed Nb.

The textures that evolve depend on the processing. The area reduction texture is different from the shear processed texture. During area reduction the predominant texture components belong to the family of $\{100\}\ \langle 110\rangle$, and for the shear deformation condition a rotated cube component i.e. $\{100\ \}$ is developed. For the shear deformation without any intermediate annealing, the texture component is offset from the rotated cube component as seen in Figure 4.4(c), and is also weaker than all the other textures. The reason for the reduced strength and offset is directly related to the rigid body rotation that the material undergoes while deforming through the die, and is a characteristic of shear deformation textures undergoing ECAE. This spreading of orientations is often attributed to rapid grain refinement and finer grain size in processed microstructures. [117, 134, 149, 11]. This is a possible explanation for the finer grain sizes that are observed at the same recrystallization temperature in the shear processed sample (20 ± 7) without intermediate annealing.

As observed from the tensile test results, the area reduced sample shows very similar flow characteristics in perpendicular directions LD and CD. The major texture component in this sample is: [101]||LD, [010]||RD. A cross product of these directions indicates that the CD direction in this sample is along $[10\overline{1}]$. This implies that the tensile test for this sample was conducted along two $\langle 110\rangle$ directions, and hence the mechanical properties are very similar. The shear processed sample that underwent intermediate annealing, indicates a major rotated cube component (100)||RD. The tensile tests for this sample were performed along $[\overline{4},\overline{3},0]$||CD and $[3,\overline{4},0]$||LD. These

rotations about the cube are not symmetry related and one does not expect the tensile properties to be similar.

For the shear processed sample without any intermediate annealing the tensile tests were carried out along: $[7,\overline{8},0]\|$ LD, and $[7,\ 6,\overline{2}]\|$ CD. In general the strain to failure is very similar in most cases. This could be a result of polycrystalline deformation, where multiple slip systems are available for deformation. However, it appears that the UTS, and n could be a good indicator for the differences in textural components.

The grain size banding as seen in the shear processed sample which underwent intermediate annealing may have led to a decrease in the strain hardening exponent in the CD direction, suggesting localized deformation. The effect of banding on the strain to failure is however unclear. Further, work in this area including micro-texture characterization can provide insight into the nature of microstructural bands and their possible causes and strategies to eliminate them.

4.6 Conclusions

The processing methodology proposed is suitable for obtaining fine grain sizes, and textures in a seamless Nb tube with a grainsize of 20 μm and ductility over 40 percent% by shear processing steps. This processing approach has an unlimited strain space to refine the microstructure and could lead to a tube with fine grain size and favorable texture for hydroforming applications.

5. SUMMARY AND CONCLUSIONS

This chapter contains a summary of the key findings and conclusions that are supported by results presented and discussed thus far.

5.1 Key Findings

5.1.1 Nb bi-crystal study

- The deformation of the bi-crystal depends on the initial orientations of the individual crystals. Crystal I deforms predominantly in the form of bands in a matrix; whereas Crystal 2 deforms in a homogeneous manner. The effect of the grain to grain interactions appear to be localized in the GB region at least during the first ECAE pass.

- Irrespective of the initial orientations the initial strong texture of the large grain Nb material reduces by orientation splitting, and new orientations are created during the process. The new orientations created do not follow the ideal simple shear texture proposed. However, they are oriented such that the $\{110\} \parallel$ SSP, and $\langle 111 \rangle \parallel$ SSD. Grain refinement in a large grain sample occurs by different regions splitting to different stable components

- Different regions in the individual crystal of the bi-crystal oriented towards similar stable orientations after two ECAE passes. regions around the GB also oriented towards these stable orientations.

- One of the common notion that Route 2C is not a preferred route for grain refinement is misleading. The HAGBs created were found to depend on orientation, for the same processing route. In the case of Crystal 2, the percent of HAGBs after deformation was up to 40%.

5.1.2 Microstructures in Nb bars produced by ECAE

- ECAE can be employed effectively in thermomechanical processing of Nb to obtain grain size control ranging from grain sizes of tens to hundreds of microns by controlling the heat treatment and processing routes.

- Texture strengths produced during multi-pass ECAE depends on the processing route. Processing dependence on the route in terms of decreasing the initial texture was found to follow this relationship: 4B⟩4A⟩4E⟩4B$_c$. On recrystallization heat treatment of the as worked ECAE material, the texture strength drops further. 4B$_c$ had the lowest texture strength after recrystallization.

- Tight grain size control around 20μm was obtained in Nb bars that were processed by multi pass ECAE and recrystallization.

- Nb processed by different routes of multi pass ECAE, and recrystallization on further deformation in a Cu matrix maintained their circularity, small deviations in cross section were noticed because of end effects created by ECAE.

5.1.3 Microstructure in Seamless Nb tubes

- The ECAE process could be successfully employed to process Nb tubes. Using this novel technique an EB welded Nb tube was processed to improve the mechanical properties of the weld. The weld and the parent material were homogenized in terms of mechanical properties. The strength and ductility of the weld and the parent material were comparable after the thermomechanicalprocessing operation.

- A new process for processing Nb tubes directly by simple shear called t-ECAE, was developed.

- Microstructures produced by t-ECAE show grain refinement in as extruded tubes; and evolution of new texture components such as {111}‖ ED after simple shear processing.

The conclusions reached over the course of this study are numerous and are varying in significance. In no specific order these conclusions are as follows:

- The Bi-crystal study indicates that the initial Nb deformation is dependent on the initial orientations, and so does the HAGB ratios after processing. This is critical to the development of processes that need uniform recrystallization.

- The convergence of orientations also implies that processing schedules could be created to create a consistently same Nb product with different starting Nb material provided that the chemistry is the same.

- Simple crystal plasticity theories (example: Taylor) fail to predict the spatially varied deformation seen in a bi-crystal. The question of how a grain reaches a stable orientation in a particular region spatially seems to be a challenge for models. This experiment shows why a microstructure model that tracks microstructure variables spatially is needed. For all technological applications spatial variation in microstructure are important, as they are correlated to important processing operations such as annealing, recrystallization and precipitate formation.

- ECAE of polycrystals can be ideally used to create low texture fine grain size poly crystalline material in fcc, and bcc cubic metals through processing and annealing related phenomenon

REFERENCES

[1] M Al-Maharbi, I Karaman, IJ Beyerlein, D Foley, KT Hartwig, LJ Kecskes, and SN Mathaudhu. Microstructure, crystallographic texture, and plastic anisotropy evolution in an mg alloy during equal channel angular extrusion processing. *Materials Science and Engineering: A*, 528(25):7616–7627, 2011.

[2] S Balachandran, RE Barber, Y Huang, H Miao, JA Parrell, RB Griffin, and KT Hartwig. Influences of different ecae routes on filament deformation in cu clad nb composite wires. *Applied Superconductivity, IEEE Transactions on*, 21(3):2584–2587, 2011.

[3] S Balachandran, RE Barber, Y Huang, H Miao, JA Parrell, S Hong, RB Griffin, and KT Hartwig. Fine grained nb for internal tin nbsn conductors. In *AIP Conference Proceedings*, volume 1219, page 216, 2010.

[4] S Balachandran, R Elwell, D Kang, R Barber, T Bieler, and K Hartwig. Nb tubes for seamless srf cavities. *IEEE Transactions on Applied Superconductivity*, 23(3):7100904–7100904, 2013.

[5] S Balachandran, KT Hartwig, DC Baars, SN Mathaudhu, TR Bieler, T Pyon, and RE Barber. Fabrication of tantalum sheet for superconductor diffusion barriers. *Applied Superconductivity, IEEE Transactions on*, 19(3):2606–2609, 2009.

[6] S Balachandran, N Seymour, R Mezyenski, R Barber, and KT Hartwig. Microstructure and mechanical properties of fine grain seamless nb tube by a novel shear deformation process. In *ADVANCES IN CRYOGENIC ENGI-*

NEERING: Transactions of the International Cryogenic Materials Conference ICMC Volume 60, volume 1574, pages 197–203. AIP Publishing, 2014.

[7] GW Bang and M Meshi. Deformation of pure and oxygen-doped niobium single-crystals with tensile axis on (111)-(011) at 77 k. In *JOURNAL OF METALS*, volume 32, pages 61–61. Minerals Metals Materials Society 420 Commonwealth Dr, Warrendale, PA 15086, 1980.

[8] RE Barber, T Dudo, PB Yasskin, and KT Hartwig. Product yield for ecae processing. *Scripta materialia*, 51(5):373–377, 2004.

[9] E Barzi, N Andreev, B Bordini, L Del Frate, VV Kashikhin, D Turrioni, R Yamada, and AV Zlobin. Instabilities in transport current measurements of nb 3 sn strands. *Applied Superconductivity, IEEE Transactions on*, 15(2):3364–3367, 2005.

[10] IJ Beyerlein, RD Field, KT Hartwig, and CT Necker. Texture development in two-pass ecae-processed beryllium. *Journal of Materials Science*, 43(23-24):7465–7473, 2008.

[11] Irene J Beyerlein and LS Tóth. Texture evolution in equal-channel angular extrusion. *Progress in Materials Science*, 54(4):427–510, 2009.

[12] A Bhowmik, S Biswas, S Suwas, RK Ray, and D Bhattacharjee. Evolution of grain-boundary microstructure and texture in interstitial-free steel processed by equal-channel angular extrusion. *Metallurgical and Materials Transactions A*, 40(11):2729–2742, 2009.

[13] TR Bieler, NT Wright, F Pourboghrat, C Compton, KT Hartwig, D Baars, A Zamiri, S Chandrasekaran, P Darbandi, H Jiang, et al. Physical and me-

chanical metallurgy of high purity nb for accelerator cavities. *Physical Review Special Topics-Accelerators and Beams*, 13(3):031002, 2010.

[14] DK Bowen, JW Christian, and G Taylor. Deformation properties of niobium single crystals. *Canadian Journal of Physics*, 45(2):903–938, 1967.

[15] TH Carnes. Ultra fine grained production in rrr niobium for rf cavities by ecae. 2009.

[16] JW Christian. Some surprising features of the plastic deformation of body-centered cubic metals and alloys. *Metallurgical Transactions A*, 14(7):1237–1256, 1983.

[17] JB Clark, RK Garrett, TL Jungling, RA Vandermeer, and CL Vold. Effect of processing variables on texture and texture gradients in tantalum. *Metallurgical Transactions A*, 22(9):2039–2048, 1991.

[18] JB Clark Jr, RK Garrett Jr, TL Jungling, and RI Asfahani. Influence of initial ingot breakdown on the microstructural and textural development of high-purity tantalum. *Metallurgical Transactions A*, 22(12):2959–2968, 1991.

[19] LD Cooley, D Burk, C Cooper, N Dhanaraj, M Foley, D Ford, K Gould, D Hicks, R Novitski, A Romanenko, et al. Impact of forming, welding, and electropolishing on pitting and the surface finish of srf cavity niobium. *IEEE Transactions on Applied Superconductivity*, 21(3):2609–2614, 2011.

[20] LR Cornwall, KT Hartwig, RE Goforth, and SL Semiatin. The equal channel angular extrusion process for materials processing. *Materials characterization*, 37(5):295–300, 1996.

[21] R Crooks et al. Production of seamless superconducting radio frequency cavities from ultra-fine grained niobium, phase ii final report. Technical report, Black Laboratories, LLC, 2009.

[22] DR Dietderich and A Godeke. Nb_3sn research and development in the usa–wires and cables. *Cryogenics*, 48(7):331–340, 2008.

[23] IL Dillamore and H Katoh. A comparison of the observed and predicted deformation textures in cubic metals. *Metal science*, 8(1):21–27, 1974.

[24] D Dorner, S Zaefferer, and D Raabe. Retention of the goss orientation between microbands during cold rolling of an fe3% si single crystal. *Acta Materialia*, 55(7):2519–2530, 2007.

[25] MS Duesbery and RA Foxall. A detailed study of the deformation of high purity niobium single crystals. *Philosophical Magazine*, 20(166):719–751, 1969.

[26] MS Duesbery, RA Foxall, and PB Hirsch. The plasticity of pure niobium single crystals. *Le Journal de Physique Colloques*, 27(C3):C3–193, 1966.

[27] CG Dunn. Cold-rolled and primary recrystallization textures in cold-rolled single crystals of silicon iron. *Acta metallurgica*, 2(2):173–183, 1954.

[28] JW Edington. The mechanical properties, dislocation sub-structure and density in niobium single crystals deformed at high strain rates. *Philosophical Magazine*, 20(165):531–538, 1969.

[29] O Engler, CN Tomé, and M-Y Huh. A study of through-thickness texture gradients in rolled sheets. *Metallurgical and Materials Transactions A*, 31(9):2299–2315, 2000.

[30] PRV Evans. Dislocation etch pit studies in annealed and deformed polycrystalline niobium. *Journal of the Less Common Metals*, 6(4):253–265, 1964.

[31] S Ferrasse, KT Hartwig, RE Goforth, and VM Segal. Microstructure and properties of copper and aluminum alloy 3003 heavily worked by equal channel angular extrusion. *Metallurgical and Materials Transactions A*, 28(4):1047–1057, 1997.

[32] S Ferrasse, VM Segal, SR Kalidindi, and F Alford. Texture evolution during equal channel angular extrusion: Part i. effect of route, number of passes and initial texture. *Materials Science and Engineering: A*, 368(1):28–40, 2004.

[33] M Field, Y Zhang, H Miao, M Gerace, and J Parrell. Optimizing nb_3sn conductors for high field magnet applications. 2014.

[34] DC Foley, M Al-Maharbi, KT Hartwig, I Karaman, LJ Kecskes, and SN Mathaudhu. Grain refinement vs. crystallographic texture: Mechanical anisotropy in a magnesium alloy. *Scripta Materialia*, 64(2):193–196, 2011.

[35] RA Foxall, MS Duesbery, and PB Hirsch. The deformation of niobium single crystals. *Canadian Journal of Physics*, 45(2):607–629, 1967.

[36] Y Fukuda, K Oh-ishi, M Furukawa, Z Horita, and TG Langdon. The application of equal-channel angular pressing to an aluminum single crystal. *Acta materialia*, 52(6):1387–1395, 2004.

[37] Y Fukuda, K Oh-ishi, M Furukawa, Z Horita, and TG Langdon. Influence of crystal orientation on ecap of aluminum single crystals. *Materials Science and Engineering: A*, 420(1):79–86, 2006.

[38] Y Fukuda, K Oh-Ishi, M Furukawa, Z Horita, and TG Langdon. Influence of crystal orientation on the processing of copper single crystals by ecap. *Journal of materials science*, 42(5):1501–1511, 2007.

[39] M Furukawa, Y Fukuda, K Oh-Ishi, ZJ Horita, and TG Langdon. An investigation of deformation in copper single crystals using equal-channel angular pressing. In *Materials Science Forum*, volume 503, pages 113–118. Trans Tech Publ, 2006.

[40] AJ Garratt-Reed and G Taylor. Optical and electron microscopy of niobium crystals deformed below room temperature. *Philosophical Magazine A*, 39(5):597–646, 1979.

[41] AA Gazder, W Cao, CHJ Davies, and EV Pereloma. An ebsd investigation of interstitial-free steel subjected to equal channel angular extrusion. *Materials Science and Engineering: A*, 497(1):341–352, 2008.

[42] AK Ghosh, LD Cooley, and AR Moodenbaugh. Investigation of instability in high j_c nb_3sn strands. *Applied Superconductivity, IEEE Transactions on*, 15(2):3360–3363, 2005.

[43] A Godeke, MC Jewell, CM Fischer, AA Squitieri, PJ Lee, and DC Larbalestier. The upper critical field of filamentary nb_3sn conductors. *Journal of applied physics*, 97(9):093909, 2005.

[44] I Gonin, TESLA Collaboration, et al. *Hydroforming Test of Back Extruded Niobium Tube*. Dt. Elektronen-Synchrotron DESY, MHF-SL Group, 1998.

[45] D Goran, JJ Fundenberger, E Bouzy, W Skrotzki, S Suwas, T Grosdidier, and LS Toth. Local texture and microstructure in cube-oriented nickel single

crystal deformed by equal channel angular extrusion. *Philosophical Magazine*, 91(2):281–299, 2011.

[46] RA Graham. Single crystal technology for making rrr niobium sheet. In *Single Crystal-Large Grain Niobium Technology: International Niobium Workshop*, volume 927, pages 21–40. AIP Publishing, 2007.

[47] MA Grinfeld. The stress driven instability in elastic crystals: Mathematical models and physical manifestations. *Journal of Nonlinear Science*, 3(1):35–83, 1993.

[48] T Grosdidier, J-J Fundenberger, D Goran, E Bouzy, S Suwas, W Skrotzki, and LS Tóth. On microstructure and texture heterogeneities in single crystals deformed by equal channel angular extrusion. *Scripta Materialia*, 59(10):1087–1090, 2008.

[49] CF Gu and LS Tóth. The origin of strain reversal texture in equal channel angular pressing. *Acta Materialia*, 59(14):5749–5757, 2011.

[50] CF Gu, LS Tóth, and CHJ Davies. Effect of strain reversal on texture and grain refinement in route c equal channel angular pressed copper. *Scripta materialia*, 65(2):167–170, 2011.

[51] CK Gupta and AK Suri. *Extractive metallurgy of niobium*. CRC press, 1993.

[52] K Han, JD Embury, JR Sims, LJ Campbell, H-J Schneider-Muntau, VI Pantsyrnyi, A Shikov, Al Nikulin, and A Vorobieva. The fabrication, properties and microstructure of cu–ag and cu–nb composite conductors. *Materials Science and Engineering: A*, 267(1):99–114, 1999.

[53] W Han, S Wu, C Huang, S Li, and Z Zhang. Orientation design for enhancing deformation twinning in cu single crystal subjected to equal channel angular pressing. *Advanced Engineering Materials*, 10(12):1110–1113, 2008.

[54] N Hansen, RF Mehl, et al. New discoveries in deformed metals. *Metallurgical and materials transactions A*, 32(12):2917–2935, 2001.

[55] M Haouaoui and EA Hartwig, KTand Payzant. Effect of strain path on texture and annealing microstructure development in bulk pure copper processed by simple shear. *Acta materialia*, 53(3):801–810, 2005.

[56] B Harris. Solution hardening in niobium. *physica status solidi (b)*, 18(2):715–730, 1966.

[57] KT Hartwig, SN Mathaudhu, HJ Maier, and I Karaman. Hardness and microstructure changes in severely deformed and recrystallized tantalum. *Ultrafine Grained Materials II*, pages 151–160, 2002.

[58] JJ Hauser and B Chalmers. The plastic deformation of bicrystals of fcc metals. *Acta Metallurgica*, 9(9):802–818, 1961.

[59] CD Hawes, PJ Lee, and DC Larbalestier. Measurements of the microstructural, microchemical and transition temperature gradients of a15 layers in a high-performance nb3sn powder-in-tube superconducting strand. *Superconductor Science and Technology*, 19(3):S27, 2006.

[60] SS Hazra, EV Pereloma, and AA Gazder. Microstructure and mechanical properties after annealing of equal-channel angular pressed interstitial-free steel. *Acta Materialia*, 59(10):4015–4029, 2011.

[61] RWK Honeycombe. The plastic deformation of metals. *Edward Arnold, London W 1 Z 8 LL. 1975, 477 p(Book).*, 1975.

[62] SI Hong and MA Hill. Microstructural stability of cu–nb microcomposite wires fabricated by the bundling and drawing process. *Materials Science and Engineering: A*, 281(1):189–197, 2000.

[63] Sun Ig Hong, MA Hill, Y Sakai, JT Wood, and JD Embury. On the stability of cold drawn, two-phase wires. *Acta metallurgica et materialia*, 43(9):3313–3323, 1995.

[64] M Hoseini, M Meratian, M R Toroghinejad, and JA Szpunar. Texture contribution in grain refinement effectiveness of different routes during ecap. *Materials Science and Engineering: A*, 497(1):87–92, 2008.

[65] MF Hupalo and HRZ Sandim. The annealing behavior of oligocrystalline tantalum deformed by cold swaging. *Materials Science and Engineering: A*, 318(1):216–223, 2001.

[66] S Ikeno and E Furubayashi. Dislocation behavior in pure niobium at low temperatures. *physica status solidi (a)*, 27(2):581–590, 1975.

[67] P Jepson, H Uhlenhut, and P Kumar. Refractory metal plates with uniform texture and methods of making the same, February 20 2002. US Patent App. 10/079,286.

[68] H Jiang, D Baars, A Zamiri, C Antonie, P Bauer, TR Bieler, F Pourboghrat, C Compton, and TL Grimm. Mechanical properties of high rrr niobium with different texture. *Applied Superconductivity, IEEE Transactions on*, 17(2):1291–1294, 2007.

[69] H Jiang, TR Bieler, C Compton, and TL Grimm. Cold rolling evolution in high purity niobium using a tapered wedge specimen. *Physica C: Superconductivity*, 441(1):118–121, 2006.

[70] JS Kallend, UF Kocks, AD Rollett, and H-R Wenk. Operational texture analysis. *Materials Science and Engineering: A*, 132:1–11, 1991.

[71] D Kang, DC Baars, TR Bieler, G Ciovati, C Compton, TL Grimm, and AA Kolka. Characterization of large grain nb ingot microstructure using oim and laue methods. In *Proc. 15th Int. Conf. on RF Superconductivity*, pages 890–897, 2011.

[72] Peter Kneisel, GR Myneni, G Ciovati, J Sekutowicz, and T Carneiro. Development of large grain/single crystal niobium cavity technology at jefferson lab. In *Single Crystal- Large Grain Niobium Technology: Proceedings of the International Niobium Workshop(AIP Conference Proceedings Volume 927)*, volume 927, pages 84–97, 2007.

[73] UF Kocks, T Hasegawa, and RO Scattergood. On the origin of cell walls and of lattice misorientations during deformation. *Scripta metallurgica*, 14(4):449–454, 1980.

[74] CS Lee and BJ Duggan. A simple theory for the development of inhomogeneous rolling textures. *Metallurgical Transactions A*, 22(11):2637–2643, 1991.

[75] CS Lee and BJ Duggan. Deformation banding and copper-type rolling textures. *Acta metallurgica et materialia*, 41(9):2691–2699, 1993.

[76] PJ Lee, CM Fischer, MT Naus, AA Squitieri, and DC Larbalestier. The microstructure and microchemistry of high critical current nb_3sn strands manu-

factured by the bronze, internal-sn and pit techniques. *Applied Superconductivity, IEEE Transactions on*, 13(2):3422–3425, 2003.

[77] PJ Lee and DC Larbalestier. Compositional and microstructural profiles across nb $_3$ sn filaments produced by different fabrication methods. *Applied Superconductivity, IEEE Transactions on*, 11(1):3671–3674, 2001.

[78] PJ Lee and DC Larbalestier. Microstructure, microchemistry and the development of very high nb $_3$ sn layer critical current density. *Applied Superconductivity, IEEE Transactions on*, 15(2):3474–3477, 2005.

[79] PJ Lee and DC Larbalestier. Microstructural factors important for the development of high critical current density nb_3sn strand. *Cryogenics*, 48(7):283–292, 2008.

[80] S Li, IJ Beyerlein, DJ Alexander, and SC Vogel. Texture evolution during equal channel angular extrusion: effect of initial texture from experiment and simulation. *Scripta materialia*, 52(11):1099–1104, 2005.

[81] S Li, AA Gazder, IJ Beyerlein, EV Pereloma, and CHJ Davies. Effect of processing route on microstructure and texture development in equal channel angular extrusion of interstitial-free steel. *Acta materialia*, 54(4):1087–1100, 2006.

[82] F Louchet and LP Kubin. Dislocation substructures in the anomalous slip plane of single crystal niobium strained at 50 k. *Acta Metallurgica*, 23(1):17–21, 1975.

[83] SN Mathaudhu, S Blum, RE Barber, and KT Hartwig. Severe plastic deformation of bulk nb for nb 3 sn superconductors. *Applied Superconductivity, IEEE Transactions on*, 15(2):3438–3441, 2005.

[84] SN Mathaudhu and KT Hartwig. Grain refinement and recrystallization of heavily worked tantalum. *Materials Science and Engineering: A*, 426(1):128–142, 2006.

[85] PS Mathur and WA Backofen. Mechanical contributions to the plane-strain deformation and recrystallization textures of aluminum-killed steel. *Metallurgical Transactions*, 4(3):643–651, 1973.

[86] M Matsuo, T Sakai, and Y Suga. Origin and development of through-the-thickness variations of texture in the processing of grain-oriented silicon steel. *Metallurgical Transactions A*, 17(8):1313–1322, 1986.

[87] CA Michaluk, MM Nowell, and RA Witt. Quantifying the recrystallization texture of tantalum. *JOM*, 54(3):51–54, 2002.

[88] C Mishra, Sand Därmann and K Lücke. On the development of the goss texture in iron-3% silicon. *Acta Metallurgica*, 32(12):2185–2201, 1984.

[89] TE Mitchell, RA Foxall, and PB Hirsch. Work-hardening in niobium single crystals. *Philosophical Magazine*, 8(95):1895–1920, 1963.

[90] TE Mitchell and WA Spitzig. Three-stage hardening in tantalum single crystals. *Acta metallurgica*, 13(11):1169–1179, 1965.

[91] H Miyamoto, U Erb, T Koyama, T Mimaki, A Vinogradov, and S Hashimoto. Microstructure and texture development of copper single crystals deformed by

equal-channel angular pressing. *Philosophical magazine letters*, 84(4):235–243, 2004.

[92] H Miyamoto, A Vinogradov, S Hashimoto, and R Yoda. Formation of deformation twins and related shear bands in a copper single crystal deformed by equal-channel angular pressing for one pass at room temperature. *Materials transactions*, 50(8):1924–1929, 2009.

[93] BL Mordike and G Rudolph. Three-stage hardening in tantalum deformed in compression. *Journal of Materials Science*, 2(4):332–338, 1967.

[94] H Mughrabi. Dislocation wall and cell structures and long-range internal stresses in deformed metal crystals. *Acta metallurgica*, 31(9):1367–1379, 1983.

[95] A Nadai. Theory of flow and fracture of solids, v. 2. 1950.

[96] J Nagakawa and M Meshii. The deformation of niobium single crystals at temperatures between 77 and 4.2 k. *Philosophical Magazine A*, 44(5):1165–1191, 1981.

[97] EV Nesterova, B Bacroix, and C Teodosiu. Experimental observation of microstructure evolution under strain-path changes in low-carbon if steel. *Materials Science and Engineering: A*, 309:495–499, 2001.

[98] V Palmieri. Spinning of tesla-type cavities: Status of art. In *Proc. of the 9th Workshop on RF superconductivity, Santa Fe, USA*, pages 532–537, 1999.

[99] V Palmieri. Advancements on spinning of seamless multicell reentrant cavities. In *Proc. 11th Int. Workshop on RF Superconductivity*, pages 357–361, 2003.

[100] V Palmieri, R Preciso, VL Ruzinov, S Yu Stark, and S Gambalonga. Forming of seamless high beta accelerating cavities by the spinning technique. *Nuclear*

Instruments and Methods in Physics Research Section A: Accelerators, Spectrometers, Detectors and Associated Equipment, 342(2):353–356, 1994.

[101] Z Pan, F Xu, SN Mathaudhu, LJ Kecskes, WH Yin, XY Zhang, KT Hartwig, and Q Wei. Microstructural evolution and mechanical properties of niobium processed by equal channel angular extrusion up to 24 passes. *Acta Materialia*, 60(5):2310–2323, 2012.

[102] JA Parrell, Y Zhang, MB Field, P Cisek, and S Hong. High field nb_3sn conductor development at oxford superconducting technology. *Applied Superconductivity, IEEE Transactions on*, 13(2):3470–3473, 2003.

[103] JA Parrell, Y Zhang, MB Field, M Meinesz, Y Huang, H Miao, S Hong, N Cheggour, and L Goodrich. Internal tin conductors engineered for fusion and particle accelerator applications. *Applied Superconductivity, IEEE Transactions on*, 19(3):2573–2579, 2009.

[104] G Purcek, O Saray, O Kul, I Karaman, GG Yapici, M Haouaoui, and HJ Maier. Mechanical and wear properties of ultrafine-grained pure ti produced by multi-pass equal-channel angular extrusion. *Materials Science and Engineering: A*, 517(1):97–104, 2009.

[105] Dierk Raabe and K Lücke. Rolling and annealing textures of bcc metals. In *Materials Science Forum*, volume 157, pages 597–610. Trans Tech Publ, 1994.

[106] V Randle and O Engler. *Introduction to texture analysis: macrotexture, microtexture and orientation mapping*. CRC Press, 2000.

[107] CN Reid, A Gilbert, and GT Hahn. Twinning, slip and catastrophic flow in niobium. *Acta metallurgica*, 14(8):975–983, 1966.

[108] M Richert, Q Liu, and N Hansen. Microstructural evolution over a large strain range in aluminium deformed by cyclic-extrusion–compression. *Materials Science and Engineering: A*, 260(1):275–283, 1999.

[109] HG Salem, RE Goforth, and KT Hartwig. Influence of intense plastic straining on grain refinement, precipitation, and mechanical properties of al-cu-li-based alloys. *Metallurgical and Materials Transactions A*, 34(5):1153–1161, 2003.

[110] HRZ Sandim, HH Bernardi, Bert Verlinden, and D Raabe. Equal channel angular extrusion of niobium single crystals. *Materials Science and Engineering: A*, 467(1):44–52, 2007.

[111] HRZ Sandim, RE Bolmaro, RA Renzetti, MJR Sandim, KT Hartwig, SC Vogel, and D Raabe. Texture evolution as determined by in situ neutron diffraction during annealing of iron deformed by equal channel angular pressing. *Metallurgical and Materials Transactions A*, 45(10):4235–4246, 2014.

[112] HRZ Sandim, JP Martins, AL Pinto, and AF Padilha. Recrystallization of oligocrystalline tantalum deformed by cold rolling. *Materials Science and Engineering: A*, 392(1):209–221, 2005.

[113] HRZ Sandim and D Raabe. An ebsd study on orientation effects during recrystallization of coarse-grained niobium. In *Materials Science Forum*, volume 467, pages 519–524. Trans Tech Publ, 2004.

[114] HRZ Sandim and D Raabe. Ebsd study of grain subdivision of a goss grain in coarse-grained cold-rolled niobium. *Scripta materialia*, 53(2):207–212, 2005.

[115] H Schaeben, R Hielscher, and F Bachmann. Texture analysis with mtex–free and open source software toolbox. *Solid State Phenomena*, 160:63–68, 2010.

[116] VM Segal. Materials processing by simple shear. *Materials Science and Engineering: A*, 197(2):157–164, 1995.

[117] VM Segal. Equal channel angular extrusion: from macromechanics to structure formation. *Materials Science and Engineering: A*, 271(1):322–333, 1999.

[118] VM Segal, VI Reznikov, AE Drobyshevskiy, and VI Kopylov. Russian metallurgy. *Engl. Transl*, 1:115, 1981.

[119] PJ Sherwood, F Guiu, Ho-Chul Kim, and Po L Pratt. Plastic anisotropy of tantalum, niobium, and molybdenum. *Canadian Journal of Physics*, 45(2):1075–1089, 1967.

[120] Y Shimizu, Y Ito, and Y Iida. Formation of the goss orientation near the surface of 3 pct silicon steel during hot rolling. *Metallurgical Transactions A*, 17(8):1323–1334, 1986.

[121] W Singer. Seamless/bonded niobium cavities. *Physica C: Superconductivity*, 441(1):89–94, 2006.

[122] W Singer. Srf cavity fabrication and materials. 2014.

[123] W Singer, H Kaiser, X Singer, G Weichert, I Jelezov, T Khabibuline, A Skasyrskaia, P Kneisel, T Fujino, and K Saito. Hydroforming of superconducting tesla cavities. In *Proc. in the 10th Workshop on RF Superconductivity, Tsukuba, Japan*, 2001.

[124] X Singer, W Singer, I Jelezov, A Matheisen, DESY P Kneisel, et al. Hydroforming of multi-cell niobium and nbcu-clad cavities. *Thomas Jefferson National Accelerator Facility, Newport News, VA*, 2009.

[125] WA Spitzig and PD Krotz. Comparison of the strengths and microstructures of cu-20% ta and cu-20% nb in situ composites. *Acta Metallurgica*, 36(7):1709–1715, 1988.

[126] WA Spitzig, AR Pelton, and FC Laabs. Characterization of the strength and microstructure of heavily cold worked cu? nb composites. *Acta Metallurgica*, 35(10):2427–2442, 1987.

[127] R Srinivasan, GB Viswanathan, VI Levit, and HL Fraser. Orientation effect on recovery and recrystallization of cold rolled niobium single crystals. *Materials Science and Engineering: A*, 507(1):179–189, 2009.

[128] JO Stiegler, CKH Dubose, RE Reed Sr, and CJ McHargue. Dislocations in deformed and annealed niobium single crystals. *Acta Metallurgica*, 11(8):851–860, 1963.

[129] T Tajima. Success stories of rf superconductivity in the field of particle accelerators. Technical report, Los Alamos National Laboratory (LANL), 2013.

[130] S Takeuchi, T Hashimoto, and K Maeda. Plastic deformation of b. c. c. metal single crystals at very low temperature. *Trans. Jpn. Inst. Met.*, 23(2):60–69, 1982.

[131] G Taylor and JW Christian. Experiments on the deformation of niobium single crystals. i. stress versus strain curves and slip systems in compression and tension. *Philosophical Magazine*, 15(137):873–892, 1967.

[132] L Thilly, J Colin, F Lecouturier, JP Peyrade, J Grilhé, and S Askénazy. Interface instability in the drawing process of copper/tantalum conductors. *Acta materialia*, 47(3):853–857, 1999.

[133] MG Ulitchny and R Gibala. The effects of interstitial solute additions on the mechanical properties of niobium and tantalum single crystals. *Journal of the Less Common Metals*, 33(1):105–116, 1973.

[134] RZ Valiev and TG Langdon. Principles of equal-channel angular pressing as a processing tool for grain refinement. *Progress in Materials Science*, 51(7):881–981, 2006.

[135] RA Vandermeer and JB Bernal. Deformation zone geometry and texture gradients in cold rolled niobium. *Textures of Crystalline Solids*, 2:183–203, 1977.

[136] RA Vandermeer and JC Ogle. Development of preffered orientations in cold-rolled niobium (columbium). Technical report, Oak Ridge National Lab., Tenn., 1968.

[137] W Wasserbäch. Anomalous slip in high-purity niobium and tantalum single crystals. *Physica status solidi (a)*, 147(2):417–446, 1995.

[138] Q Wei, T Jiao, SN Mathaudhu, E Ma, KT Hartwig, and KT Ramesh. Microstructure and mechanical properties of tantalum after equal channel angular extrusion (ecae). *Materials Science and Engineering: A*, 358(1):266–272, 2003.

[139] H Wenk. Preferred orientation in deformed metals and rocks, an introduction to modern texture analysis. 1985.

[140] HR Wenk and Paul Van Houtte. Texture and anisotropy. *Reports on Progress in Physics*, 67(8):1367, 2004.

[141] Walter D Wilkinson. Fabrication of refractory metals. Technical report, 1970.

[142] DV Wilson and PS Bate. Influences of cell walls and grain boundaries on transient responses of an if steel to changes in strain path. *Acta metallurgica et materialia*, 42(4):1099–1111, 1994.

[143] GG Yapici, I Karaman, and Z-P Luo. Mechanical twinning and texture evolution in severely deformed ti–6al–4v at high temperatures. *Acta materialia*, 54(14):3755–3771, 2006.

[144] GG Yapici, I Karaman, ZP Luo, and H Rack. Microstructure and mechanical properties of severely deformed powder processed ti–6al–4v using equal channel angular extrusion. *Scripta materialia*, 49(10):1021–1027, 2003.

[145] AP Zhilyaev and TG Langdon. Using high-pressure torsion for metal processing: Fundamentals and applications. *Progress in Materials Science*, 53(6):893–979, 2008.

[146] L Zhu, HRZ Sandim, M Seefeldt, and B Verlinden. Ebsd characterization of an ecap deformed nb single crystal. *Journal of materials science*, 45(17):4672–4681, 2010.

[147] L Zhu, M Seefeldt, and B Verlinden. Three nb single crystals processed by equal-channel angular pressingxpart i: Dislocation substructure. *Acta Materialia*, 61(12):4490–4503, 2013.

[148] L Zhu, M Seefeldt, and B Verlinden. Three nb single crystals processed by equal-channel angular pressingxpart ii: Mesoscopic bands. *Acta Materialia*, 61(12):4504–4511, 2013.

[149] YT Zhu and TC Lowe. Observations and issues on mechanisms of grain refinement during ecap process. *Materials Science and Engineering: A*, 291(1):46–53, 2000.

APPENDIX A

GRAIN GROWTH IN RG NB

In order to determine the grain growth characteristics of RG Nb. ECAE processed Nb was recrystallized at temperatures ranging from 700^{o}C- 1400^{o}C for a duration of 90 min. The optical micrographs of the recrystallized samples are as shown in Figure A.1, and Figure A.2.Complete recrystallization does not take place until 800^{o}C the grain size is uniform, and the average grain size is 12$\pm$3μm at this temperature. As the temperature is increased from 800^{o}C there is a bi-modal microstructure development suggesting preferential growth of certain textures over others upto 1200^{o}C, above which the grain sizes are large but does not indicate any banding in microstructure.

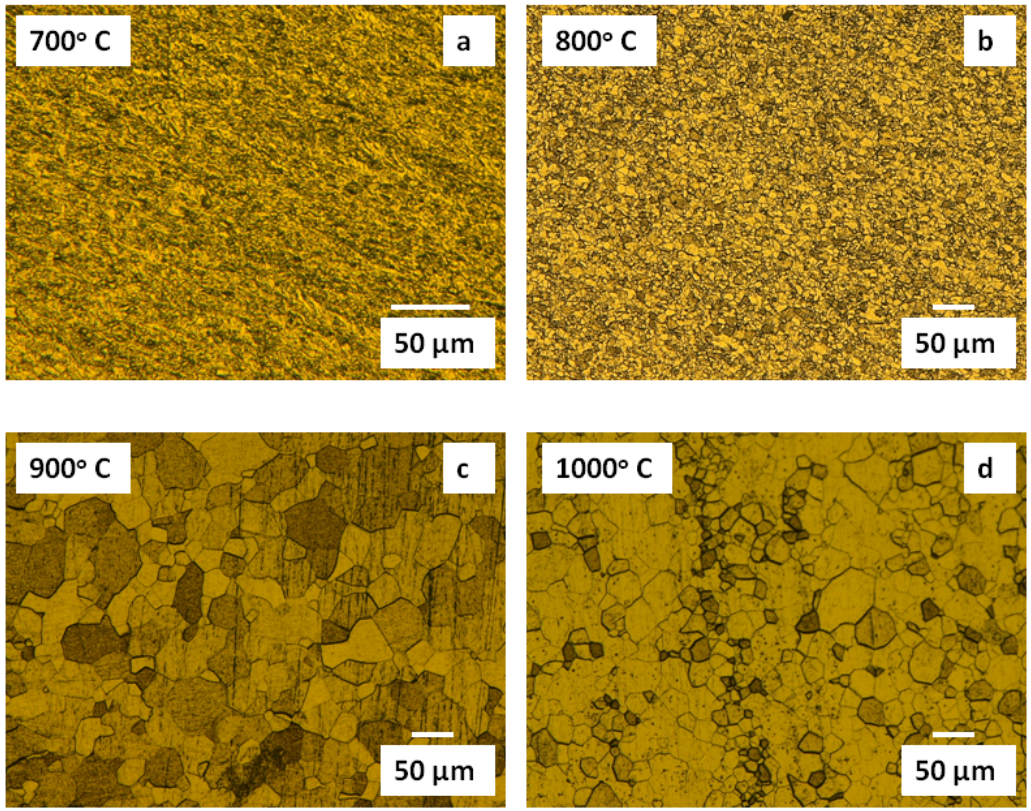

Figure A.1: Optical micrographs of ECAE processed Nb heat treated for 90 min in a vacuum of 2-8 x 10^{-6} torr at temperatures of: a) 700^{o}C, b) 800^{o}C, c) 900^{o}C, and d) 1000^{o}C

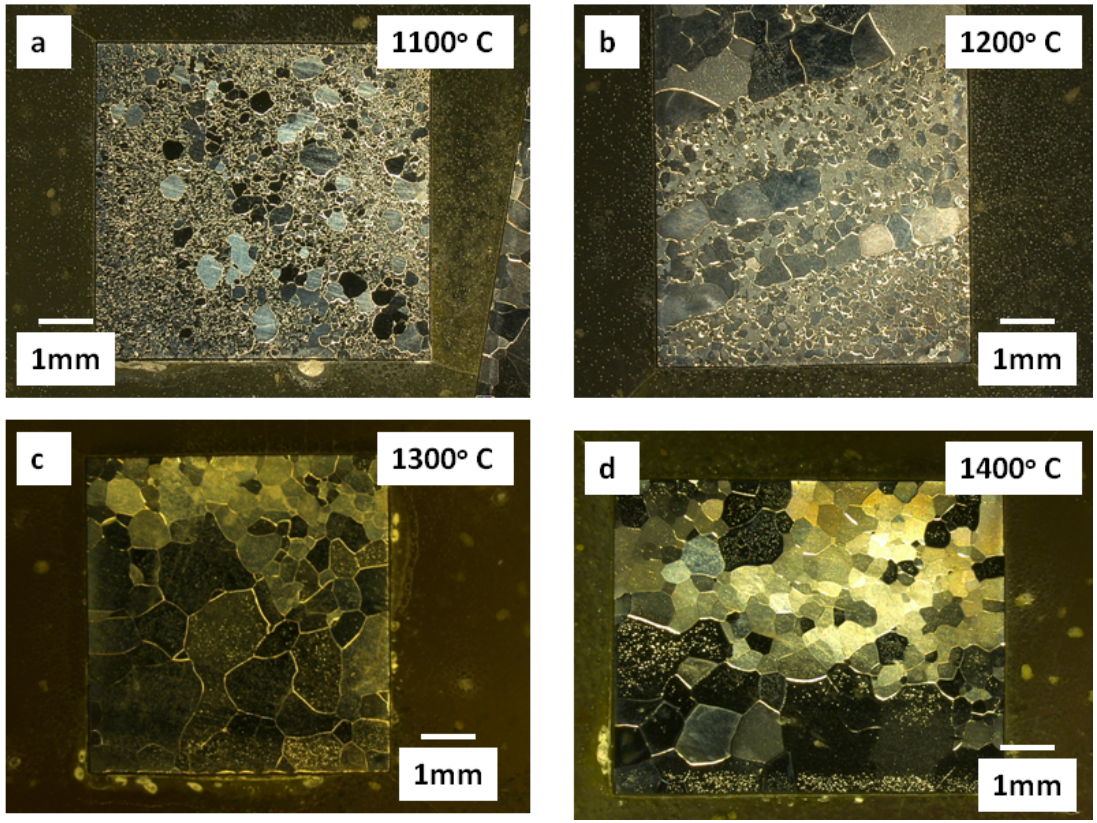

Figure A.2: Optical micrographs of ECAE processed Nb heat treated for 90 min in a vacuum of 2-8 x 10^{-6} torr at temperatures of: a) 1100^{o}C, b) 1200^{o}C, c) 1300^{o}C, and d) 1400^{o}C

APPENDIX B

WELD HEALING OF A RRR NB TUBE BY MULTI PASS ECAE AND RECRYSTALLIZATION HEAT TREATMENTS

B.1 Background

There is a need for seamless niobium (Nb) tubes that have high chemical purity, high ductility, isotropic mechanical properties, and excellent deformability by hydroforming into 9-cell SRF cavity strings. With such tubing, SRF cavities could presumably be fabricated without equatorial welds and with better reproducibility (in final shape and surface characteristics). The absence of equatorial welds holds promise for improved cavity performance. The improved formability should lead to higher cavity yields (fewer cavities that fail qualification) and a lower overall fabrication cost per cavity-string. The material microstructure leading to these improvements (grain refinement, texture, and long range uniformity) might foster additional improvements in cavity operating performance (improved surface characteristics). A spin-off benefit could be improved fabrication methods appropriate for other Nb and Ta products (bar, plate, sheet, and small diameter tube) for superconductor applications.

The problem is that presently available commercial high purity (RRR grade) Nb sheet used to make SRF cavity halves by deep drawing often deforms non-uniformly resulting in an inconsistently shaped cavity, formed-shape spring-back inconsistencies, and unwanted internal surface roughness. These problems stem from material with an inconsistent microstructure within a given sheet, and from sheet to sheet. We know this is true because material deformation behavior is dependent on mi-

crostructural characteristics including grain size, texture, and short and long range uniformity, and RRR Nb sheet for SRF cavities is known to have an inconsistent microstructure.

Experience has shown that it is very difficult to break up the microstructure of cast Nb because of a very large initial grain size, strong texture, the directional nature of conventional working operations, and the persistence of the original Nb texture [SRF 2010]. Lingering features in the microstructure inhibit efficient breakdown by conventional methods (area reduction extrusion, forging and rolling) - the result is often texture bands, grain size banding, and regions of partially recrystallized material if the annealing temperature is too low. It is the non-uniform microstructure and undesirable texture in Nb sheet that leads to non-uniform deformation characteristics, inconsistent spring-back behavior, and surface roughness problems. A related problem of non-uniform microstructure influencing mechanical deformation characteristics is also seen as the poor morphology and net shape retainment during initial stages of drawing of Grade 1 Nb bars used in the rod-restack process (RRP). Nb microstructure improvements leading to better deformability as been demonstrated in proof of concept Cu-Nb experiments (Chapter 2 of this thesis).

An opportunity exists to engineer mirostructure for lower cost fabrication of Nb tube with improved deformation behavior for hydroforming into multi-cell SRF cavity strings. The approach is to process seam-welded tube by equal channel angular extrusion (ECAE is a severe plastic deformation (SPD) method) and intermediate recrystallization annealing. The result of such processing is expected to be Nb tubing with a consistent fine grain microstructure including a somewhat healed seam weld and associated heat affected zone.

B.2 Raw Material, processing Strategy, and characterization: Weld Healing

The inital raw material for making a seam welded tube was a RRR-300 Nb sheet of nominal dimensions of 120mm x 200mm x 1.25mm, obtained from FNAL. The seam welded tube was produced by bending the sheet into a cylinder and electron beam welding (EBW) of the end to create a seam welded tube of dimensions 38mm OD, 3mm wall thickness, and 200mm in length. The EBW of the tube was done at NSCL-MSU. The as obtained tube was encapsulated in a square copper billet of 50mm x 50 mm, and a length of 250mm. The composite was processed by severe plastic deformation by ECAE, the total strain the material received was 4.6 (Route B_c). Figure B.1. shows the crossection of Nb tube before, and after processing. The tube after ECAE resembles an ellipse, with a major axis of 31 mm and a minor axis of 29mm. There is a slight increase in thicjkness from an initial value of 1.25mm to a 1.4mm. To study the microstructure of the recrystallized tube, tube crossections were heated at 700^{o}C for 1200 sec under medium vacuum conditions of 2-5x 10^{-6} torr.

Microstructure characterization and hardness methods

Optical microscopy (OM) was performed using the Keyence microscope with digital zoom. Xray diffraction (XRD) was performed on the polished sample sections using a Bruker D8 Discover Diffractometer with a Cu Ka radiation at 40KV and 40mA. The slit width used was 1mm in all cases. Microtexture measurements were performed using OIM on recrystallized samples. The working distance for all measurements was 17mm, and a standard 70o tilt was used. A step size of 2-5m was used depending upon the grain size of the sample. Vickers microhardness measurements were done on well-polished and flat specimens using a Leco (LM 300 AT) hardness tester. The load and dwell time for all measurements were 300 grams and 13s respectively; the

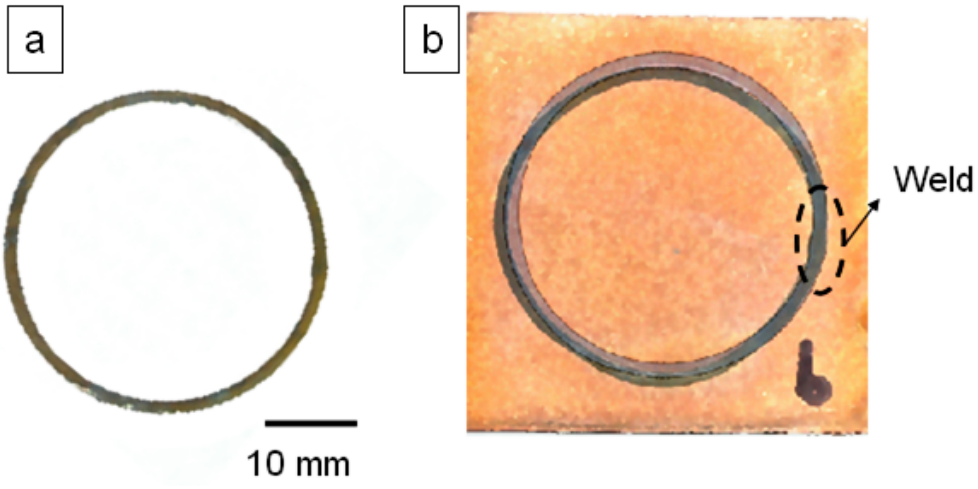

Figure B.1: Crossection of a the Nb tube: a) Before ECAE processing, and b) After ECAE propcessing, the light gray overlap is the initial crossection. The crossection of the tube after ECAE processing is elliptical rather than circular.

measurements were done in accordance with ASTM-E384.

B.3 Results

EBW and Healed tubes- Microstructure

The starting microstructures in the EBW welded tubes depends on the location of the sample along the circumference of the tube. Figure **??**, shows the microstructure of the EBW tube, as recieved and after ECAE processing and heat treatment at 800^oC. In the as welded tube, the fusion zone (FZ) extends to about 2mm along the circumference, heat affected zone (HAZ) extends to about 750-1000μm on either side of the weld and the remaining part of the tube is characterized by the parent material(PM). In the EBW condition the grain size varies from 500μm-1000μm in the FZ, to 300μm-100μm in the HAZ, and the base material has a grain size of 30$\pm$20μm. After ECAE processing and heat treatment, the grain sizes are normalized. The gradient in the grain sizes between the regions are significantly decreased, with the FZ grain size being the finest as seen in the OM's in Figure B.2 (f). The average

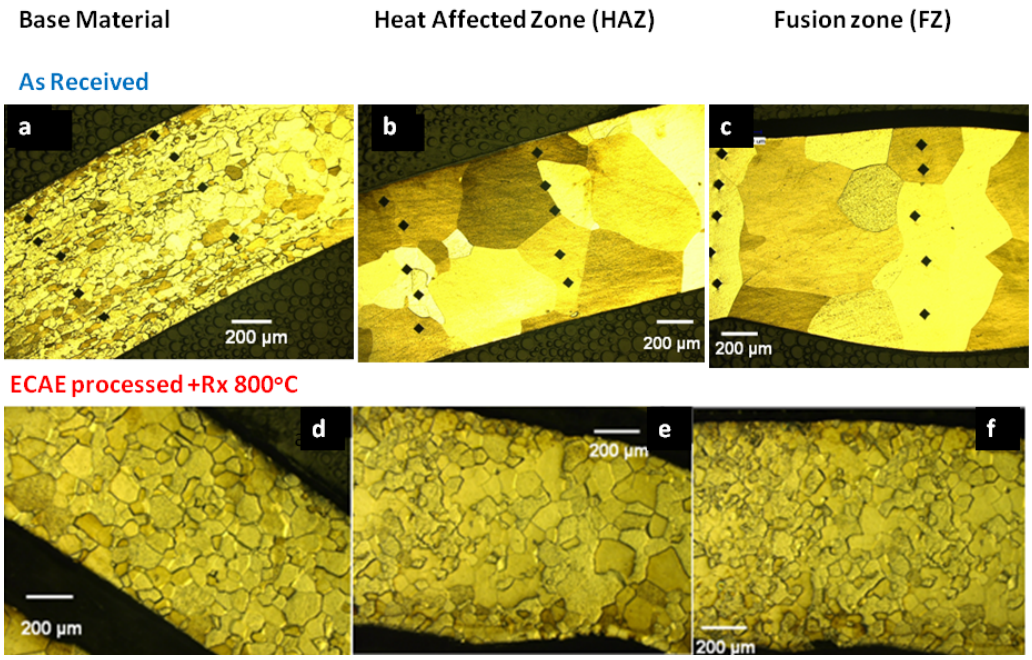

Figure B.2: Optical micrographs of EBW tube before and after ECAE processing and heat tretament. a-c, d-f correspond to the microstrctures of the different regions before and after the processing.

grain size of the all the regions is $50\mu m$. The standard deviations of the grain sizes are very different in the FZ, $30\mu m$ as compared to the HAZ and PM which are 21μm, and 8μm respectively.

Figure

A complete description of the microstructure is obtained from the IPF maps in the tube radial direction for the as welded and processed tubs as shown in Figure B.3 indicated in the IPF the FZ has grains greater than $500\mu m$. The texture strength is high 7.2 m.rd, and the individual grains can be distinguished from the pole figures (B.3 c) . The PM has a typical bcc rolling texture as expected consisting of $\{111\}\|$ND and $\{100\}\|$ND orientations as shown in Figure (B.3 d). The texture strength is lower as compared to FZ and is about 4.0 m.r.d. The tube after

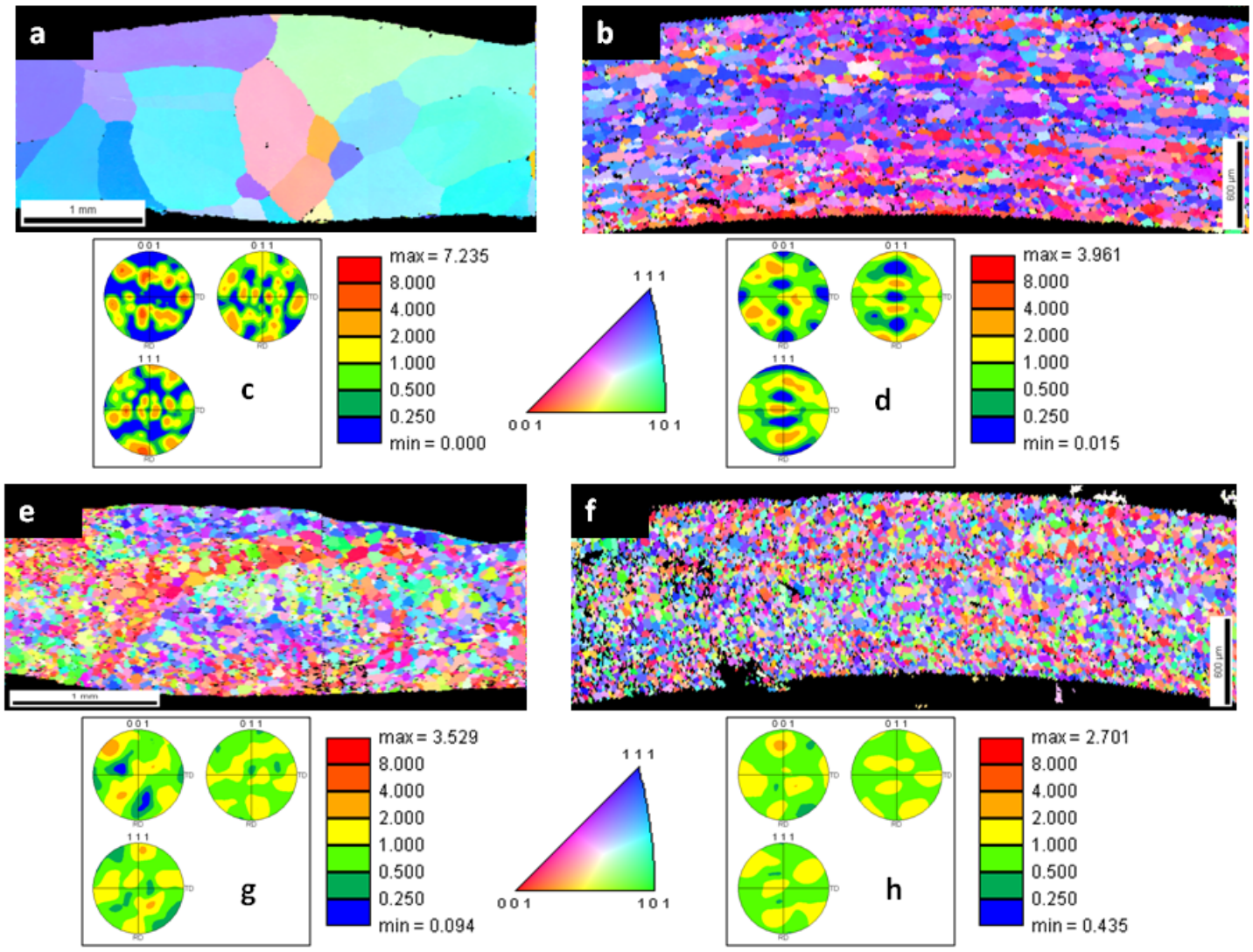

Figure B.3: IPF maps in the sheet normal direction of the FZ, and the PM before after ECAE processing. a-b. IPF of the FZ ,and PM is EBW condition, and c-d are the corresponding PF's. e-f. IPF of the FZ ,and PM after ECAE processing and heat treatment at 700^oC, and g-h are the corresponding PF's

ECAE processing shows heavy breakdown in microstructure in FZ, the prior grain boundaries of the large grains are distinguishable although very heavily deformed. However, the texture strength is significantly lower from the initial FZ , and PM and the maximum intensity is about 3.5 m.r.d. there is an emergence of {111}‖ND, {100}‖ND , {110}‖ND shear texture. The as processed PZ microstructure is significantly different from the initial PZ microstructure, the texture strength of 2.7 m.r.d is the lowest among all the other microstructure. The crystal orientations are randomized, and correspond to weak shear textures.

EBW and Healed tubes-Mechanical Properties

The hardness along the circumference of the tube over a 90 section is shown in Figure B.4, there is no significant difference in the hardness along the circumference in the as received Nb tube irrespective of the region in the tube. The maximum hardness in the as received tube along this section was 64±8, and occurs in the PM, whereas the minimum hardness is 53±8 occurs in the FZ. As the Nb tube is worked, there is an overall increase in the hardness. The hardness of the initial FZ is varies between 133±6 to 147±9. The PM hardness varies between 130±4 to 140±8. The hardness values along the tube section after recrystallization heat treatment of 800^oC is very similar to as received tube. The minimum and maximum hardness values of 54±1, and 70±7 both occur in the original PM region.

The stress-strain curves are presented in Figure B.5 and associated tensile properties are calculated from the tensile curves as shown in Table B.1. For the as-received sheet and as-welded tube parent metal (PM) are similar. This is expected, and confirms that the mechanical properties of the as-received annealed sheet do not change much by forming the sheet into tube geometry for relatively large bending radii and associated small levels of plastic strain. The tensile behavior of the FZ in the as-

Table B.1: Summary of tensile testing data of EBW, and ECAE processed Nb tube

Condition	**Orientation**	**Yield (0.2% Strain) MPa**	**UTS**	**Ductility (%)**	**n**
As received sheet	parallel to axis of tube	74	167	27.8	0.28
As formed tube	180 deg to weld	74	156	26.7	0.32
	Weld	74	107	13.7	0.13
ECAE processed and recrystallized (8E + 750oC)	180 deg to weld	80	177	20.1	0.23
	Weld	81	185	19.9	0.28

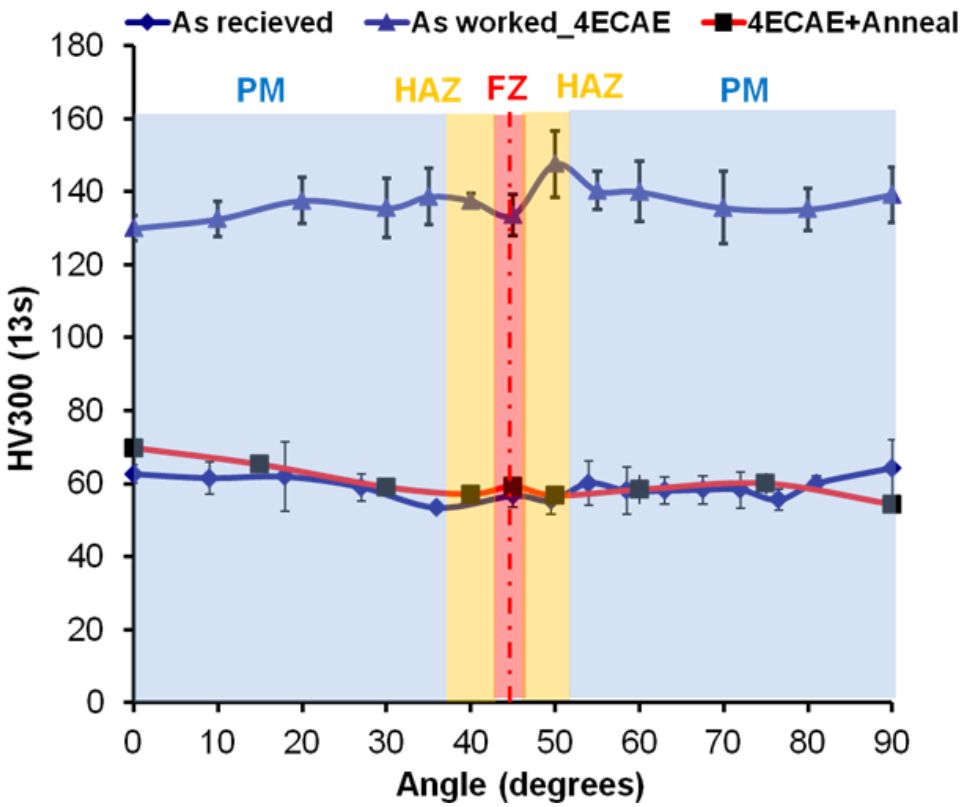

Figure B.4: Hardness along the tube crossections along the PM, HAZ and FZ in the as-recieved, as worked, and ECAE processed and annealed conditions.

welded tube exhibits substantially lower properties than the parent metal (i.e. UTS and ductility values of 107 MPa and 14% versus 156 MPa and 27%,respectively). The ECAE plus recrystallization tube parent metal YS and UTS are above those of the as-received sheet and as-welded tube Pm, while the corresponding ductilities are lower. The tensile properties in the FZ and PM for the ECAE plus recrystallization tube are similar. This result is notable, and forecasts better overall tube deformability for the ECAE processed tube, compared to the as-welded tube.

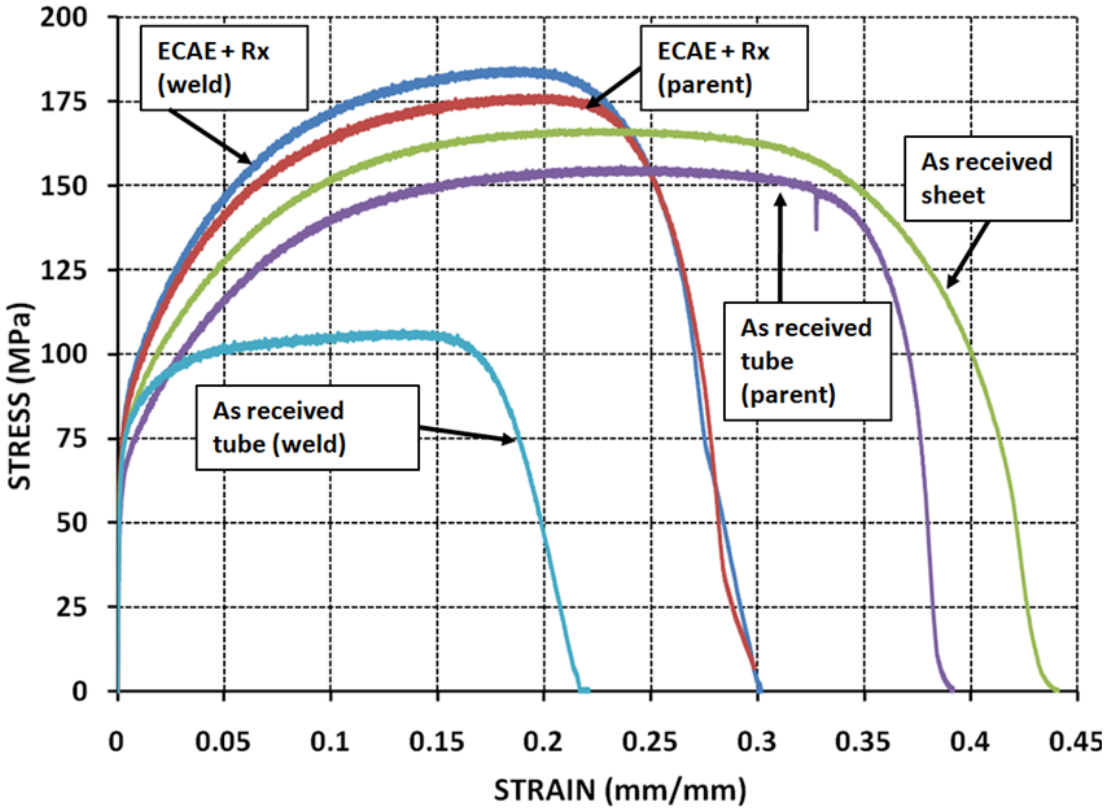

Figure B.5: Tensile tests of samples cut along the axis of the tube corresponding to the FZ, and PM before and after thermomecghanical processing by ECAE. Note the converegence in the mechanical property of the FZ and PM after ECAE and heat treatment at 650^{o}C